Aachen University of Technology
Germany

Materials Science Institute
Univ.-Prof. Dr. techn. E. Lugscheider

Engineering Thesis

Developments in Optimisation Methods for Plasma Spraying of Functional Coatings and the Utilisation of High-Speed Pyrometry for On-line Process Control of Al_2O_3/TiO_2 Coatings

Author: Frank Ladru
Supervisor: Dipl.-Ing. R. Mathesius
Research field: Thermal Spraying

Aachen, June 1994

TU Delft

Technische Universiteit Delft

AFSTUDEERCOLLOQUIUM

Development in optimisation methods for Plasma Spraying of Functional Coatings and the utilisation of High-Speed Pyrometry for On-line Process Control of Al_2O_3/TiO_2 Coatings

Datum	-	vrijdag 8 juli 1994
Plaats	-	zaal B, Laboratorium voor Materiaalkunde
Aanvang	-	10.00 uur
Spreker	-	Frank Ladru
Afstudeerdocent	-	Prof.Dr.Ir. M.H. van de Voorde

Foreword:
This engineering thesis has been carried out at "Lehr- und Forschungsgebiet Werkwissenschaften" of Univ.-Prof.Dr.techn. E. Lugscheider, "Rheinisch-Westfalische Technische Hochschule Aachen". Graduation outside the University of Technology Delft was made possible with support of Prof.Dr.Ir. M.H. van de Voorde.

Summary:
Functional coating systems to protect high-performance machine parts against environmental attack as wear, oxidation, (hot-)corrosion and chemical attack are gaining more and more interest in aerospace, transport, chemical and offshore industries. The enormous flexibility of the Thermal Spray process makes it very important for coating high-performance parts; all kinds of metallic and non-metallic can be sprayed on a wide variety of materials.

Many studies have been devoted to improve and optimise Plasma Spraying of functional coatings. Most of the time it has been done empirically, by trial and error. Over 80 parameters (e.g. power, gas flow and composition, powder rate and spraying distance) influence the coating process. An optimised adjustment of the Plasma Spray system to spray high quality coatings is difficult to determine. Better fundamental understanding of relations between adjustment parameters and resulting coating quality parameters is desirable.

Methods which can help with this optimisation are noncontact optical measurement methods, Statistical Experiment Planning, Simulation and Process modelling and ultrasound measurements. An introduction to these methods will be given.

A high-speed pyrometric system has been used for noncontact on-line monitoring of substrate surface temperatures during Plasma Spraying of Al_2O_3/TiO_2 (87/13) coatings. The goal is to determine heat-input and temperature stability of the process. Measured temperature profiles will be brought in relation to mechanical properties and microstructure. Future optimistic view is use of Pyrometric process control systems for on-line quality control (QC).

Werkstoff-wissenschaften
Univ.-Prof. Dr. techn. E. Lugscheider

RWTH RHEINISCH-WESTFÄLISCHE TECHNISCHE HOCHSCHULE AACHEN

J/93.131/VdV

Scriptievoordracht

door

Frank Ladru

plaats: Laboratorium voor Materiaalkunde, zaal C

Datum: 17 december 1993

Tijd: 10.00 uur

Titel: *Optimisation of Thermally Sprayed Functional Coating Systems with Help of Noncontact Optical Measurements, Statistical Design of Experiments and Process Modelling and - Simulation.*

Samenvatting:

Thermisch spuiten (Thermal Spraying) is een veelzijdige mehode voor het maken van relatief dikke funktionele deklagen (coatings). Alle combinaties tussen substraat en deklaag van metalen, keramieken en cermets zijn mogelijk. Er worden zelfs anti-slijtagelagen aangebracht op vezelversterkte kunststoffen.
Deze deklagen worden onder andere aangebracht tegen slijtage, tegen corrosie en oxidatie en als warmte-isolatie(Thermal Barrier Coatings) en zijn van groot belang in met name hoge temperatuur toepassingen, maar ook op implantaten. Bij deze laatste groep draagt de coating zorg voor lichaamsverdraaglijkheid en het substraat voor de mechanische eigenschappen.
In de laatste decennia werden deze substraat-coating-systemen op empirische wijze geoptimaliseerd. Een goede coating heeft een hoge weerstand tegen zijn milieu, is stabiel tijdens zijn levensduur en heeft een sterke binding met het substraat.
Thermisch spuiten is een gecompliceerd proces met meer dan 80 proces parameters en is dus moeilijk te optimaliseren. Die huidige ontwikkelingen die bijdragen aan kennis van de physische processen zijn kontaktloze optische meettechnieken (Pyrometrie en Laser-Doppler-Anemometry); wiskundige, statistische hulpmiddelen en het simuleren en modelleren van het Thermisch Spuiten. Geen van bovengenoemde methoden zijn in staat het proces alleen te optimaliseren en zullen vaak gecombineerd moeten worden.
Al dit onderzoek is van groot belang om bestaande en toekomstige coatings te verbeteren om zo levensduur en bedrijfszekerheid te vergroten.

Keywords

Atmospheric Plasma Spraying, Ceramics, Coating, High-Speed Pyrometry, On-line Process Control, Monitoring, Optimisation.

Acknowledgements

I am very grateful to both professor van de Voorde and professor Lugscheider for offering me the possibility to fulfil my engineering thesis at the Materials Science Institute in Aachen, Germany. Furthermore I would like to thank Robert Mathesius and Peter Remer for their great support.

Foreword

This engineering thesis is the last of three parts of the authors' studies Materials Science in Engineering at the University of Technology Delft. It follows a literature survey and a practical work. The engineering thesis is being fulfilled at the Materials Science Institute of Univ.-Prof. Dr. techn. E. Lugscheider, University of Technology Aachen. Graduation outside the University of Technology Delft was made possible with the support of Prof. Dr. Ir. M.H. van de Voorde.

Table of Contents

Assignment of the Engineering Thesis

Thema: Untersuchungen zum Zusammenhang von Plasma-, Partikel- und Schichteigenschaften mittels optischer Meßverfahren

Bei den thermischen Spritzverfahren und insbesondere beim Plasmaspritzen ist eine Einstellung gewünschter Schichteigenschaften bislang nur über umfangreiche, kostenintensive Spritzversuche möglich. Wenn es gelingt, die Partikeleigenschaften und den Temperaturverlauf der aufwachsenden Schicht meßtechnisch zu erfassen und gezielt einzustellen, ist die Grundlage für eine wesentlich effizientere, anlagenunabhängige Schichtentwicklung und Qualitätssicherung geschaffen.

Im Rahmen eines Forschungsprojektes soll in Zusammenarbeit mit der Bundeswehrhochschule München der Zusammenhang zwischen einstellbaren Spritzparametern, Plasmaeigenschaften und Partikeleigenschaften ermittelt werden.
Zu diesem Zweck wird vom Münchener Partner ein mobiles, automatisiertes Laser-Doppler-Anemometer (LDA) mit integrierter Charge-Coupled-Device- (CCD) und Micro-Channel-Plate- (MCP) Technik verwendet, um sowohl Lage und Stabilität des Plasmastrahls zu erfassen als auch die Geschwindigkeits-, Größen- und Flugbahnverteilung im Spritzstrahl zu ermitteln.
Vom Aachener Projektpartner wird ein vorhandenes Hochgeschwindigkeits-Pyrometer (HGP) eingesetzt, um on-line während des Beschichtungsprozesses Mittelwert und Schwankungen der Oberflächentemperatur zu messen. Die Schwankungen der Oberflächentemperatur sollen mit den Stabilitätsuntersuchungen des Plasmastrahls und der Stationaritätsmessung des Partikelstroms korreliert werden, um den Zusammenhang zwischen Partikel- bzw. Strahleigenschaften sowie den Oberflächentemperaturen einerseits und den erzielten Schichtqualitäten andererseits zu bestimmen.
Die Arbeiten beim Aachener Partner umfassen dabei im einzelnen:

- Einarbeitung in die Beschichtungstechnik unter Einbeziehung unterschiedlicher Verfahren und Brennertypen.
- Erarbeiten der theoretischen Grundlagen der Temperaturmessung an Oberflächen unter besonderer Berücksichtigung der Infrarot-Pyrometrie (IRP).
- Einarbeitung in die Funktionsweise des am Institut befindlichen HGPs und grundlegende Beschichtungsversuche mit verschiedenen Keramiken, um das HGP-System auf die spezielle Aufgabe einzustellen.
- Koordination der sowohl in Aachen als auch in München stattfindenden Beschichtungsversuche.
- Durchführung von Beschichtungsversuchen mit unterschiedlichen Keramiken (sowohl getrennt von als auch in Zusammenhang mit LDA-Messungen im Spritzstrahl), zum einen im Mikrozeitmeßbereich, um Instabilitäten des Brenners und der Pulverfördereinrichtung zu erfassen und zum anderen im Makrozeitmeßbereich zur Aufnahme von Temperaturverläufen und -schwankungen, die durch das Einwirken und die Veränderung von Prozeßparametern wie Beschichtungsverfahren, Brennerleistung, Art des Beschichtungswerkstoffes, Pulverförderrate und Pulvergasrate verursacht werden.
- Beurteilung der produzierten Schichtqualitäten anhand diverser metallographischer und werkstoffwissenschaftlicher Untersuchungen, wie Gefügeuntersuchungen mit Licht- und Elektronenmikroskopie sowie Porositäts- und Härtemessungen und Haft- und Verschleißprüfungen.
- Ermittlung des Zusammenhangs zwischen Primärparametern, Plasma- und Partikeleigenschaften, Temperaturbeeinflußung der Substratoberfläche und Schichtqualitäten.

Summary

This text describes the author's engineering thesis of his studies Materials Science in engineering. The work has been realised at the Materials Science Institute, Aachen University of Technology.

The experimental work is the forms part of a research project to investigate the relations between primary parameters and process parameters in Atmospheric Plasma Spraying of functional coatings. Primary parameters such as power level, spray distance and powder feed rate indirectly determine resulting coating quality. Monitoring process parameters such as particle velocities and substrate temperatures is a much better starting point for quality improvement, control and optimisation.

For this purpose a High-Speed Pyrometer system has been adapted and employed to measure substrate temperature profiles during Plasma Spraying of Al_2O_3/TiO_2 (87/13) coatings. This is important to determine, because it indicates the heat-input and stability of the Plasma Spraying process.

The Plasma Spraying technique and the coating procedure has been described. A widespread introduction to developments in optimisation methods is given. The physical principle of electromagnetic radiation exchange on which pyrometric temperature measurement is based, is extensively described.

In one procedure after samples for microscopy and samples for wear resistance as well as adhesive strength in tension test, had been sprayed, the temperature profile was recorded. Parameters that were expected to influence the heat-input, e.g. power level and powder feed rate, have been optimised.

Microscopic evaluation and mechanical destructive testing do not give explicit and indisputable the best adjustment of parameters and exactly this underlines the usage of process control methods as Pyrometry to monitor the process. Although the pyrometric measurements do not totally convince to be 'the solution' for process control and optimisation, the results encourage further research.

Zusammenfassung

Die vorliegende Arbeit ist eine Diplomarbeit des Studienfachs Werstoffkunde. Sie wurde im Lehr- und Forschungsgebiet Werkstoffwissenschaften an der Rheinisch-Westfälischen Technischen Hochschule Aachen durchgeführt.

Diese experimentelle Arbeit ist Teil eines Forschungsprojektes mit der Aufgabenstellung, den Zusammenhang von Plasma-, Partikel- und Schichteigenschaften mittels optischer Meßverfahren zu untersuchen. Primäre Parameter, wie z.B. Leistung, Spritzabstand und Pulverförderrate, bestimmen indirekt die resultierende Schichtqualität. Die Erfassung von Prozeßparametern, wie z.B. Teilchengeschwindigkeit und Substrattemperatur, führt zu einer wesentlich besseren und gezielteren Optimierung.

Zu diesem Zweck wurde ein Hochgeschwindigkeitspyrometer installiert und modifiziert, um die Temperaturprofile während des Beschichtungsprozesses von Al_2O_3/TiO_2 (87/13) meßtechnisch zu erfassen.

Zu Beginn der Arbeit erhählt der Leser eine kurze Einführung in die Plasmaspritztechnologie und in den Schichtentstehungsprozeß. Die bestehenden und die in der Entwicklung befindlichen Optimierungsmethoden sind Gegenstand des 4. Kapitels. Anschließend wird das physikalische Prinzip des elektromagnetischen Strahlungsaustausches, auf welchem die Pyrometrie basiert, im Detail beschrieben.

Die Proben für Mikroskopie, Verschleiß und Haftzug sind in einem Spritzdurchgang fertiggestellt worden. Während jedes Spritzdurchgangs wurde das Temperaturprofil gemessen. Parameter wie Leistung und Pulverförderrate, von denen eine Beeinflussung der Wärmeeinbringung in das Substrat zu erwarten war, wurden optimiert.

Mikroskopie und Untersuchungen über die mechanischen Eigenschaften allein, führen nicht zu einer optimalen Anpassung der Einflußparameter. Die Pyrometrie hat sich als eine nützliche Meßmethode herausgestellt, um die bisherigen zerstörenden Untersuchungsverfahren zu ergänzen. Die weitere Erforschung der Pyrometrie ist notwendig, um ihren Einsatz bei der Prozeßkontrolle und -optimierung endgültig beurteilen zu können.

Samenvatting

Het afstudeerwerk dat hier wordt beschreven vond plaats in het kader van de Materiaalkunde studie van de schrijver. Het werk werd uitgevoerd aan het Materiaalkunde instituut van de Technische Hogeschool Aachen.

Het experimenteel werk maakt deel uit van een onderzoeksproject waarbij met optische metingen de relaties tussen primaire en proces parameters bij Plasma Spuiten van functionele coatings onderzocht worden. Parameters zoals vermogen, spuit afstand en poeder massa stroom bepalen indirect de coating kwaliteit. Proces controle van parameters, zoals deeltjes snelheid en substraat temperatuur, vormt een betere uitgangspositie voor kwaliteits controle, -verbetering en coating optimalisatie.

Ten behoeve hiervan werd een Hogesnelheids Pyrometer systeem aangepast en ingezet voor metingen van substraat temperaturen tijdens het Atmosferische Plasma Spuiten van Al_2O_3/TiO_2 (87/13) coatings. Dit is uiterst belangrijk om te bepalen, omdat de warmte inbreng een beeld geeft over de stabiliteit van het Plasma Spuit proces.

Het Plasma Spuiten en fabriceren van coatings wordt kort beschreven. Een uitgebreide inleiding over de ontwikkelingen op het gebied van optimalisatie methoden wordt gegeven. Het fysische basis principe van stralings uitwisseling, waarop de Pyrometrie is gebaseerd, wordt uitvoering beschreven.

In een stap worden achtereenvolgens proefstukken voor microscopische, slijtage en treksterkte gespoten en daarna direct wordt een temperatuur profiel opgenomen. Voor de optimalisatie is gekozen voor parameters van wie verwacht werd een meetbare invloed op de temperatuur profielen te hebben. Dit waren vermogen en poeder massa stroom.

Microscopisch onderzoek en destructieve slijtage en treksterkte testen leverden geen onweerlegbare en duidelijke optimale instelling op. Dit is nu precies de reden, waarom zoveel waarde wordt gegeven op de ontwikkeling en toepassing van proces controle met o.a. Pyrometrie. Alhoewel ook de pyrometrische metingen niet volledig overtuigen, moedigen ze toch aan tot verder onderzoek.

1. Introduction

Technological progress requires high quality materials and processing. Exposure of materials to their ultimate limits of performance demands for extended research. The constantly increasing stresses and surface temperatures lead to stimulate new developments.

By combining different materials which have specific properties products with unique characteristics can be processed. Coated surfaces to give better protection against environmental attack such as wear, oxidation, erosion and (hot-)corrosion is long established and has found application in many forms across a wide variety of disciplines.
Some examples of surface layers are uranium fuel coatings in nuclear reactors, painted or varnished ironwork and wear coatings on high speed tools. Despite the great variety of coating types and their utilisation, the basic requirements are generally the same for all systems: good environmental resistance, long term stability and strong adhesion of the protective layer to the substrate.

Within surface technologies Thermal Spraying, especially Plasma Spraying, is one of the most important technique for depositing relatively 'thick' functional coatings. A wide variety of combinations between metals, ceramics and plastics between coating and substrate material can be fabricated. Thermal Spraying has become a standard coating method, because it is reliable and manifold in operation. The enormous flexibility of the Thermal Spray process makes it very important for coating high-performance parts in aerospace, automotive, chemical and offshore industries.

Many studies have been devoted to the improvement and optimisation of Plasma Sprayed functional coatings. Most of the time the optimisation is empirical, by trial and error, because there are more than 80 parameters (e.g. power, gas flow and composition, powder rate and spraying distance) that may influence the coating process. Therefore it is difficult to determine the optimized adjustment of the Plasma Spray system to spray high quality coatings. For this reason extensive and expensive research is necessary, concerned to resources, time and manpower.

The usual way to find the best possible substrate coating system starts with the deposition process. This is followed by a destructive characterisation of microstructure and investigation of the mechanical properties. After modification of the process, the deposition is done again. For each substrate-coating-system this highly expensive process has to be repeated many times. Final coating quality to be used in practice is 'approved' by statistics, due to the destructive nature of the testing methods.

New developments in measurement methods are important to make new progress in Quality Control (QC), quality improvement, optimisation and process control. These include Noncontact Optical Methods, Statistical Experiment Planning (SEP), Process Modelling and Simulation as well as Non Destructive Testing (NDT).

In order to find a solution for the problems mentioned above, the Materials Science Institute, Aachen University of Technology and the Faculty of Electronics, München University of armed forces, started a co-operative research project (AIF 9622). The goal is to research the relations between primary parameters on one hand and heat-input, coating quality and plasma and particle properties on the other hand.
The München work group employ a Laser Doppler Anemometry system to determine plasma and particle properties and the Aachen Thermal Spraying group use a High-Speed pyrometric system (HS-Pyrometry) for measuring temperature profiles during Atmospheric Plasma Spraying. Heat-input and

temperature stability of the process will be determined by on-line temperature measurements. Fluctuations and deviations of the observed temperature indicate to irregularities.

For coatings examination, various destructive testing methods will be applied. In addition to that data, light microscopy will provide information over the microstructure.

The coating to be investigated is ceramic Al_2O_3/TiO_2 (87/13). Combination of measured temperature profiles and the results of mechanical tests and microstructure research may show relations and may lead to a better fundamental understanding of the process.

The research aims to the usage of HS-Pyrometry as a process control system.. Good knowledge of temperature profiles provides the operator with an on-line process control tool. By monitoring the process, deviations of the ideal temperature or increase of the temperature scattering, caused by any instability, informs over irregularies. The operator can well aimed change the setting of the Plasma Spraying equipment to realise the ideal temperature again.

In this engineering thesis the reader will be provided with sufficient information about the wide Thermal Spraying and coating field. Furthermore a review of developments in coating optimisation methods will be given. After treatment of the basics of Pyrometry and a description of the adaptation of the Pyrometric Process Control System (PPCS), the results of the optimisation will be given.

2. Methods of Thermal Spraying

The manifold Thermal Spraying processes base generally on materials in form of wire, powder or rods that melt in a concentrated heat-source and accelerate and transported onto a substrate. It is a line-of-sight process, where the molten material deposit, in form of small liquid droplets, only onto surfaces that are directly in line with the droplets. On a prepared surface (substrate) forms a coating that has a typical pancake-like, lamellar structure (Fig. 2.1).
The coating has the benefits of rapid solidification processing (RPS), with the advantage of only small interactions of substrate and coating (no liquefying and no decomposition effect of the substrate). Benefits of RPS are good homogeneity, fine grain size and metastable phases.
The Thermal Spraying methods can be classified according to heat source (chemical or electrical), form of the spray-material or application of the substrate-coating-system (Fig. 2.2). Here we follow the classification according to heat source. The next paragraphs only give short, compact descriptions of the Thermal Spraying methods, because of the numerous published books and articles [1-13].

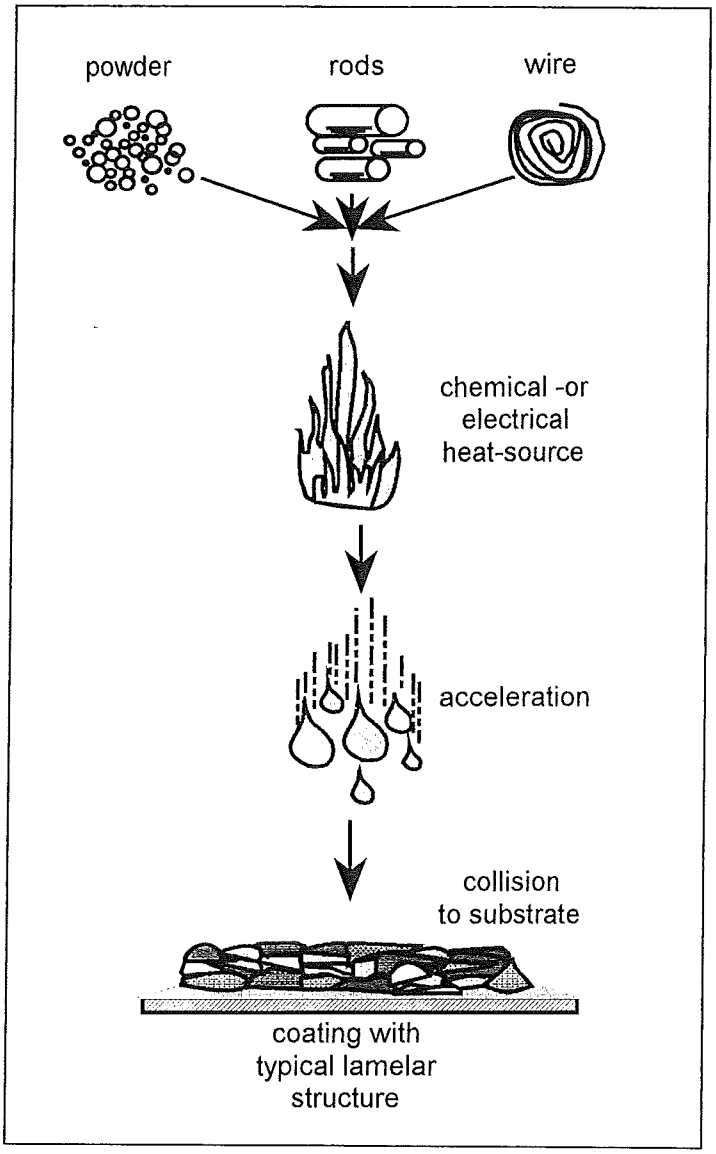

Fig. 2.1. Basic principle of Thermal Spraying.

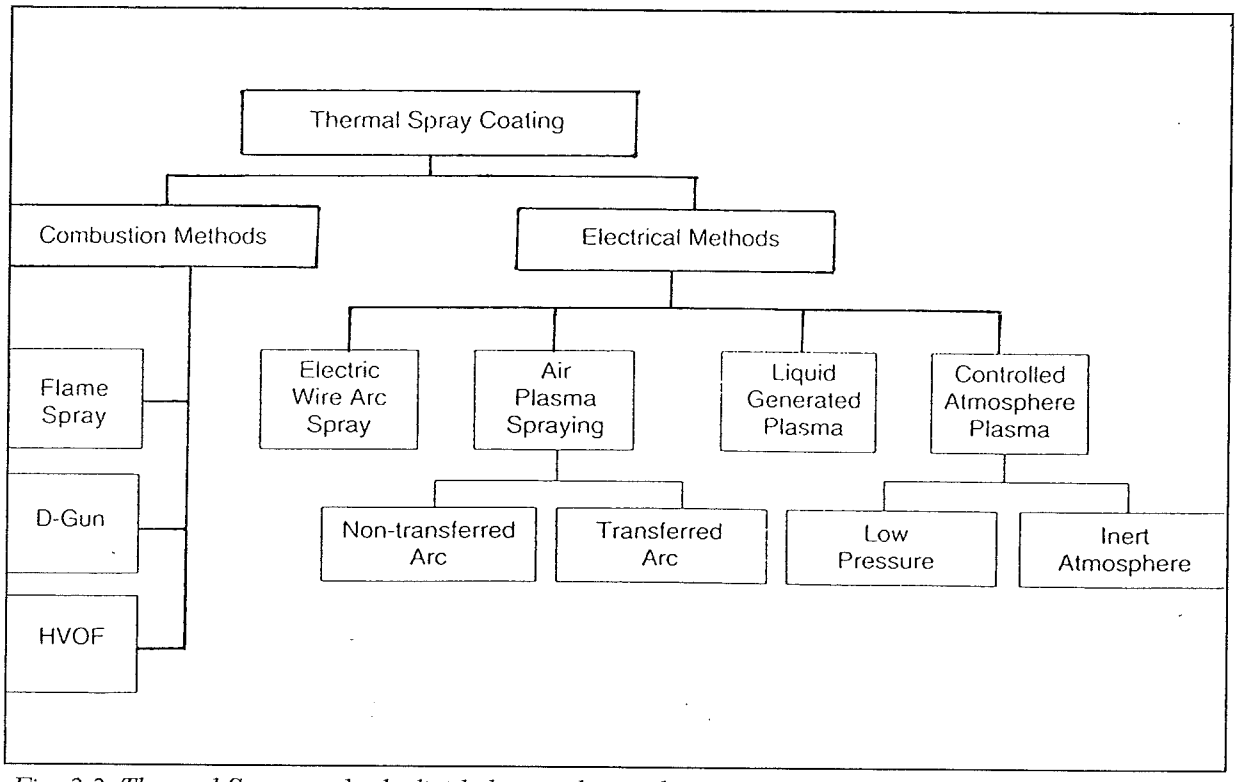

Fig. 2.2. Thermal Spray methods divided according to heat-source [4].

2.1. Chemical Heat-source

2.1.1. Flame Spraying

The early Thermal Spraying methods use an oxygen-fuel gas flame as heat-source. Metals and alloys (wire or powder) and ceramic materials (powder or rods) can be sprayed. The fuel gases commonly used are acetylene, propylene or hydrogen. The carrier gas may be oxygen, fuel gas or some other, usually inert gas. The combustion flame may be shrouded with a stream of compressed air or inert gas. Flame Sprayed coatings have a thickness from 50 m up to some millimetres [2].

2.1.1.1. Wire Flame Spraying

Through the centre of a combustion flame a wire, with a typical diameter of 1,6-5 mm, is fed at a controlled rate. The wire tip melts off and compressed air, which flows annular around the nozzle accelerates the molten or semi-molten particles to a velocity of ~100 ms^{-1} [3]. The fuel gas used is generally acetylene and the flame can reach a temperature of 3150 °C [10]. Air flow, gasflow, gas pressure, wire diameter and wire feed rate influence the coating morphology (Fig. 2.3).
Wire Flame Spraying process is economical seen very interesting and nowadays used extensively in wide ranges of industries. Wire Spraying equipment is portable and the guns are used manually, which makes them attractive for on-site applications. A fairly wide selection of ferrous and non-ferrous metals can be sprayed successfully; various steels, Al, Zn, Cu, Mo and Ni-alloys.

2.1.1.2. Powder Flame Spraying

In Powder Flame Spraying a powder suspended in a carrier gas stream, is introduced in an oxygen-fuel gas flame (Fig. 2.4). The fuel gases commonly used are acetylene or hydrogen. A particular material will define the spraying parameters (e.g. the choice of gases, the geometry of the spray head and the gas and powder flows).

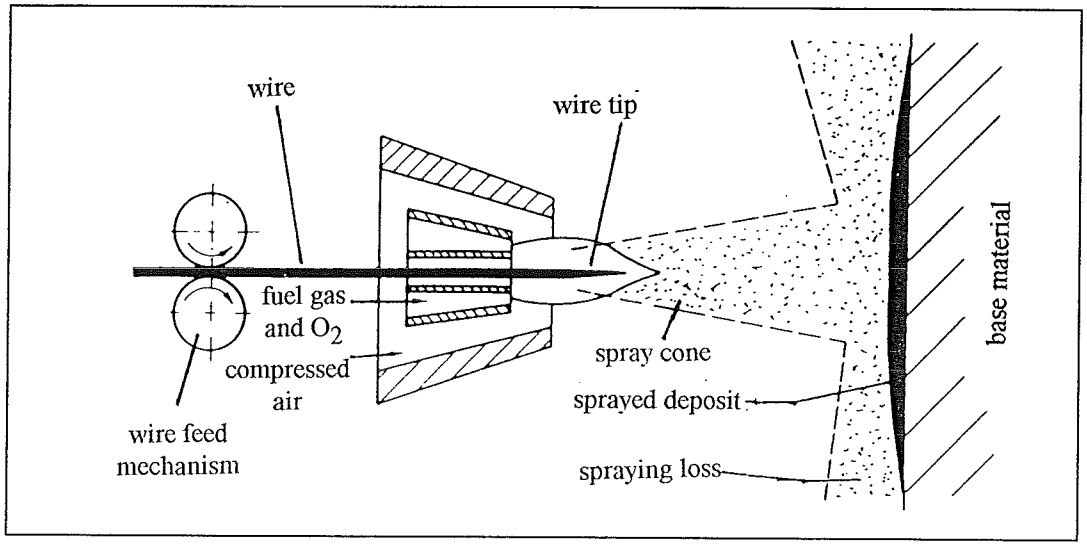

Fig. 2.3. Wire Flame Spraying [2].

The Powder Flame Spraying process extends the choice of materials to those which are available in powder form. This leads to the spraying of various carbides, oxide ceramics and cermets. Modified torches are extensively in use for applying plastic coatings onto large components [3].

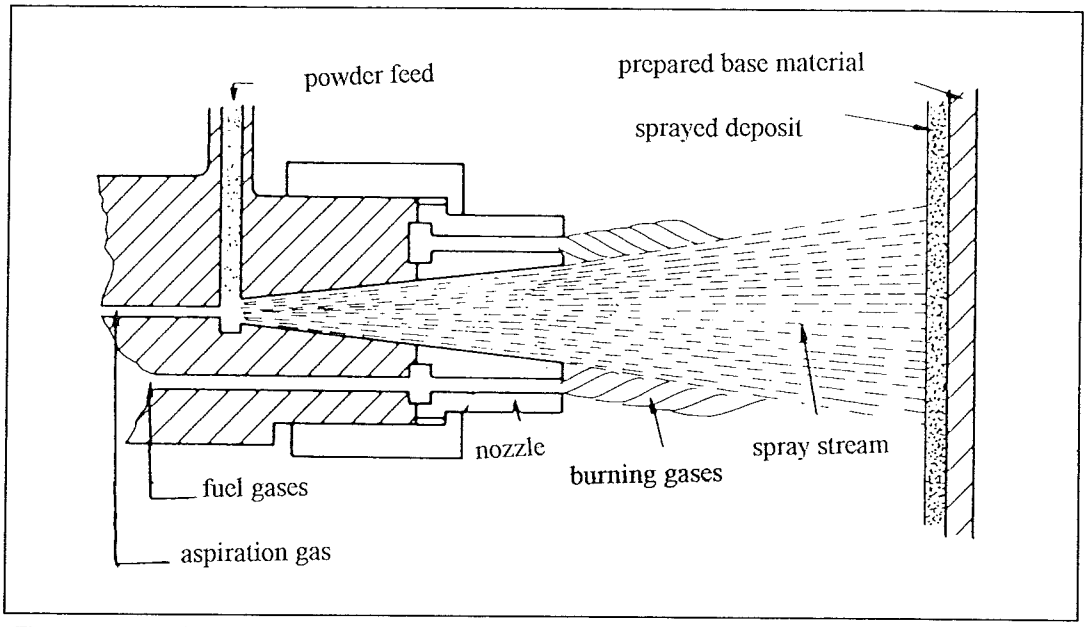

Fig. 2.4. Powder Flame Spraying [2].

2.1.2. Detonation Gun

The Detonation Gun equipment is housed in a double-walled sound-proof barrel of 1-1,5 m long and 20-30 mm internal diameter into which the gas mixture is injected (Fig. 2.5). A spark plug ignites the gas mixture consisting of acetylene, oxygen and shrouded gas (and the powder). During a short burn period the flame front accelerates, compressing and heating the unreacted gases in front of it. After reaching of the critical temperature, self-ignition produces a detonation or shock wave, which moves at a speed of approximately 3000 ms^{-1} and has a temperature of about 4700 °C. As the detonation wave passes through the suspended particles they heat up and accelerate up to velocities exceeding 700 ms^{-1}.
The molten particles leave the gun barrel at a high velocity and produce a high density layer on their impact. Complete is the cycle after opening of a nitrogen valve and a purge stream to sweep out the gaseous combustion products. Depending on the type of coating applied, this cycle is repeated 4 to 8 times a second.
The bond strengths of Detonation gun sprayed coatings to their substrates are extremely high and have a porosity level, compared to most plasma sprayed coatings. Materials deposited with D-gun are metals, various metallic alloys, Ni-alloys, Co-alloys, WC/Co/Co and oxide-ceramics.

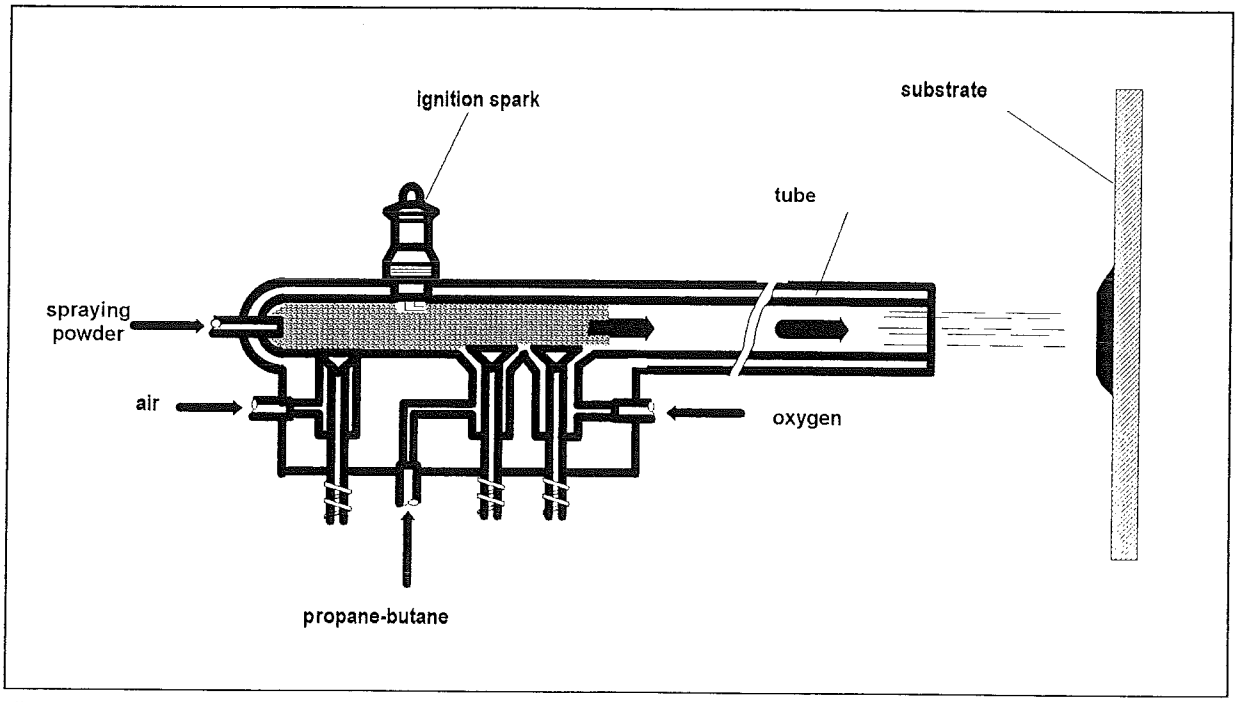

Fig. 2.5. Detonation gun.

2.1.3. High Velocity Oxygen Fuel Spraying

In the eighties several competitive High Velocity Oxygen-fuel Flame (HVOF) spraying methods were launched into the Thermal Spraying market, starting with the Jet-Kote® process. The principle is generation of flames with high velocities by burning oxygen-fuel gas mixtures in a gun with special nozzle geometry (Fig. 2.6). The fuels used are hydrogen, propane, butane and propylene, which are pre-pressurised. Gas velocity and temperature are 1300 ms^{-1} and 3400 °C respectively. Sprayable are powders with high melting points of approximately 1700 °C. The particles reach velocities up to 1000 ms^{-1}. Processing of all steels, nickel and cobalt alloys and some ceramics is possible.

2.2. Electrical Heat-source

2.2.1. Electric Arc Spraying

In Electric Arc Spraying two wires are fed through two angled electrode holders, with a DC potential between them. As the tips almost contact each other an electric arc is generated, producing high temperatures of around 6250 °C. The wires' tips melt and atomise by a jet of high-pressure gas (usually compressed air) producing a spray stream (Fig. 2.7). The wire materials used in this process are often similar to those used in the Wire Flame Spraying process.

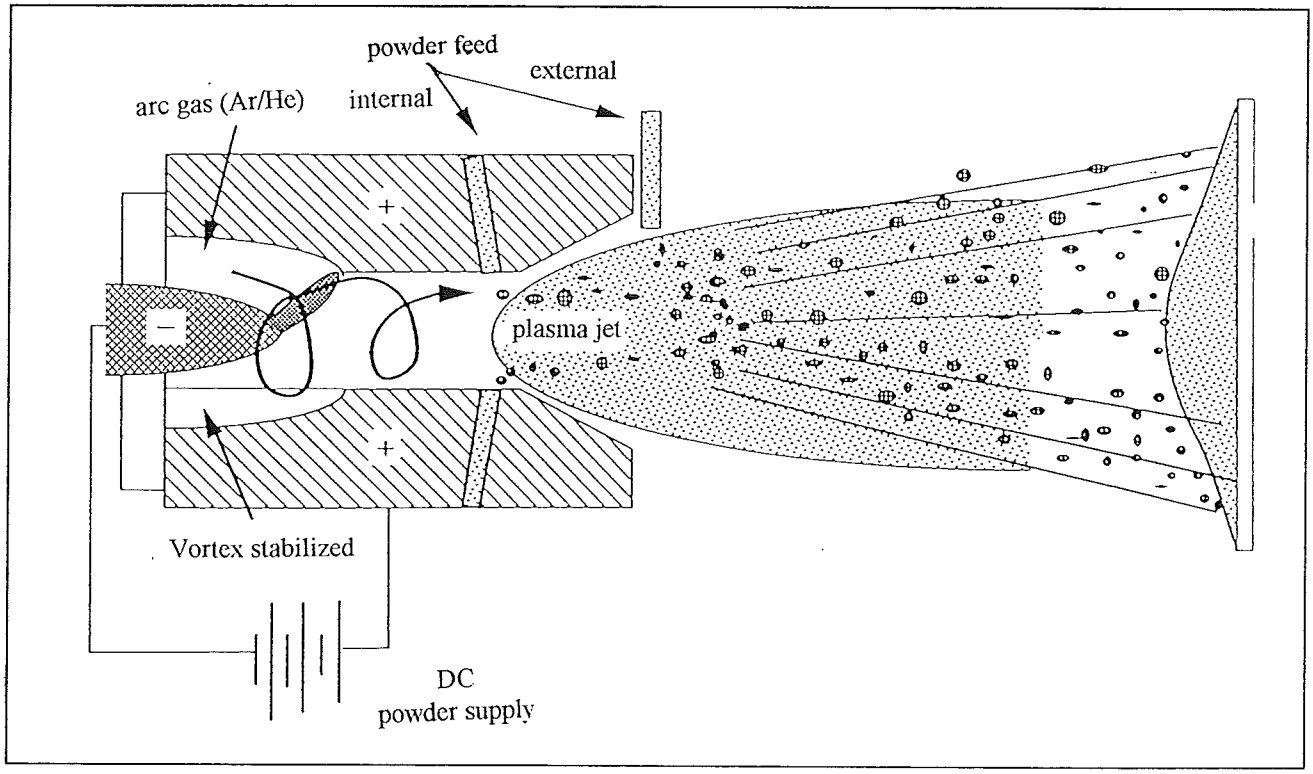

Fig. 2.8. Cross section of a Plasma Spray gun [4].

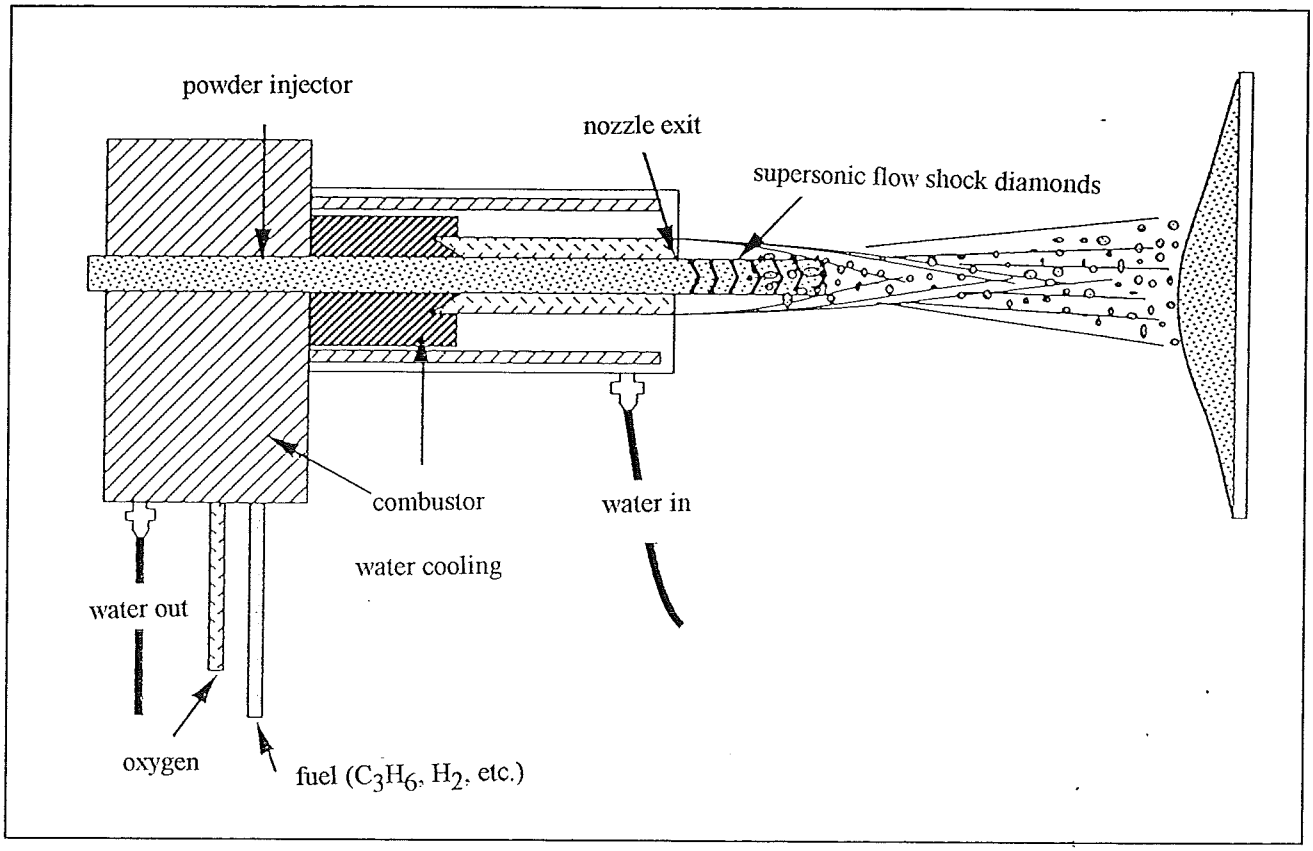

Fig. 2.6. High Velocity Oxygen Fuel Spraying [4].

However, differences exist in the resulting coatings, due to different heating processes involved. For example, initial particle temperatures tend to be higher with this process. The process is particularly well suited for high speed deposition relatively thick coatings on large components.
Only electrical conducting materials can be sprayed. This process may be used too, to produce coatings of mixed metals (pseudo-alloys), by feeding two different wires through the electrodes. The most commonly used materials are: carbon and low-alloy steels, Al and Zn.

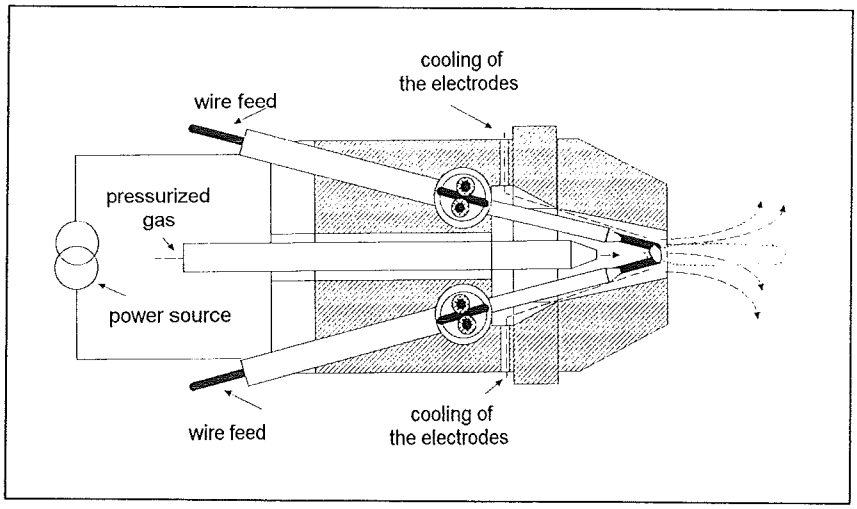

Fig. 2.7. Electric Arc Spraying.

2.2.1. Plasma Spraying

Among Thermal Spray technologies, Plasma Spraying is considered to be the most universal coating technique. One of the reasons is the different Plasma Spray variants available. Almost every substrate-coating combination is possible. Plasma Sprayed coatings offer technical advantages over common combustion coatings for the following reasons:

- The heat source is more efficient, caused by the high energy state of the plasma;
- The heat source is inert, thereby minimising oxidation of the substrate and coating;
- Higher plasma temperatures permit spraying of high melting materials.

Besides high melting metals, oxides, carbides and almost all known ceramics and materials with a very low melting point (even plastics) can be plasma sprayed. Fig. 2.8 gives a sectional drawing of a plasma gun.

2.2.1.1. Atmospheric Plasma Spraying

A plasma is often referred to as the fourth matter of state and consist of a mixture of electrons and ions conducting very well. At high temperatures a stable plasma forms in electric and electromagnetic fields. Fig. 2.8. shows a Plasma Spray gun. Between an anode nozzle of copper and a tungsten cathode a DC arc dissociates and ionises the gases passing through. The nozzle ejects, at velocities of several hundred meters per second, a plasma jet. The velocity increase comes from special nozzle geometry and volume expansion of the gases, by the dissociation and ionisation. Most devices use argon as main plasma gas, often with small additions of hydrogen (this increases the power and enthalpy of the plasma) or nitrogen or in special cases helium. The plasma reaches temperatures of 16.000 °C.
Powders, suspended in an inert carrier gas stream (argon), are injected in the plasma stream at a position depending on the melting point of the material. Energy transfer to the powder particles is very efficient.
Most of the guns developed for Plasma Spraying can be hand held, but because of high noise levels (~120 dB) and strong UV radiation operators do need appropriate protection. To meet improved safety legislation and the modern requirements for quality control, most systems are now fully automated.

2.2.1.2. Vacuum Plasma Spraying

A common disadvantage of all Thermal Spraying techniques is that there can be some interaction between the molten particles and the ambient atmosphere. Even though plasmas, which are essentially inert, turbulence trap air, resulting in unacceptable levels of oxides in coatings. In Vacuum Plasma Spraying (VPS) the process is carried out in a chamber held at a low pressure (Fig. 2.9). Another advantage is that higher particle reach higher velocities than by APS, which results in coatings with higher densities. The chamber pressures vary from 30-200 mbar [14].
Inert Plasma Spraying (IPS) also uses the vacuum chamber. The air in the chamber is than evacuated and replaced by an inert atmosphere of nitrogen or argon.

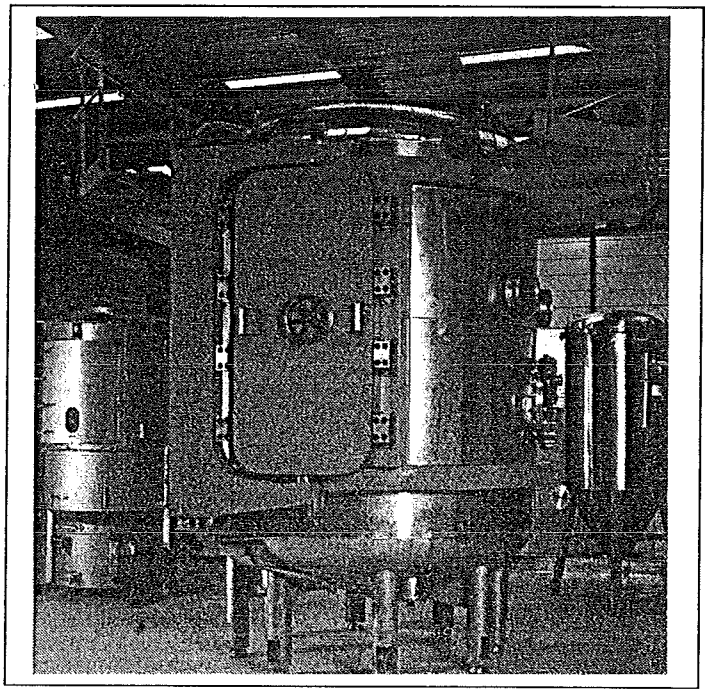

Fig. 2.9. Vacuum Plasma Spraying system [10].

2.2.1.3. Underwater Plasma Spraying

In Underwater Plasma Spraying (UPS), the coating is fabricated under water. Advantages are noise, dust and radiation reduction. The process is interesting for offshore and marine applications and to spray toxic materials. All materials that can be processed with inert or vacuum plasma spraying also can be sprayed with UPS. UPS is very suitable for thermal sensitive materials such as plastics by the efficient cooling of the water [15].

2.2.1.4. Shrouded Plasma Spraying

Other new process developments deal with the so-called Shrouded Plasma Spraying (SPS). The plasma gun uses an inert gas shroud to protect the molten particles from air during the spray process. Shrouded Plasma Spraying is of decisive importance to coat large components with oxidation sensitive materials.

2.2.1.5. Controlled Atmosphere Plasma Spraying

Controlled Atmosphere Plasma Spraying (CAPS) can handle all plasma process variants by one plasma spray system (except for UPS). Such a system covers all process variants of APS, IPS, SPS and VPS (Fig. 2.10-11).

Newly published is the Controlled Aspiration Process (CAP) [16]. The liquid metals become atomised in a supersonic nozzle in this process. The process is suitable to apply coatings on components to a near-net shape. The process itself consists of a gas heater that supplies heated pressurised gas to an also heated supersonic nozzle/tundish assembly. The tundish is independently pressurised as a means of forcing the liquid metal through a small orifice in the nozzle throat where it's atomised and forced into the supersonic gas flow.

2.2.3. Laser Spraying

Laser Spraying is a recent and novel innovation [11][17]. The heating source for Thermal Spraying is a high-power laser. Two different processes:

- In the 'one step process', powder or paste with special binder, is injected into the laser-beam. The paste is molten by the laser and the forms the coating.
- The 'two step process' consists of the coating fabrication with an arbitrary Thermal Spraying technique, followed by a laser heat-treatment. Improvement of coating quality, like density, structure and adhesion strength are obtained.

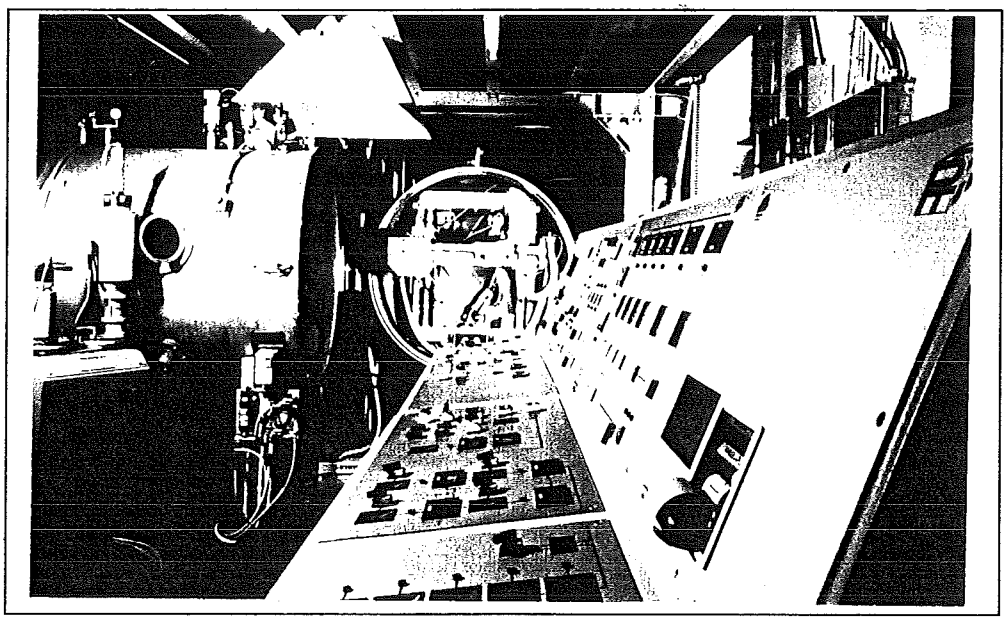

Fig. 2.10. Controlled Atmosphere Plasma Spraying system.

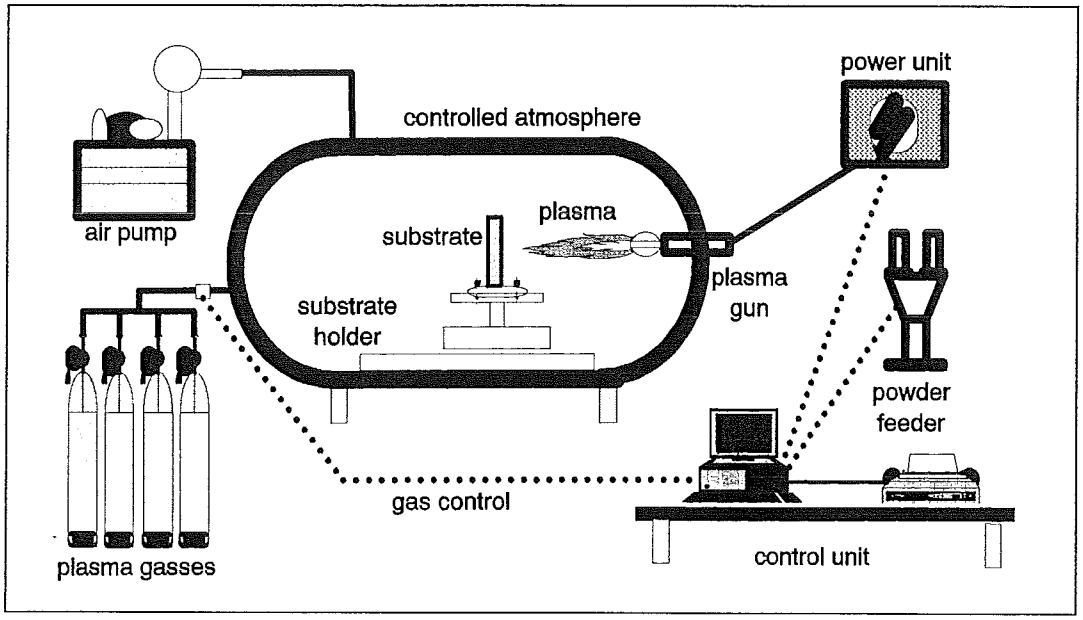

Fig. 2.11. Schematically drawing of a CAPS equipment.

3. Functional Coating Systems

No limitation of the Thermal Spraying technology is set by substrate and/or coating material. Metallic hard materials, like the different carbides and nitrides, non-metallic hard materials, oxide-ceramics and intermetallics can be sprayed [18]. All combinations with metals, cermets, high-alloy-steels, hard-alloys, MCrAlY-type materials and Ni- and Co-super-alloys can be processed. Even plastic-metal combinations and metallic or ceramic coatings on fibre reinforced plastics, are being fabricated today [19]. The following paragraphs give a more detailed review of different coatings [2-13,19].
Before spraying of a coating, which has a good bonding cleaning the substrate surface is very important. Preparation of the surface describes paragraph 3.1. Paragraph 3.2 describes the adherence of the coating to the substrate. A review of the functional coatings and their applications described in $3.3 and $3.4.

3.1. Preparation of Substrate Surface

The condition of the substrate surface determines very much the quality of the resulting coating. The removing of contaminants, as oils, grease, paint, rust, scale and moisture, is the first step in the substrate surface preparation. Available methods are:

- vapour degreasing to remove of oil, grease and other solvent soluble organic compounds. (commonly used solvents are trichlorethylene, perchloethylen and 1,1,1-trichloroethane);
- baking at 300 to 350 °C for a few hours will vaporise and remove deeply penetrated oils [4];
- ultrasonic cleaning is applied to dislodge contaminants in confined or hidden areas;
- wet abrasive blasting uses a water slurry, comprising the abrasive media, which is projected by air through a jet onto a surface to remove corrosion products, paint, grease and oil;
- dry abrasive blasting uses high pressure compressed air, which carries the abrasive media, to remove old sprayed coatings, mil scale, paint, corrosion products and oxides.

Experience has shown that, without exception, all sprayed coatings have significantly higher bond strengths on roughened surfaces. The principle methods for this step in preparation of the surface are, dry abrasive grit blasting, machining or macro roughening. Grit blasting has the disadvantage that some substrate materials may be too hard to roughen, while other can work-harden. Inevitably always a few grit particles remain embedded in the surface. After grit blasting of the surface it's activated and will give good bonding to the impacting particles.

Often a bond coating is sprayed to the substrate, e.g. MeCrAlY for ZrO_2 and NiCr, NiAl, Mo for ceramics (see 3.4.).

Areas that do not require coating material, are usually masked (also during grit-blasting) to prevent build-up of overspray coatings. Masking-methods are: metal shadow masks, tough high temperature tape and paint.

3.2. Bonding Mechanisms of Coatings

The strength of a coating system depends on the weakest link in the chain of the following three forces:

- Bonding strength of the coating;
- Strength of the substrate material;
- Strength of the coating material.

In Thermally Sprayed coatings the weakest link is usually the bonding strength of the coating [21]. The coating is bonded to the substrate by [4]:

- mechanical interlocking;
- fusion (melting) of contact surfaces;
- diffusion of element species.

Mechanical interlocking is the most important mechanism for Thermal Spray coating adherence (Fig. 3.1). The arriving molten particles flow around irregularities on the substrate. After shrinkage caused by solidification the mechanical interlocking is a fact.
When the surface is clean and active and the particles are able to reach the surface very closely adsorption-forces can contribute to the bonding. These forces however are weak. After formation of the initial coating layers, which are in direct contact with the base material, self-cohesion strength determines the bonding of the next coating layers.
Negative influences to bonding strength have oxides, dirt or oils. These may interfere with the liquid flow and will reduce or prevent local bonding.

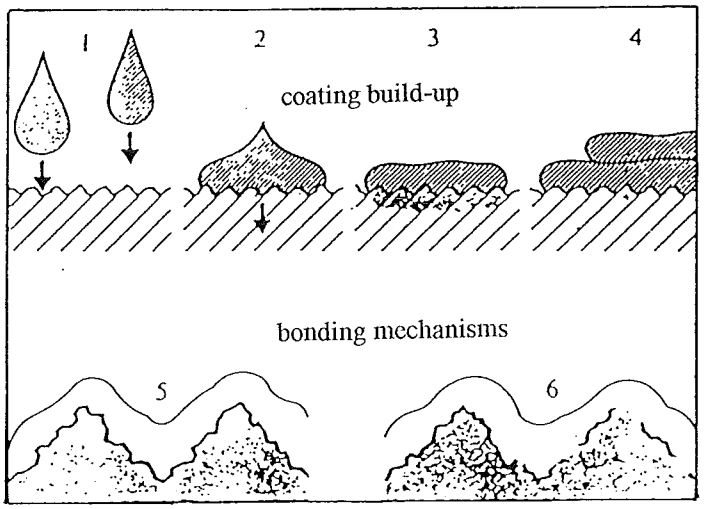

1. Flight of molten droplets
2. Collsion to the surface
3. Heat transfer to substrate
4. Stiffen and shrink of coating material
5. Mechanical bonding
6. Local welding

Fig. 3.1. Mechanical bonding [21].

3.3. Functions of Coatings

Coatings manufactured with Thermal Spraying have become very important to enhance performance of base materials used in three industry groups: aerospace, land-based turbine engines for power generation and other that include chemical processing plants, oil industry, paper and steel mills, etc. Table 3.1. gives a brief compilation of some typical parts used in the various industries that rely on thermally sprayed wear coatings.

Different functions of coatings, which can be distinguished are:

- wear coatings to resist abrasion, erosion, cavitation and fretting and to reduce friction;
- thermal insulation coatings to reduce heat conduction to the base material (Thermal Barrier Coating, TBC);
- corrosion and oxidation resistant coatings;
- hot corrosion coatings to resist the combination of high temperature corrosion and salt attack;
- clearance control coatings in turbines to ensure efficient flow of engine working fluids (air in the compressor and fuel combustion products/air in the turbine) over turbine blades [13];
- electrically conductive and electrically resistive coating;
- dimensional restorative coatings to repair or re-surface worn and/or corroded parts;
- medically compatible coatings on implants in both dental and orthopaedic devices;
- polymer coatings to protect against chemical attack, corrosion or abrasion.

Table 3.1. Compilation of some typical parts used in various industries [20].

Flight gas turbines	Land-based turbines	Others
turbine and compressor blades, vanes	Turbine and compressor buckets, vanes, nozzles	feed rolls, pump sleeves
gas path seals	piston rings	shaft sleeves
mid-span stiffeners	hydroelectric valves	gate valves, seats
Z-notch tip shroud	boilet tubes	rolling element bearings
combustion and nozzle assemblies	wear rings, gas path seals	dies and moulds, diesel engine cylinder
blade dovetails	impeller shafts	hip joint prosthesis
flap and slat tracks	impeller pump housings	hydraulic press sleeves
compressor stators		grinding hammers, agricultural knives, biological implants

3.4. Overview of Functional Coatings

We can distinguish five main coating groups:

- Metallic coatings:

Aluminium, zinc and cobalt are for corrosion protection. Aluminium layers suite well to protection against SO_2-atmospheres. Ni and Mo are in use as bonding layers for the actual functional coatings. Molybdenum is also as wear resistant coating.

- Metallic-alloy coatings:

NiAl and NiCr are in use as bonding coating. Nickel forms intermetallic phases with aluminium or chromium. Widely used are the metallic MeCrAlY-type coatings (Me=Fe, Ni, Co). These coatings are in use for hot-corrosion, erosion and chemical protection.

- Hardmetallic coatings:

These are mainly in use as wear resistant coatings, e.g. the classical WC-Co-system. Typical hard alloys are Co or Ni alloyed with B, Si and Cr. These hard alloys are very resistant to oxidising acids and alkalines.

- Intermetallic coatings:

Strong metallic forces between the atoms characterise intermetallic phases. These metallic forces give the coating good mechanical properties and high temperature resistance. The intermetallics are nickel- and titaniumaluminides and silicides. The nickel- and cobalt-superalloys are being applied to approximately temperatures up to 1100 °C.

- Ceramic coatings

The use of ceramic coatings is increasing because outstanding oxidation resistance, hardness and high temperature resistance. Alloying with other oxide-ceramics can improve the brittle behaviour.

- Cermets:

Mixing ceramic with metal powder forms unique coatings for very specific applications, like hot working tools.

A summary of the Thermal Spraying materials gives in Fig 3.2 and Appendix C.

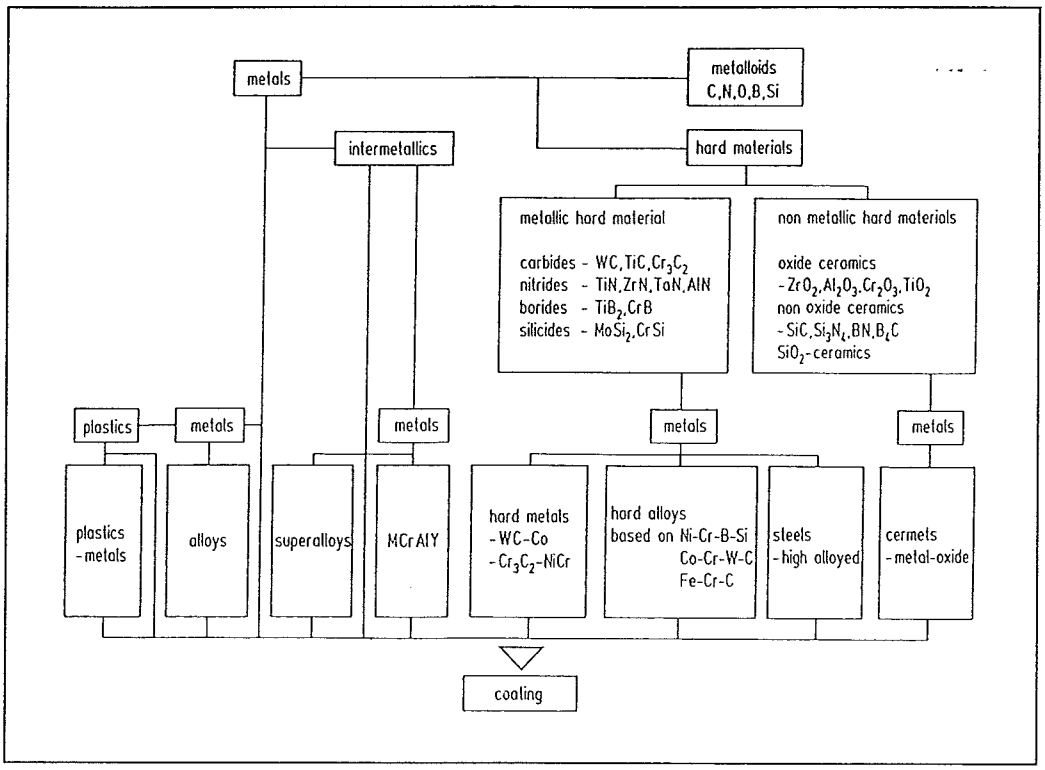

Fig.3.2. Coating materials [10].

4. Quality Improvement and Control of Thermal Sprayed Coatings

Knowledge of the relations between primary spray parameters and resulting coating morphology is very important to optimise coatings and to monitor the Plasma Spraying process. This initiated the development of various Optimisation-, Quality Control- (QC) and Non Destructive Evaluation (NDE) methods.

Paragraph 4.1 gives a selection of the numerous plasma spray and coating parameters and in paragraph 4.2. the developments in optimisation and process control methods are described.

4.1. Plasma Process Parameters which Influence Coating Quality

Thermal Spraying is a complex process; coating quality, e.g. density, homogeneity and bonding, is determined by over 80 process parameters [9]. Fig. 4.1. give some parameters. A selection of these parameters is:

- **system:**
  - power (voltage / current)
  - spray distance
  - traverse velocity
  - primary gas (usually Ar)
  - secondary gas (H_2, N_2, He)
  - primary gas flow
  - secondary gas flow
  - flow ratio = ratio of secondary to primary gas flow
  - atmosphere (air, vacuum, inert, shrouded, reactive or water).
- **plasma gun:**
  - geometry of nozzle
  - geometry of gas distribution ring
  - powder injector: angle, distance to middle of the plasma, diameter
- **powder feeder:**
  - powder carrier gas flow
  - powder feed rate
  - heater temperature
  - stirrer
- **powder:**
  - material
  - particle distribution
  - mean particle size
  - powder morphology
- **substrate:**
  - material
  - geometry: plane / symmetrical
  - temperature (pre-heating)
  - substrate cooling
  - surface roughness
- **coating:**
  - bonding layer
  - thickness
  - number of passes
  - heat treatment
  - distance between two passes

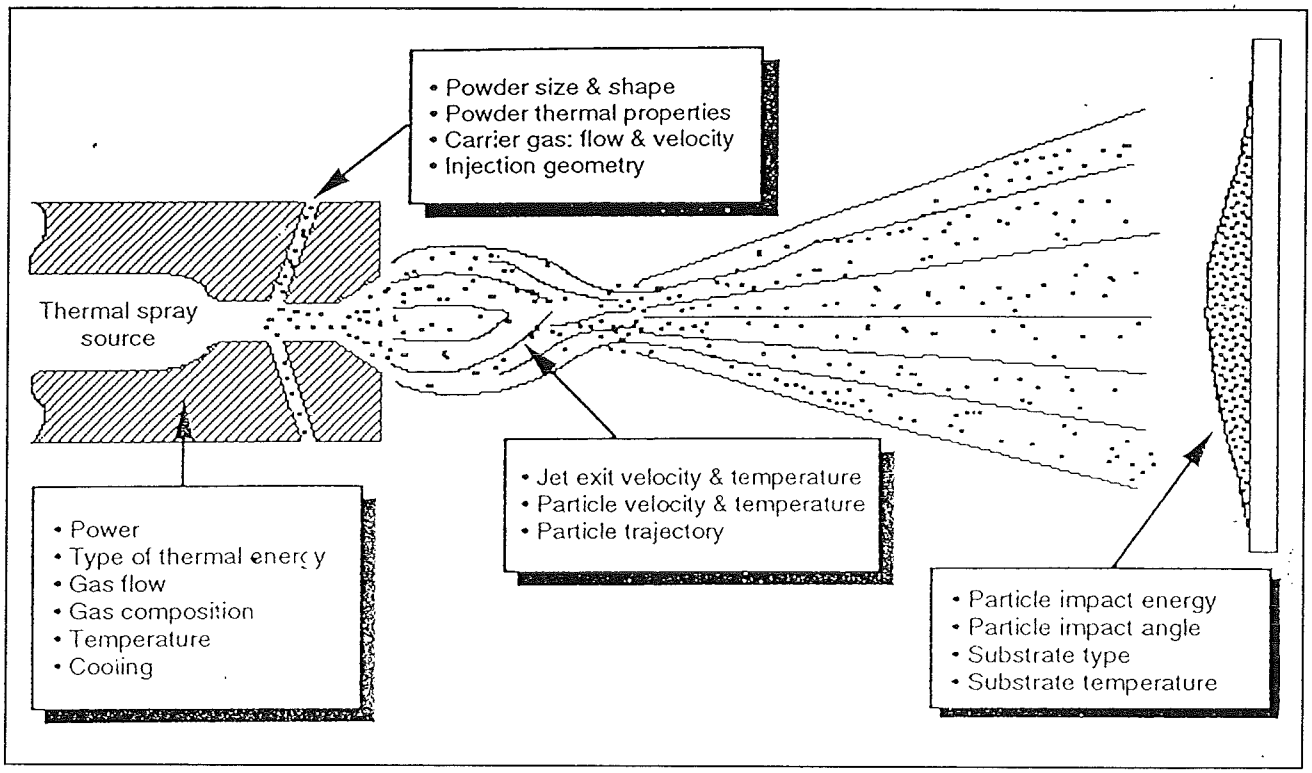

Fig. 4.1. Some of the parameters of Plasma Spraying [2].

4.2. Developments in Coating Optimisation and Process Control

The methods described here have different characteristics and intentions. The methods can be used separately or simultaneously and may complete each other. The increasing demands to coating systems form the basis for the development of coating optimisation- and process control methods. From various industries, different methods are adapted and now being used for coating optimisation. Described in this chapter are: Noncontact Optical Measurements, Simulation and Modelling, Statistical Experiment Planning (SEP) and Ultrasound Scanning.

4.2.1. Noncontact Optical Diagnostic Measurements

A significant emphasis has been placed on areas of computerised process control and unmanned operation with robots. Such developments do not only result in increased process consistency and productivity, but also distance the operator from a hazardous work environment. However, these state-of-the-art automated systems only monitor and regulate the controllable process parameters. There is no in-process monitoring of the actual coating quality or its determinants. Thus problems such as powder nozzle erosion, cable wear or powder variation often result in improper powder feed and hence deficient coating quality.

Coating quality actually depends on the behaviour of the particles in the plasma (velocity, size, melting-degree) and the impact of the particles to the substrate (heat-input and heat fluctuations).
Three noncontact optical measurement methods will be reviewed: High-Speed Pyrometry, Laser Doppler Anemometry (LDA) and Real-Time Video Imaging. It is expected that these methods are able to bridge the gap due to of the failing knowledge of the relations between primary (or indirect, macroscopic) and secondary (or resulting) parameters (Fig 4.2) [22]. More related optical methods

exist, but will not be described in this text. Pyrometry was used for the authors work and will be described more extensively in the next chapter.

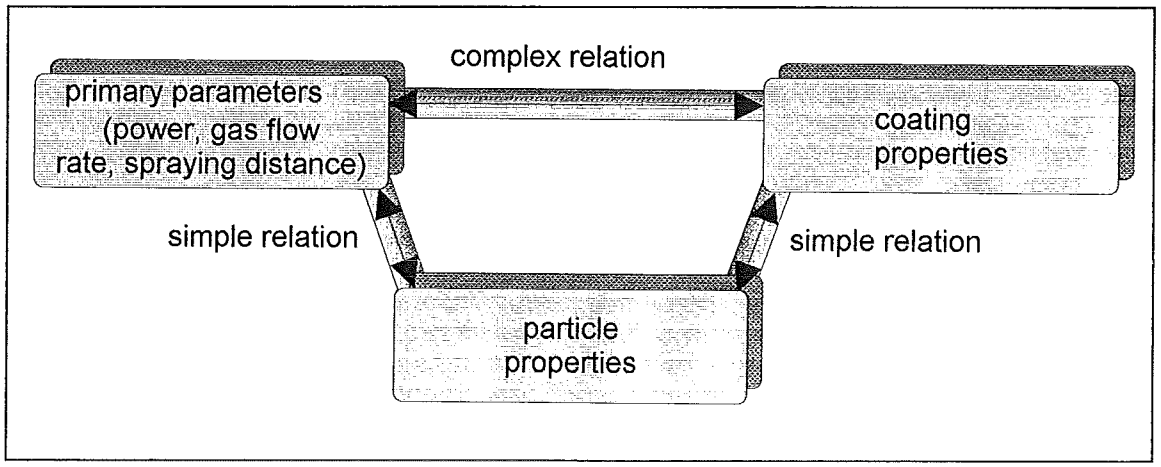

Fig. 4.2. Simple relations between primary parameters and coating properties over particle properties

4.2.1.1. Pyrometry

Use of Pyrometry for noncontact surface temperature measurement, could help in optimizing those parameters, which directly influence coating quality (Fig. 4.2). Use of Pyrometry during Thermal Spraying to monitor the process on-line may lead to process- and quality control.

All materials above the temperature zero-point in all physical states emit electromagnetic radiance energy, as a consequence of its temperature. The amount rises with temperature and above 550 °C the electromagnetic radiation can be seen by the human eye [23]. The wavelength of the emitted electromagnetic or thermal radiation varies from 10^{-3} to 10^{-8} m. The range of the spectrum is schematically given in Fig. 4.3.

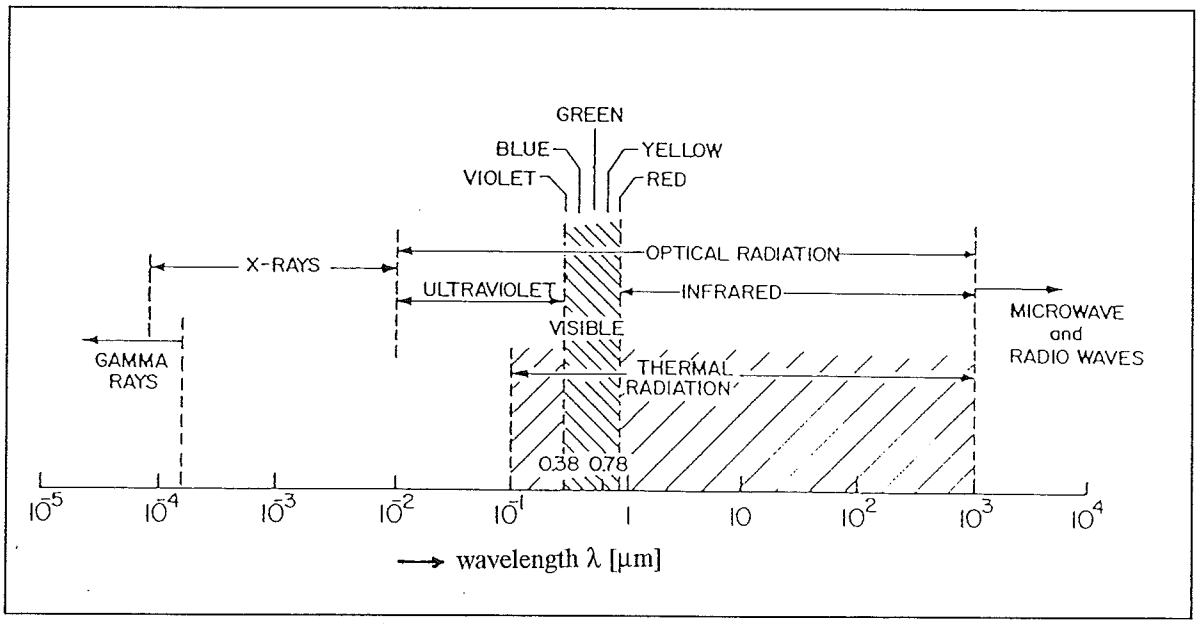

Fig. 4.3. The Electromagnetic Spectrum [88].

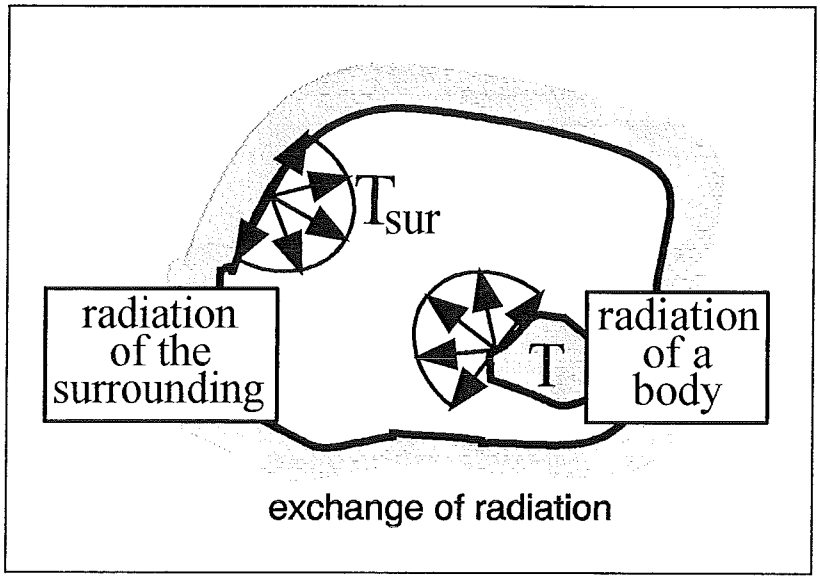

Fig. 4.4. The principle of radiation exchange.

Pyrometry uses the principle of constant radiation exchange between bodies. In a system of Fig. 4.4, the temperature T of the body in the centre will decrease until reaching of the lower temperature T_{sur} of the surrounding. Even if the bodies have the same temperature, radiation is exchanged. In such a system in balance the same amount of radiation is exchanged.

Radiation in the infrared range is caused by vibrations and oscillation of atom masses, which is caused by forces between the atoms. Visible radiation is produced by changes in energy states of the spinning electrons. Solid and liquid materials have continuous spectra with wide wavelength areas of selective emission. Gases radiate at small discrete wavelengths. This distinct behaviour is caused by a different atom structure in the three matter of states.

A relatively recent development in optimizing substrate-coating-systems is the High-Speed Pyrometer (HS-Pyrometer). Characteristic of this type of Pyrometer is a very low sampling rate (the time between two temperature measurements). These Pyrometers use sampling rates of 36 µs to 200 ns. Fig. 4.4 gives a schematic picture of a HS-Pyrometer temperature measurement. The temperature characteristics that can be obtained are given.

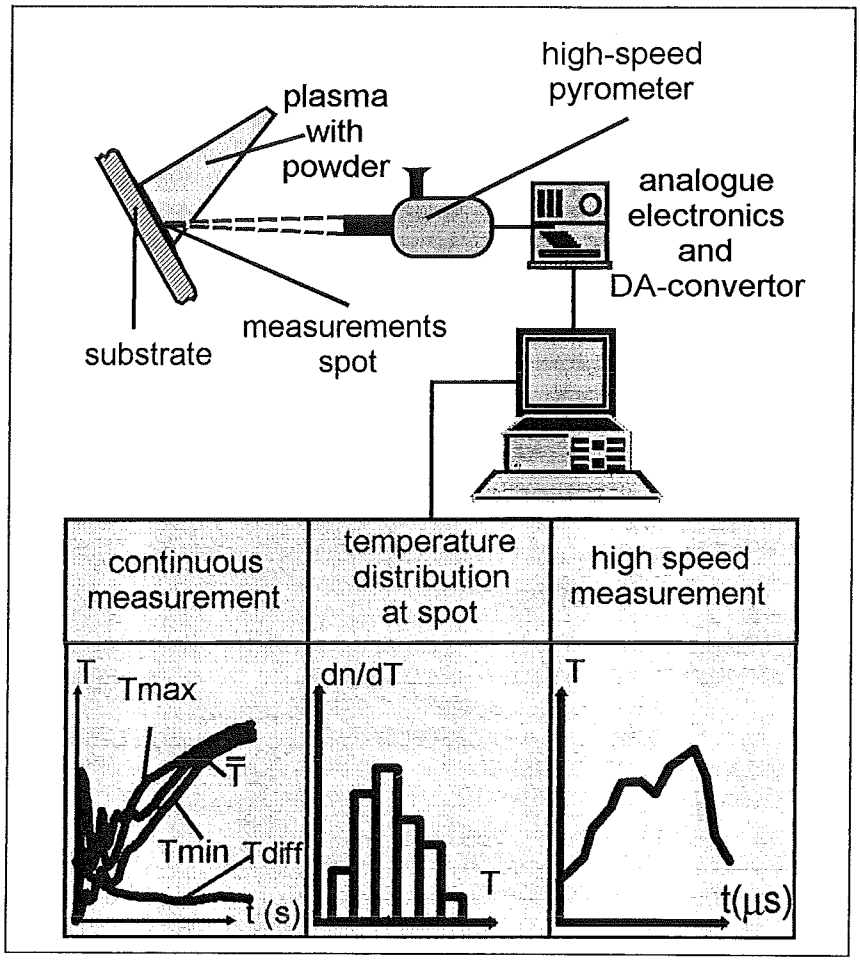

Fig. 4.5. HS-Pyrometric process control system.

The HS-Pyrometer is used in Thermal Spraying for two types of approach. On one hand on-line substrate temperature measurements determine temperature stability's of the process [24-27] and on the other hand, other focus on the fundamental behaviour of the particles and their impact on the substrate. Measured are particle velocities and distribution, mass distribution and melting- and flattening degree [22][28-32].

HS-Pyrometry has been developed to research the fundamental properties of the Plasma Spraying process. Residual stresses depend on the temperatures and gradient build-up during spraying. Thermal shock resistance and lifetime of coatings and coated components is related to these build-up internal stresses. Reduction of the thermal load, caused by the spraying process, on the substrate materials is state-of-the-art. Unfortunately this method is arbitrary and not reproducible and should be controlled to keep the temperature gradient in a defined range. To set up an effective temperature control, measurements of the coating surface temperatures at each location within the spraying spot is required.

HS-Pyrometry may lead to on-line process control (monitoring) and in the future coating qualities could be 'predicted' without destructive testing. Unsteady temperatures during Thermal Spraying may be detected and show wear of the nozzle or a changing powder rate.

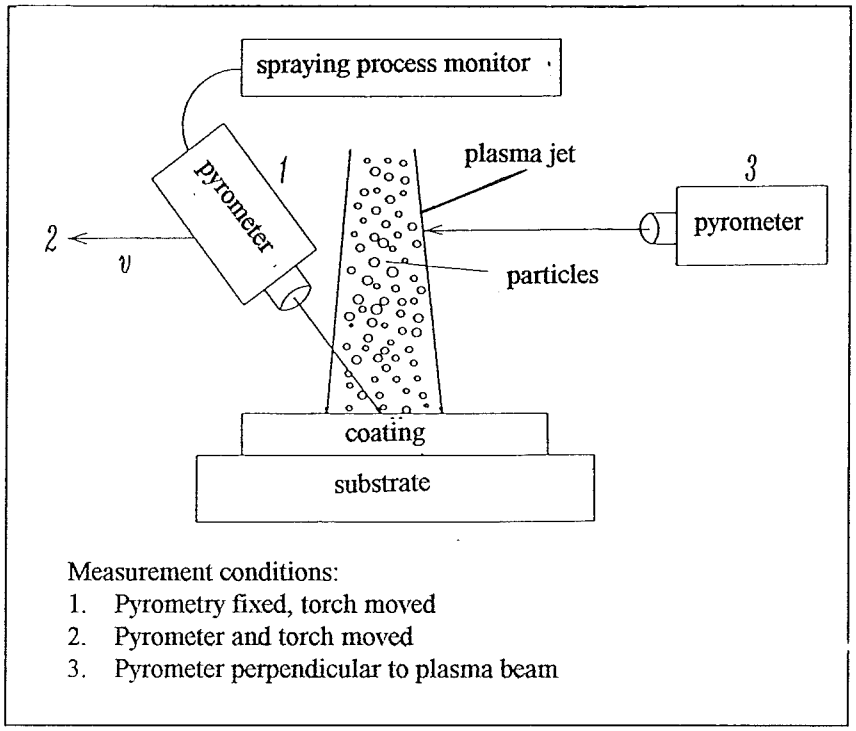

Fig. 4.6. Measurements set-up for pyrometric measurements [24].

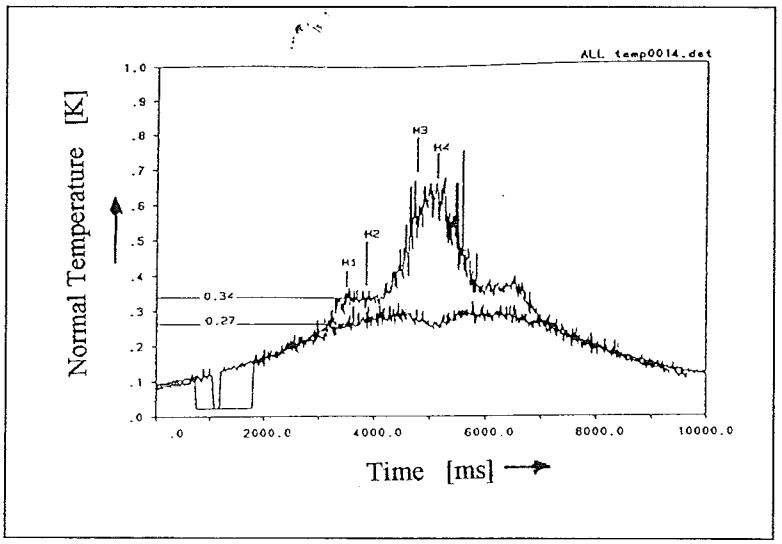

Fig. 4.7. Comparison of temperatures at 700 g/h ZrO_2 and without powder [24].

Sölter carried out experiments with a Pyrometer in three different positions [24]. Fig. 4.6 shows the set-up. The temperature image around a Plasma Spraying spot is shown in Fig. 4.7. Variation of the powder rate was detected very well. Furthermore at different powder rates temperature profiles were recorded (Fig. 4.8).

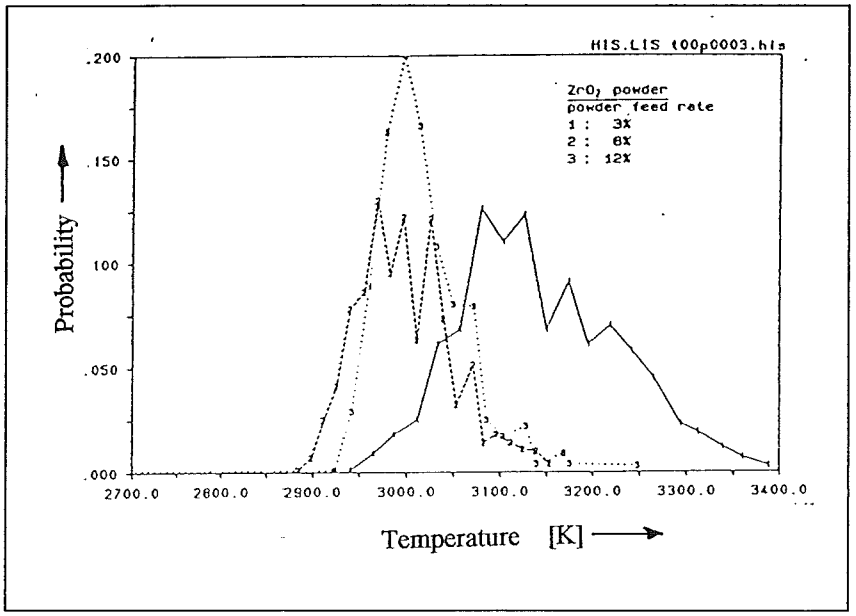

Fig. 4.8. Temperature distribution at different powder feed rates [24].

Moreau et al. use a fast optical Pyrometer to measure the flattening time of single particles [25]. They use a second fibre optic sensor (at the top of Fig 4.8) and these are both pointed at the same spot of the surface. In this way they insure that the detected signal come from particles impacting at the measurements spot and not from particles passing through and not impacting at the measurement spot. Apparent flattening time and the cooling time of the impinging droplets on glass substrates were found to depend on the substrate material (surface tension) and to decrease with surface thickness. The decrease of the apparent flattening time with the coating thickness was likely due to the higher cooling rate of the molten droplets impinging on already-deposited molybdenum lamellae.

Fauchais et al. discuss the behaviour of single particles and the influence of the impact velocity, flattening time and flattening degree (which is defined as the ratio of the diameter of the resulting splat to the diameter of the impacting droplet) of these single particles [29]. It was investigated for a cold steel substrate using two fast two colour Pyrometers (Fig. 4.10). One Pyrometer is focused 2 mm before the substrate and the other on the substrate surface. The influence of the velocity of the impinging particles (determined from the time of flight between the two focusing points of the Pyrometers) on the deformation and cooling processes were investigated. Fig. 4.11 gives the method of evaluation.

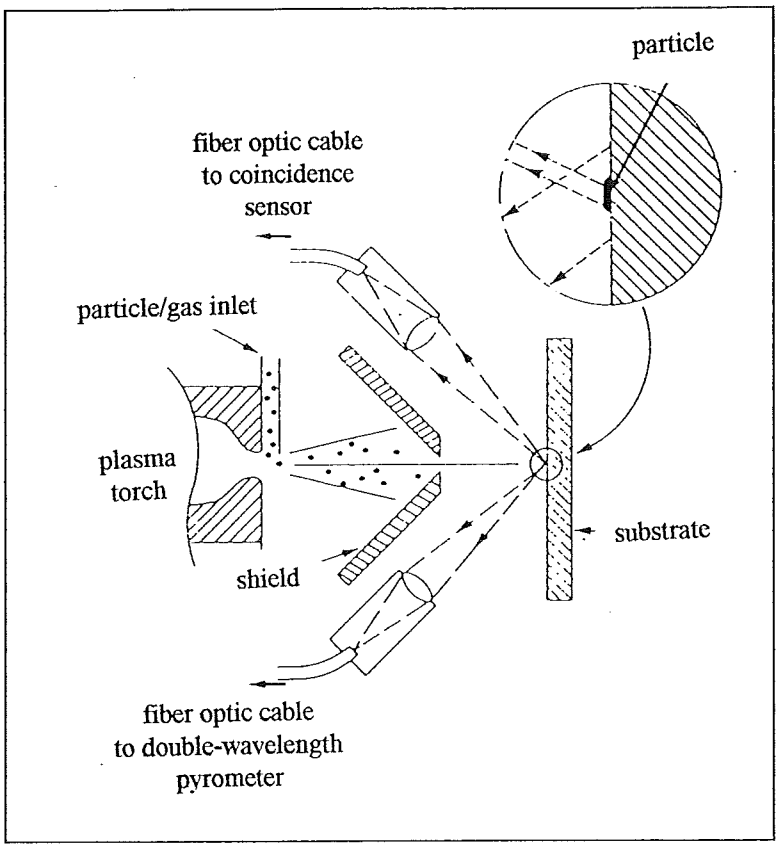

Fig. 4.9. Set-up of Moreau [25].

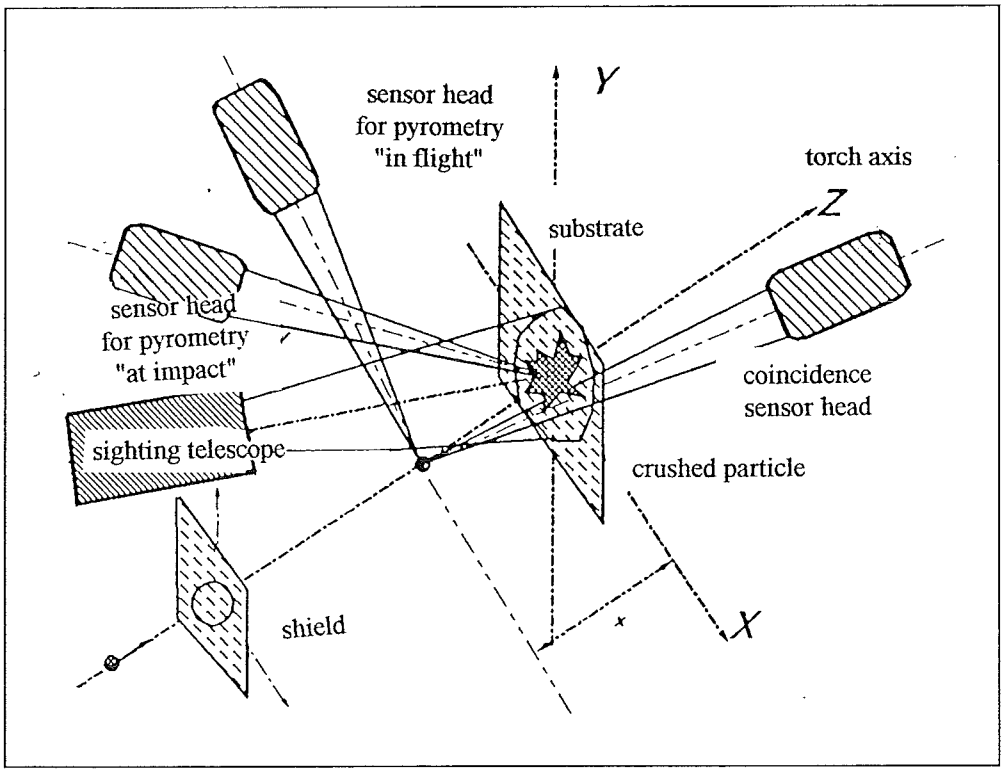

Fig. 4.10. Experimental set-up of Fauchais [29].

The particulate flattening and cooling depends strongly on particulate mass, velocity and temperature upon impact but also as underlined very recently on the substrate or previously deposited layer surface temperature [32]. Coatings are formed from successive stacking of thin lamellae (flattened particles) and their properties depend strongly on the lamellae microstructure, which depends on the cooling rate and on the type of bond between the lamellae and substrate and between the lamellae themselves.

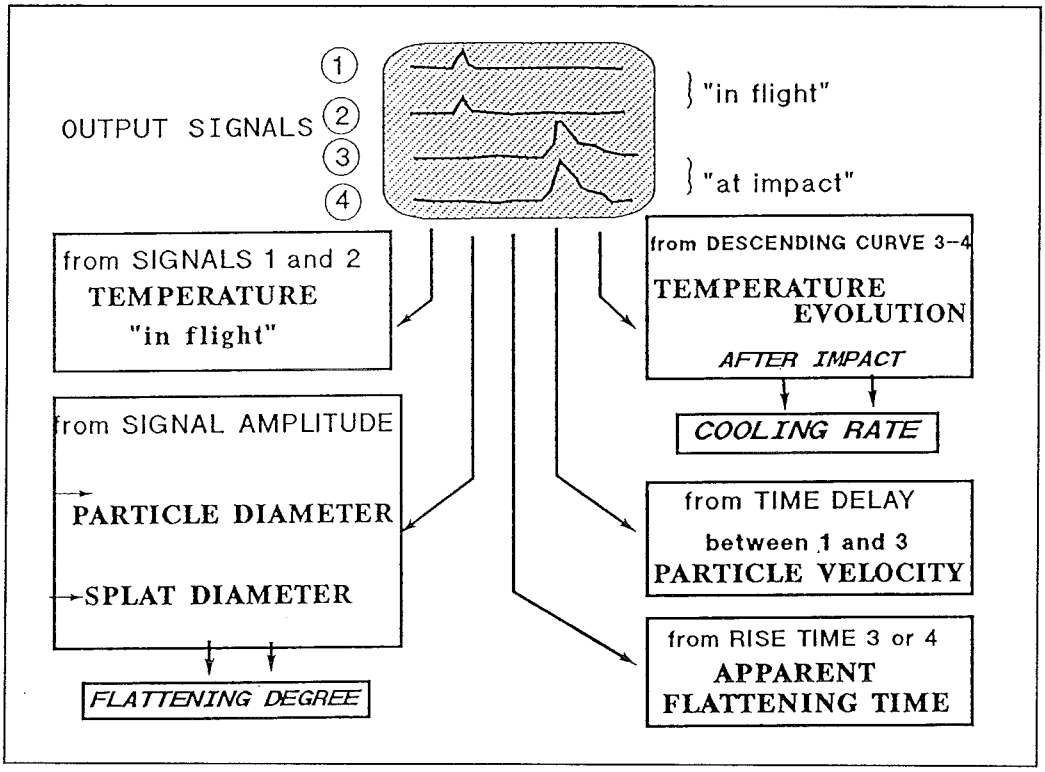

Fig. 4.11. Evaluation principle of Fauchais [29].

4.2.1.2. Laser Doppler Anemometry

Laser Doppler Anemometry (LDA) originally was developed for fluid mechanics. A total review was given by Durst et al. [33] and Wiedemann [34]. In the literature Laser Doppler Anemometry (LDA) is also referred to as Laser Doppler Velocimetry (LDV) and the latter illustrates the main property measured.

The Doppler effect, named after Christian Doppler (1803-1852), is the frequency shift an observer sees (or hears), looking (or hearing) at a moving object. The observer sees another colour or hears another tone, than the frequency of the electromagnetic radiation that originally was emitted by the moving object. This phenomenon is seen across the whole electromagnetic spectrum.
LDA uses the simple mathematic base between the Doppler frequency and the velocity of particles, which makes calibration unnecessary. After the basics are treated it will be linked to noncontact measurements in Plasma Spraying.

The Doppler frequency can be measured with the so called 'reference beam' method (Fig 4.12). A reference laser beam is split into an intense scattering beam and a weak reference beam. The reference beam is directed to a photo cathode, where it beats with the scattered strong laser beam. The frequency of the scattered light has been altered by the Doppler effect and the interference pattern of the reference beam provides the frequency difference that is directly proportional to the particle velocity.

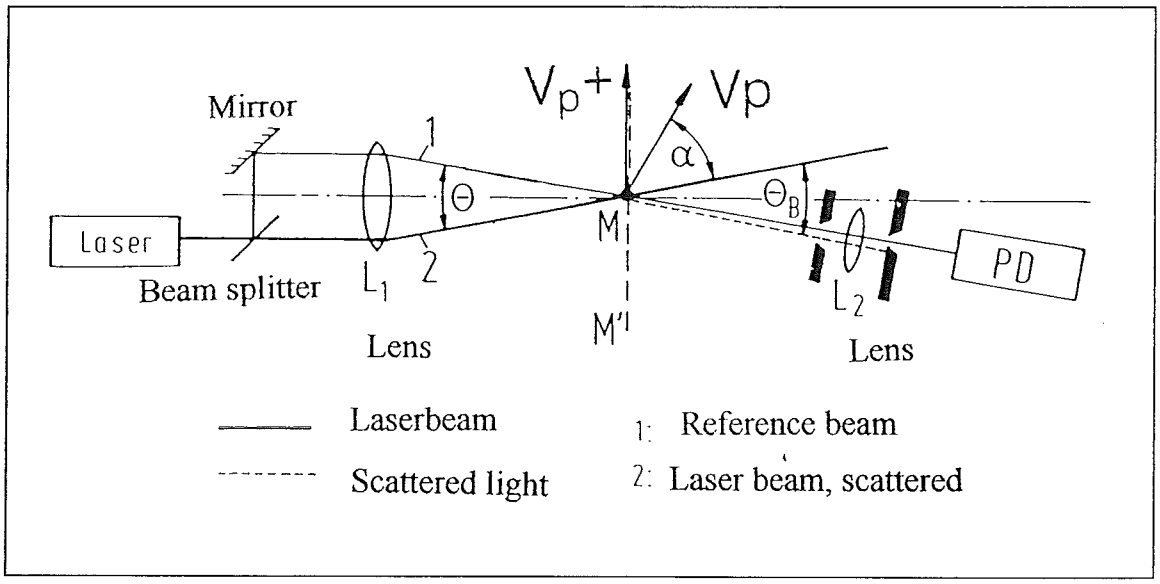

Fig. 4.12. LDA Reference beam method [34].

Another method is the 'dual beam' or 'fringe system' (Fig. 4.13). Two coherent intersecting light beams of equal intensity produce an interference pattern in the intersection volume (Fig. 4.14). As a particle crosses the fringes, the intensity of light scattered onto the photo detector rises and falls at a rate directly proportionally to the velocity.

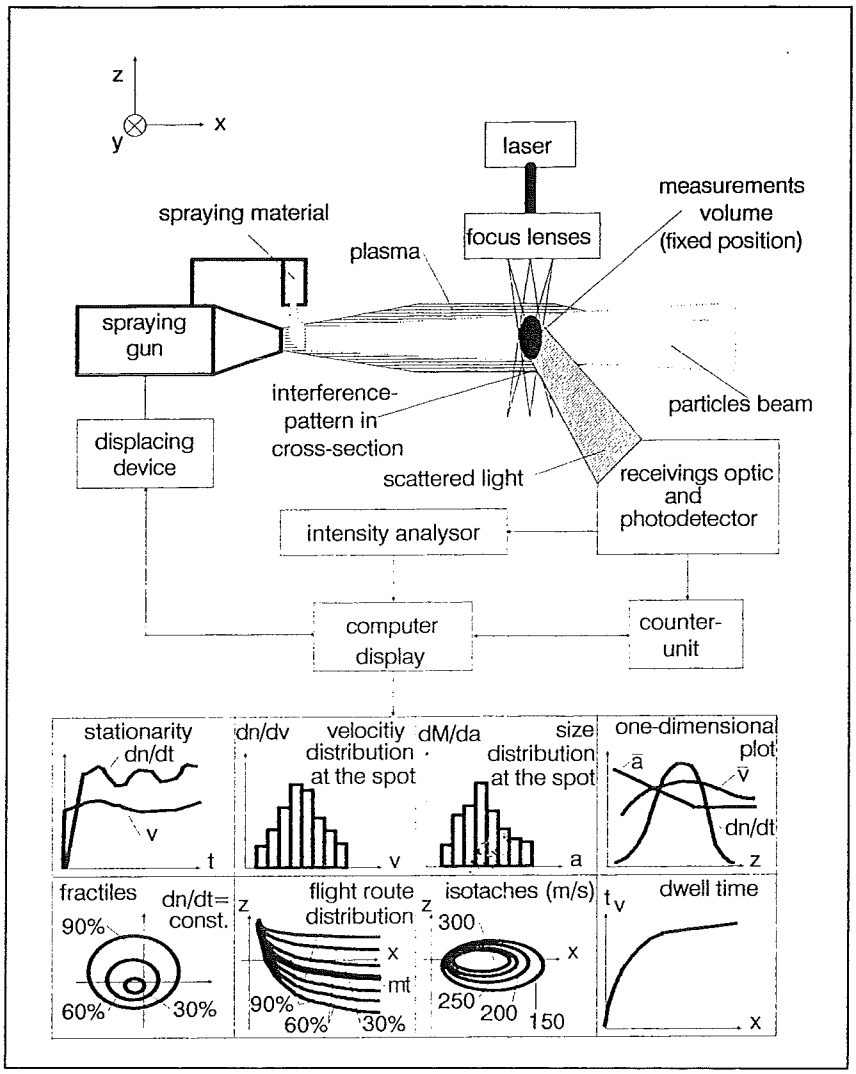

Fig. 4.15. LDA-Measurements set-up.

In Plasma Spraying LDA could be very useful and trends show more and more systematically use of LDA for optimisation and process control. A very useful review in respect to Thermal Spraying was given by Gouesbet [35]. Advantages are its non intrusive nature and because the linear response no calibration is necessary. The medium under study must be transparent to guarantee optical access.
Although the principle is extremely simple, correct LDA measurements usually require a lot of expertise, especially in a plasma environment, with high temperatures giving rise to noise due to plasma and seeding particle radiation.

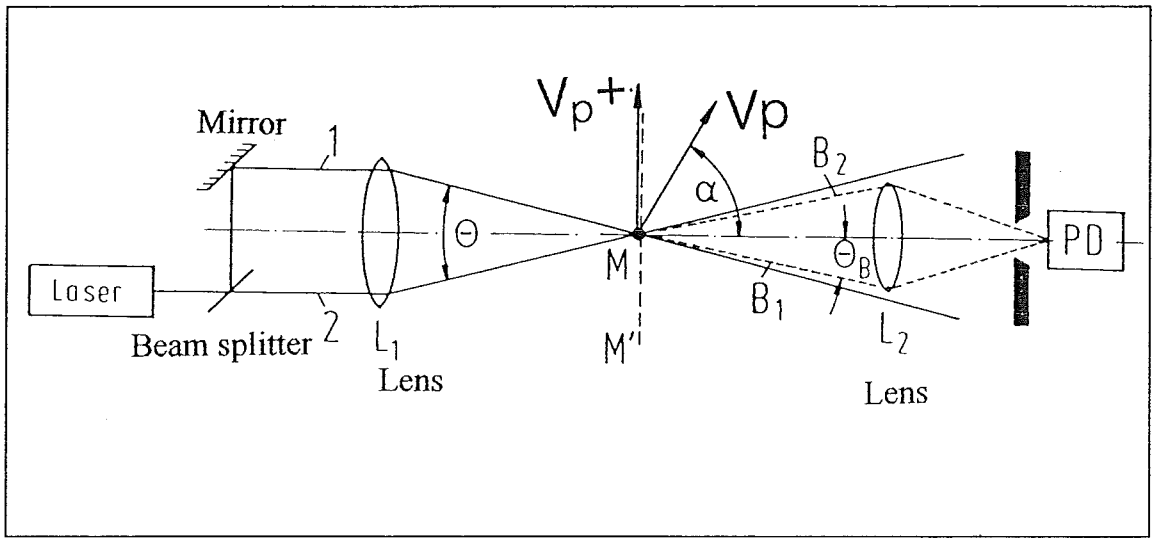

Fig. 4.13. Dual beam schematic set-up [34].

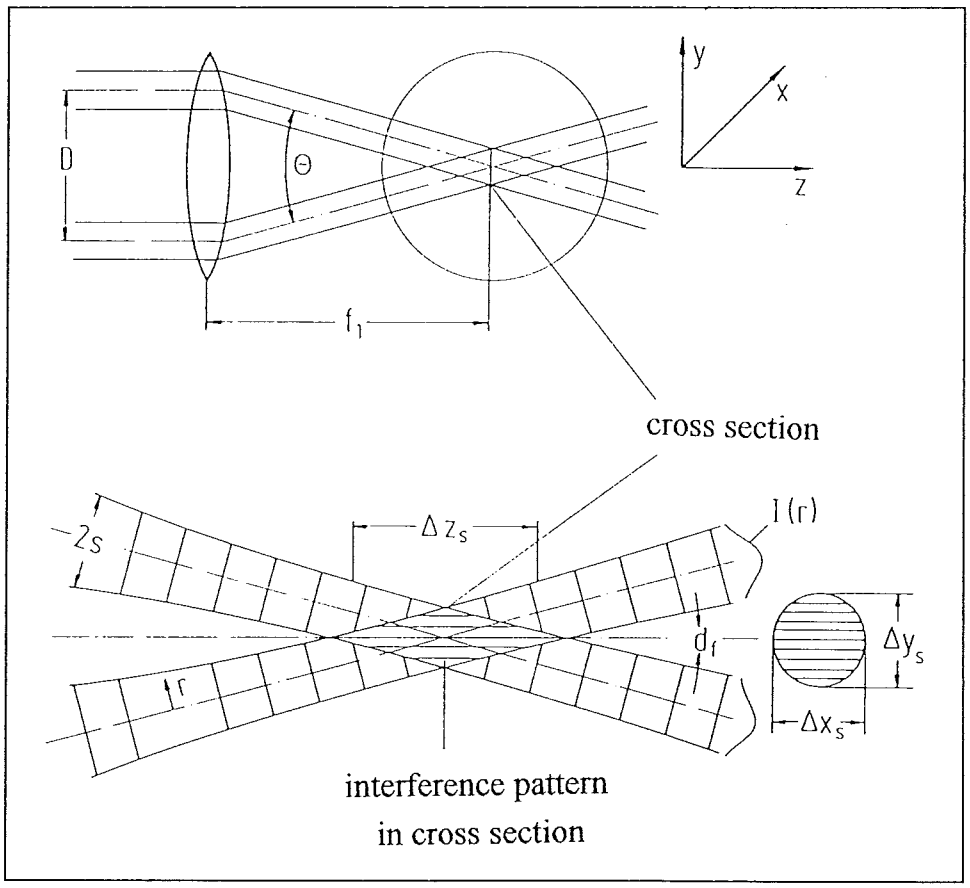

Fig. 4.14. Dual beam set-up and interference pattern [34].

Landes et al. [22] give a review of properties, being measured in Plasma Spraying, with LDA to optimise functional coating systems. Parameters as stationarity dn/dt (number of particles that reach the substrate in a specific time interval), velocity distribution dn/dv, powder mass distribution and time of flight (Fig. 4.14) are being measured and link primary with resulting parameter.

Vardelle et al. present the developments in modelling and measurement methods. Parameters that control coating quality are described [28]. Pyrometry and LDA were described for measuring surface temperatures and particle velocities and -distributions.

Flögel developed a method for on-line simultaneous measurement of particle velocity and particle size [36]. Two-dimensional particle distributions were on-line recorded and correlated to movements-models for particles in flows. The LDA system was used for experiments on a water-jet launched from a nozzle.

4.2.1.3. Real-Time Video Imaging

The problems of optimisation and on-line process monitoring have extensively been discussed and Agapakis and Hoffman describe a filming method of the spraying. By this real-time filming important properties can be determined: particle velocities, mass flow, particle pattern and vector information. These values are crucial to process development and control [37][38]. An electrical-optical viewing Stroboscopic Video camera, capable of overcoming the extreme variation in scene brightness of high-luminosity sources was developed. This system incorporates external illumination in the form of intense pulsed laser light.
Coating methods, which have been investigated were Plasma Spraying, Arc Spraying and High Velocity Oxyfuel Spraying. Process parameters that were successfully measured were particle flow patterns, plasma or flame geometry, particle velocity from comparing two recordings and particle temperature from the luminosity.

In Hoffmans latest research the measurements were extended on VPS. Through the small viewing port the spraying was filmed [39]. Difficulties have been overcome and it was made possible to see directly into the nozzle. Since VPS is used for some of the most critical Thermal Spray applications in the jet and aerospace industries, it appears that good visual access to the process can be especially beneficial.

4.2.2. Simulation and Modelling

Fundamental studies to the Plasma Spraying process have been the start of Simulation and Modelling of the process [39-42]. Simulation could be very helpful in calculating the best adjustments of the primary parameters such as gas flow and spraying distance at minimal costs by limiting the number of expensive experiments.

In a field-free plasma jet the temperature decays rapidly with increasing distance from the nozzle orifice, especially when strong turbulent mixing enhances the energy exchange between the plasma jet and the surrounding atmosphere. The powder carrier gas velocity is adjusted according to ensure particle penetration into the hot core of the plasma jet to ensure effective heat and momentum transfer to the particles. The particles entering the plasma are accelerated and heated. At a certain distance from the anode nozzle, the plasma velocity and beyond this point, the particle velocity will decrease, by the resistance of the atmosphere (Fig. 4.16-17). Ideally, the particles should arrive at the substrate at high velocities in a completely molten state (but not overheated) to form a dense coating with a low porosity level.

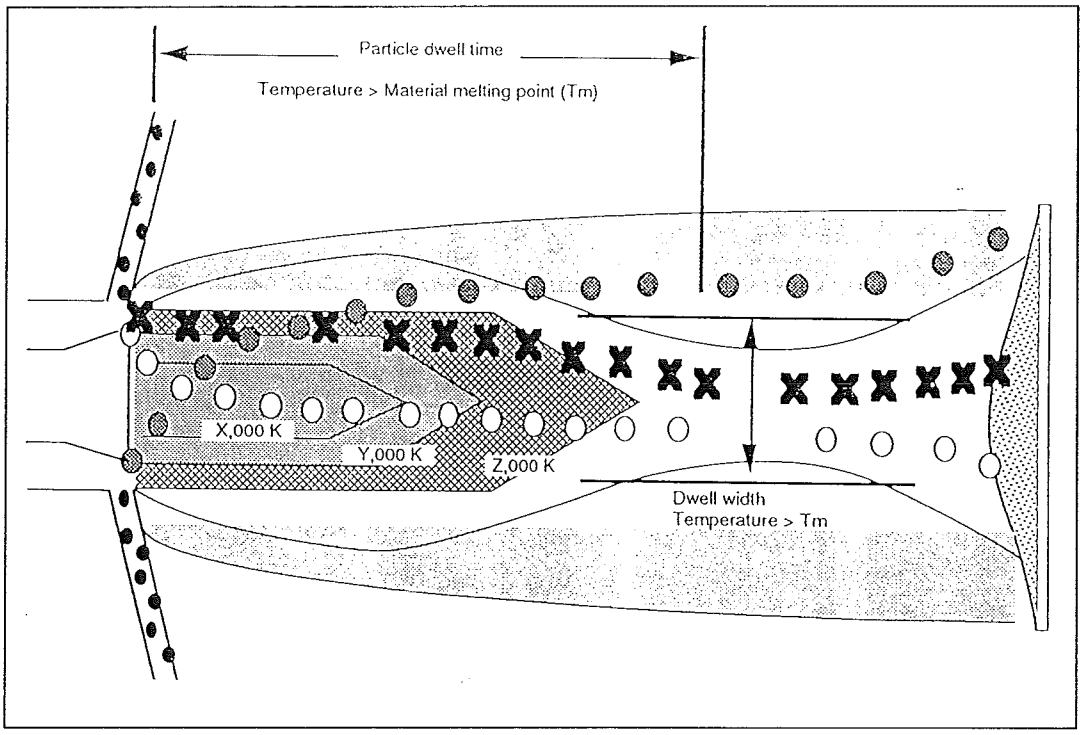

Fig. 4.16. The balance between melting degree and velocity [4].

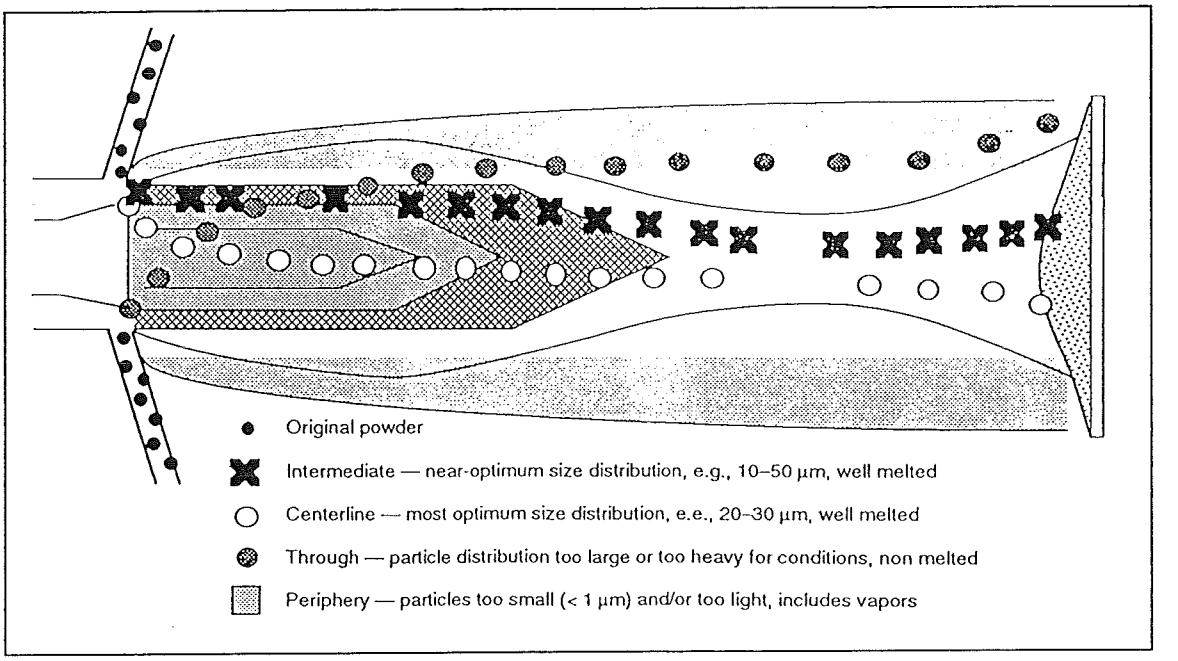

Fig. 4.17. Particle distribution in the plasma [4].

The particle dynamics and heat transfer may be affected by viscous drag, turbulence flow, particle shape, evaporation, non-steady heating and radiation, convective heat transfer, electric charging of particles [40].

With expensive in-situ noncontact diagnostic systems, like HS-Pyrometer and LDA, velocities and temperatures could be measured. These systems however are expensive and many experiments remain necessary. In the best possible situation Simulation and Modelling can predict optimum adjustment of primary parameters in relation to o achieve optimal speed and a totally molten state of the particles.
Once such a model has been developed and eventually be controlled with noncontact optical measurements and destructive testing it can 'easily' be translated to other materials and geometry's.

Knowledge of many physical constants is required; heat conduction coefficients in substrate, coating and boundary area, melting points, melting degree, melting enthalpy, heat capacity, gas flow character (lamellar, turbulent), etc. Lack of these dates makes exact calculations very difficult.

Optimisation in Thermal Spraying has been carried out for:

- surface preparation by grit blasting (this will not be discussed here);
- temperature distributions in the coating system [39-49];
- HVOF spraying process [50-53];

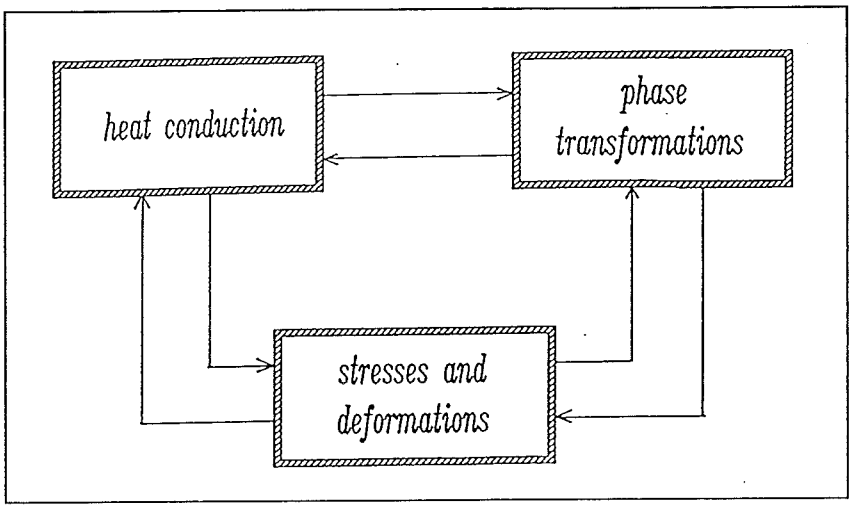

Fig. 4.18. Three factors which determine internal stresses [45].

Borgerding et al. point out the importance of controlling the internal coating stresses, which are generated by the high temperature gradients during the heating and cooling phases. Fig. 4.18 give the three most important factors of internal stresses. An effective control of the coating process requires understanding of the mechanisms responsible for the stresses build-up. The stresses occur as a result of:

- The mismatch of the modulus of elasticity and thermal expansion coefficient between topcoat, bondcoat and substrate;
- The occurrence of micro defects within the coating;
- Temperature gradients in the coating during the spraying process;
- Thermal shock during operation time.

All these factors produce superimposing effects in a rather complex manner with a corresponding impact on the coating properties. A model should define optimized parameters, e.g. thickness, thermal properties and expansion coefficient and spraying conditions for each layer in order to minimise residual stresses. The process can be divided in three sub processes, heat conduction, phase transformation and build-up of stresses and deformation and are interconnected. With a finite element analysis (FE), a ZrO_2 (8 % stabilised Y_2O_3) TBC-coating on a CoNiCrAlY bondcoat has been evaluated using this approach. The results were compared to published results out practice and application of a numerical simulation programme could be used to reduce development time for coatings and coating systems.

HVOF spraying processes are considered to be simpler than Plasma Spraying. Knotek successfully developed a computer model that uses thermodynamic laws to describe heat transfer processes, e.g. from combustion gases to particles as well as the general laws of compressible fluid flow to show the influence of the nozzle geometry and the gas mass flow rates on particle velocities and particle temperatures [53]. After a mathematical model is developed difficulties may arise in finding reliable data. In the case of HVOF Thermal Spraying the temperature dependent thermophysical properties of the materials involved are difficult to find.

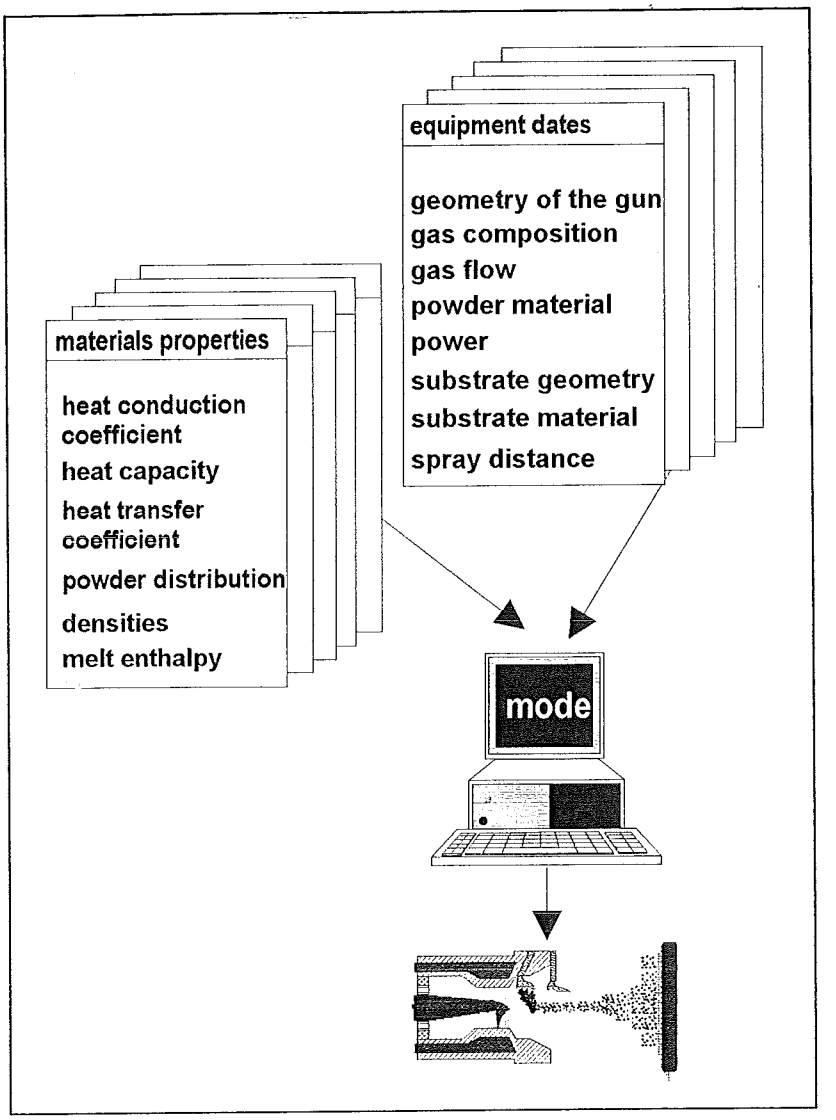

Fig. 4.19. Materials dates necessarily for process Modelling [55].

Numerical Simulation offers following advantages according to Knotek and Schnaut offer following advantages [54]:

- The iterative simulation approach leads to an improvement of the necessary scientific understanding of processes. Therefore optimisation with less prototypes;
- A better understanding of the process provides the basis for extrapolation and may suggest regions, where further experiments might be fruitful;
- Once a simulation model is verified, the time necessary between the idea and the final optimised production is shorter, due to "numerical modelling" and therefore the effort of developing the model pays off.

The advantages in comparison to statistical methods of experimental design and in-situ diagnostically methods are availability and costs.

Knepper describes the Modelling of the Plasma Spraying process. For this purpose the process is divided in three steps [55]:

- the plasma gun;
- flight phase;
- impact on the substrate.

The most important process parameters must be combined in a mathematical model. The problem here is to find the data and properties for exact calculations (Fig. 4.19)[64].

4.2.3. Statistical Experiment Planning

Statistical Mathematics is used in all fields of research to calculate mean-values, standard-deviation, etc. These results, in case of coating processing, are used to determine stability of the coating process and to 'predict' coating quality and reliability.
The goal here is to give an introduction to Statistical Experiment Planning (SEP) or Statistical Design of Experiments (SDE), which is used to limit the number of necessary experiments and to determine the relations and optimum adjustment parameters.

In the early 1920s Fisher introduces statistics in the agricultural sector for optimizing sowing and harvesting [56]. In the 1950s for chemical-industrial environment Response Surface Methods (RSM) were developed [57]. The Japanese engineer Taguchi based his theory on these early statistics and gave an enormous lift to the using of SEP for process optimisation in modern industries [58]. Another now established engineer Shainin developed SEP for optimisation of production. These four methods will be reviewed.

- Classical SEP, which can be divided into two categories:

Screening experiments are used to determine, from a set of parameters, with few experiments, the important quality influencing parameters. N-parameters are researched at two levels (+Δ and -Δ around a central chosen value). Because of symmetry and systematic its mathematically proved that only half of the 2^n experiments are necessary. The parameter should be independently from each other.
Regression experiments are used to determine relations (linear, quadratic, etc.) between adjustments- and resulting product-parameters. Only few parameters can be researched, because more experiments are necessary, than by the screening experiments.

- Responce Surface Methods (RSM):

RSM is based on sequential experimentation (optimisation through several phases). The goal is to locate the optimum and to explore its immediate surroundings, thereby gaining better understanding of the system. In the initial phase, the objective is to screen many factors to determine, which are most important. Once key factors are identified, additional experimental tests are planned to bring the process under the optimized conditions.

- Taguchi:

Taguchi based SEP is a robust product design philosophy and uses experimental design to develop products and processes, that are insensitive to variation in components and environmental factors. A disadvantage of Taguchi's methods is that its based on executing one large comprehensive experiment [59]. The way to go is independently changing of the adjustments parameters (inner array) and the disturbing parameters (outer array). Signal-to-noise-ratio (standard deviation through mean value) is used to determine the optimized parameter adjustment. Nedeß and Holst give a good summary of the difficult orthogonal tables Taguchi refers to [60].

- Shainin:

This SEP gives hand in optimizing in the production phase instead in the research phase. Optimizing well-defined processes make basic changes impossible and changes in running production difficult and with risk. Disturbing parameter should be recognised and solved. Shainin offers different methods to filter dominating disturbing parameter from all thinkable parameters.

More detailed information is given in references [61][62]. The following gives examples of SEP Plasma Spraying optimisation.

A two level statistical analyses have been applied for the optimisation of Atmospheric Plasma Sprayed Al_2O_3/TiO_2 (87/13) coatings [61]. The coatings were surface treated by a laser and the spraying parameters were statistically optimized in regard to coating-thickness and porosity. With two level statistics the significant spraying parameter were determined: current, powder feeding rate and gun traverse speed. With regression the adjustment of these was successfully determined.

Knepper uses 2 level statistics to optimise the porosity of a vacuum plasma sprayed titanium-coating [64]. The same procedure was followed; after determination of the significant parameters, with factorial analyses the porosity could well-aimed be optimized.

Steeper et al. used for the fabrication alumina-titania coated heater tubes that emulate nuclear fuel tubes Taguchi based SEP [65][66]. A Taguchi-style fractional, -factorial design of experiment was employed to evaluate the effect of seven plasma process variables on the coating quality. Concluded was that the spray distance was the most significant contributor to lowering porosity; coating thickness is dominated by powder feed rate and micro hardness was most influenced by traverse rate. Selection of the optimum levels of the design factors gave an optimized coating for this specific application.

4.2.4. Non Destructive Testing

Over the last years coatings have been optimized by a destructive testing and evaluating of the properties. Conventional destructive testing of coated components involves the testing of coupons at the same time as the actual components in a batch. In addition to the test coupons, typically a certain number of components are also evaluated destructively. Failure of a test coupon or a part to meet the specifications may cause rejection of a large number of sprayed parts, even though the failure may be an isolated incident. Worst yet, a single defect or group of defects within a batch may escape detection. Hopes are focused that coating quality can be controlled or monitored by on-line contact measurements methods, but this is very difficult to realise and for this reason non destructive testing could close the gap. Furthermore can it be a valuable non destructive testing or controlling method during the use-phase of products.

Flaws with the most deleterious effects on the lifetime of ceramic components are typically cracks, porosity and inclusions. Stresses are generally higher at surfaces than in the interiors of bodies and for this reason are surface flaws frequently found to be the main cause of failure. For example, high reliability of structural ceramic components requires detection of effects smaller than 100 µm in size [67].

To discover surface faults holographic techniques are applied [66-68]. With a laser an undisturbed recording (hologram) is made from the sample. After the sample is disturbed; by a temperature change , a vibration (sonic or ultrasonic) or by mechanical loading, the surface is rasted again. Faults at the surface, cause irregular expansion of the part and different scattering of the laser beam. Combination of the two recordings gives an interference pattern and irregularities in the surface are being discovered. Sciammarella et al. were able to detect flaws of 200 µm long and 100 µm depth. The process can be done real-time, by amplifying the disturbance.

It has been declared that with Infrared Thermography subsurface defects can be traced [70][71]. Good bonding is essential and with IR-Thermography has successfully been used to locate regions of coating/substrate separation. A controlled heat pulse is applied to one surface of the sample and an infrared (IR) camera is used to monitor the surface radiance as the part cools. The presence of sub-surface flaws such as voided regions reduce local heat flow from the heated surface to the cooler interior. The result is detection of a hot spot by the IR camera. Defects of 200 µm at a depth of 300 µm were detected [70].

The last non destructive examination (NDE) method to be described is Thermal Wave Testing [72][73]. Here also a heat-pulse is introduced in the material and the thermal waves are reflected at boundaries with materials of different thermal properties, much as an optical wave would be reflected from a medium of refractive index, causing interference and phase shift. Flaws were detected with sizes of 0.02 µm [72].

In DVS 2303 some non destructive methods to measure coating thickness are described [74]:

- bonding strength test: reduction of attachment of a permanent magnet as a value of coating thickness;
- magnetic-inductive test: change of magnetic flow by the coating;
- induction current test: change of induction current by coating;
- capacity change test: capacity change is controlled by coating thickness;
- thermo-electric test: change of thermo-voltage by the coating;
- ultrasound-impulse-echo-test: time elapsed between two echo's is measured.

5. Radiation Thermometry - Pyrometry

The primary objective of this chapter, is to present a basic concept, which relates electromagnetic radiation to use in noncontact temperature measurements. Paragraph 5.1 describes the basic laws of thermal radiation. There exist different pyrometrc basis methods and 5.2 described these. The complex calibration for measuring temperatures of non black bodies is treated in 5.3 and this chapter will be concluded by a description of the problems of the emissivity in 5.4.

5.1. Principles of Thermal Radiation

This paragraph gives the reader information about the formulae and mathematics of electromagnetic radiation and will bring more understanding to the radiation of bodies.

Paragraph 4.2.1.1 described the principle of Pyrometry (radiation exchange between bodies of different temperature). The thermal radiation range of the total electromagnetic radiation spectrum is of interest for Pyrometry (Fig. 4.4.). Especially the infrared (IR) area is interesting for Pyrometry, because 80 % of the emitted radiation is infrared [75-78]. Furthermore absorb most materials infrared radiation better. The main part of sunlight also is infrared, because the atmosphere absorbs less than visible radiation. Table 5.1 gives the ranges of the thermal radiation area.

Table 5.1. General overview of the wavelength ranges.

Name of radiation	Area	Wavelength λ [nm]	Frequency λ [10^3 Hz]
ultra violet	vacuum UV	100-200	3000-1500
	wide UV	200-280	1500-1070
	middle UV	280-315	1070-950
	close UV	315-380	950-790
visible	visible	380-780	790-385
infrared	close IR	780-3000	385-100
	middle IR	3000-50.000	100-6
	wide IR	50.000-10^6	6-0,3

Table 5.2 gives the definitions of the values to express radiation intensities and energies. These are necessary to give a mathematical description of the radiation processes. Most book that describe radiation exchange give these definitions [80][81].

Table 5.2. Radiation definitions.

quantity	description	abbreviation	dimension
radiation energy	transferred energy	Q	J
radiation flow or radiation power	transferred energy per unity time	$\Phi=dQ/dt$	$W=Js^{-1}$
radiation intensity	radiation flow per volume angle Ω	$I=d\Phi/d\Omega$	Wsr^{-1}
specific radiation	dA is a radiating surface element	$M=d\Phi/dA$	Wm^{-2}
radiation density	Angle ϑ is formed by the surface normal and the radiation direction	$L=d^2\Phi/(dA\cos\vartheta d\Omega)$	$Wm^{-2}sr^{-1}$
spectral radiation density		$L_\lambda=dL/d\lambda=$ $d^3\Phi/(dA\cos\vartheta d\Omega\, d\lambda)$	$Wm^{-3}sr^{-1}$

Pyrometric noncontact temperature measurement methods have been known for at least 60 years and are based on Planck's radiation formula (1900) for a black body or ideal radiator [23][78-81]:

$$L_{\lambda_B}=\frac{dL_B}{d\lambda}=\frac{C_1}{\pi\lambda^5[\exp(\frac{C_2}{\lambda T})-1]}, \qquad (1)$$

where $L_{\lambda B}$ the spectral radiation density for a black body in $[W\cdot m^{-3}]$, λ the wavelength [m], T the absolute temperature [K], $C_1=2\pi\cdot c_0{}^2h$ $[W\cdot m^2]$, $C_2=c_0\cdot h/k$ $[m\cdot K]$, c_0 the velocity of light in vacuum [m/s] and h Planck's constant [J•s] is. Fig. 5.1 gives the spectral radiation density as function of wavelength for some temperatures.

The radiation density of a body depends on its temperature and its surface condition [81]. A black body absorbs all incoming thermal radiation and a real- or non black body partly reflects and transmits radiation. A black body absorbs all radiation and reflects no radiation. Not all incoming radiation energy is absorbed because of reflection and transmission and thus rises the temperature less than a black body would. The absorbed visible wavelength's determine the colour of the surface.

The balance between absorbed, emitted and reflected radiation gives [23]:

$$\varepsilon_\lambda=\alpha_\lambda=1-\rho_\lambda-\tau_\lambda, \qquad (2)$$

where ε_λ the emissivity (described later), α_λ the absorption grade, ρ_λ the reflections' grade and τ_λ the transitivity is.

A surface does not absorb equally over all wavelengths: a black body can absorb visible radiation, but reflect IR radiation. The body is not black for IR radiation. Fig. 5.2. shows the simulation of a black body for all wavelengths. All reflected radiation stays in the hollow body and becomes absorbed finally.

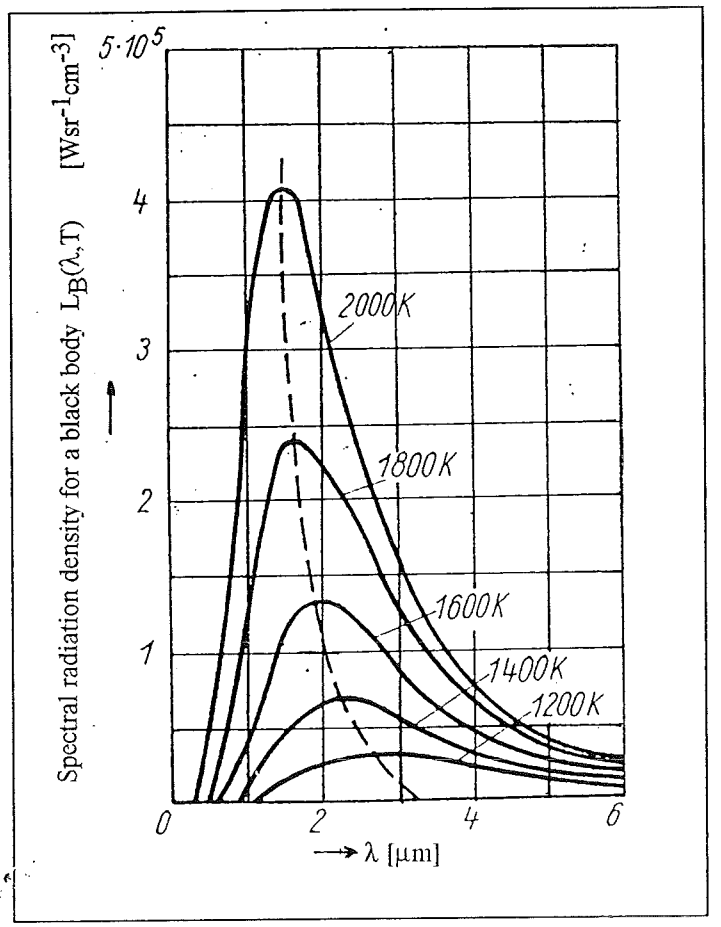

Fig. 5.1. Spectral radiation density as function of λ and T [23].

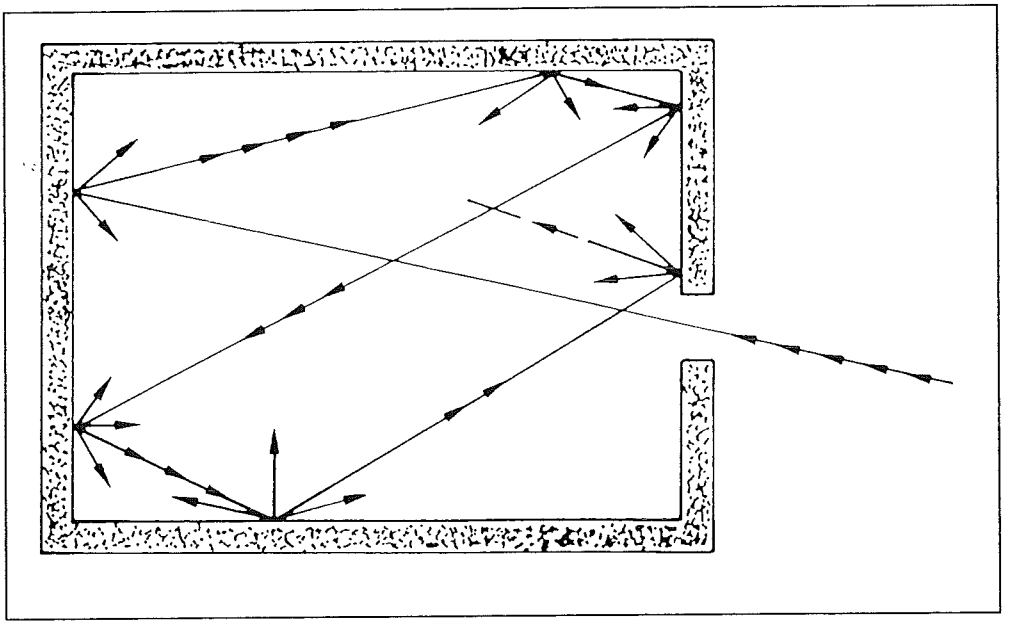

Fig 5.2. Black body simulation for all wavelengths.

The radiation law of Kirchhoff gives the relation of non black body radiation to black body radiation (1860):

$$L_\lambda = \varepsilon_\lambda \cdot L_{\lambda B}, \qquad (3)$$

where ε_λ the spectral emissivity or spectral emission coefficient of the material at wavelength λ is. The emissivity has a value between 0 and 1 and depends on temperature, wavelength, surface roughness, etc. (treatment in 5.4.). For a black body, the surface emissivity ε_λ t is independent of wavelength and temperature, and has the value ε_λ=1.

So called grey bodies have an emissivity that is constant over all wavelengths [95]. Fig. 5.3 gives the difference in spectral radiation density, of an ideal black body and a platinum body, at a temperature of 1573 °C, as function of wavelength. Unfortunately most materials have emissivities, which vary from wavelength to wavelength, and are called non grey or real bodies.

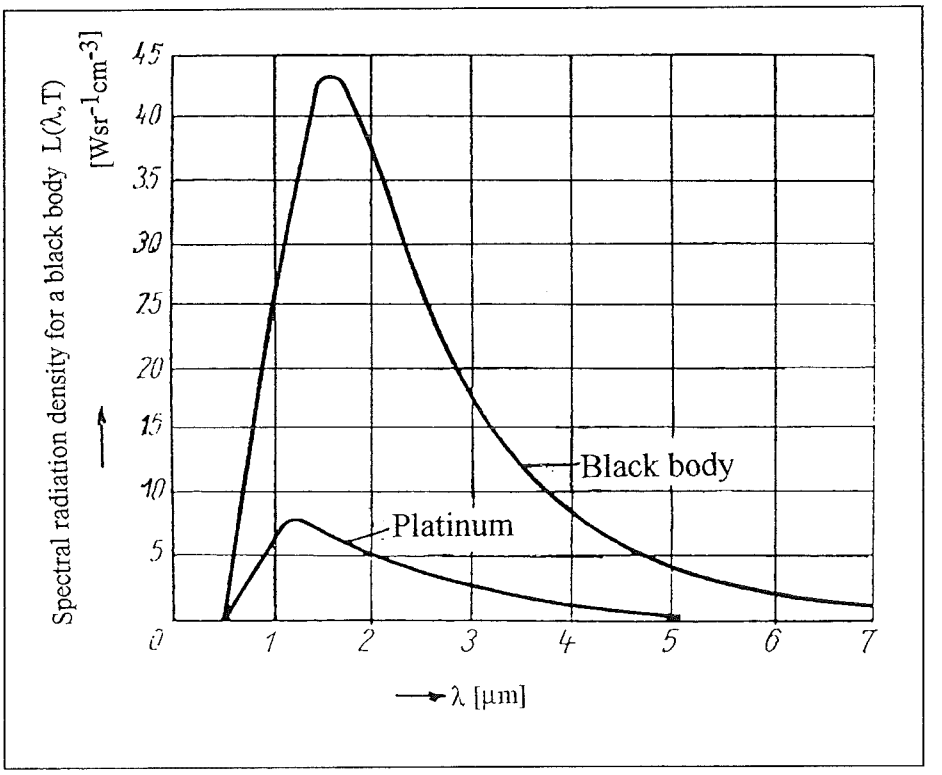

Fig. 5.3. Spectral radiation density of a black body and of Platinum at T=1573 °C [23].

Kirchhoffs law substituted in Planck's distribution law gives the general spectral radiation density for all surfaces:

$$L_\lambda = \varepsilon_\lambda \frac{C_1}{\pi\lambda^5[\exp(\frac{C_2}{\lambda T})-1]}, \qquad (4)$$

and for the emissivity ε_λ a value between 0 and 1 has to be substituted. Many Pyrometry techniques use the Wien approximation to Planck's distribution law:

$$L_\lambda \approx \varepsilon_\lambda \frac{C_1}{\pi\lambda^5}\exp\left[\frac{-C_2}{\lambda T}\right] \qquad (5)$$

We can estimate the error made because of this approximation by calculating the spectral radiation density with equation (5). Substitution of the radiation density at a temperature of 1500 K and a wavelength of λ=1,5 µm in the Wien approximation (6) gives a temperature difference of 0,4 K. The error made is 0,0026 %.

The temperature of a body also can be determined by the measurement of the total radiation emitted. The surface, under the curves in Fig. 5.4 give the total radiation density $N_B(T)$ for black bodies. The Stefan-Boltzmann equation describes the changes of the total specific radiance emittance as a function of temperature:

$$N_B(T)=\sigma \cdot T^4, \tag{6}$$

where σ is the constant of Stefan-Boltzmann. Integration of equation (1) over all wavelengths gives the total radiation density:

$$N_B(T) = \int_0^\infty L_{\lambda_B}(\lambda,T) = \int_0^\infty \frac{C_1}{\pi\lambda^5[\exp(\frac{C_2}{\lambda T}) - 1]} \tag{7}$$

and:

$$\sigma = \frac{2\pi}{15}\cdot\frac{C_1}{C_2^4} = 5{,}6697\cdot 10^{-8}\left[\mathrm{Wm^{-2}K^{-4}}\right] \tag{8}$$

Kirchhoffs law (3) gives the relation between black and real or total radiation density is:

$$N(T) = \varepsilon_t \cdot N_B(T) \tag{9}$$

and ε_t the total emissivity.

For sake of completeness of the basic radiation laws, the displacement law of Wien is given:

$$\lambda_{max}\cdot T = 2{,}8978\cdot 10^{-3}\left[\mathrm{mK}\right], \tag{10}$$

where λ_{max} is the wavelength, where at a specific temperature the spectral radiation density has its maximum. The hatched line in Fig. 5.1 and the line in Fig. 5.4 connects the peaks at different temperatures of maximum radiation densities.

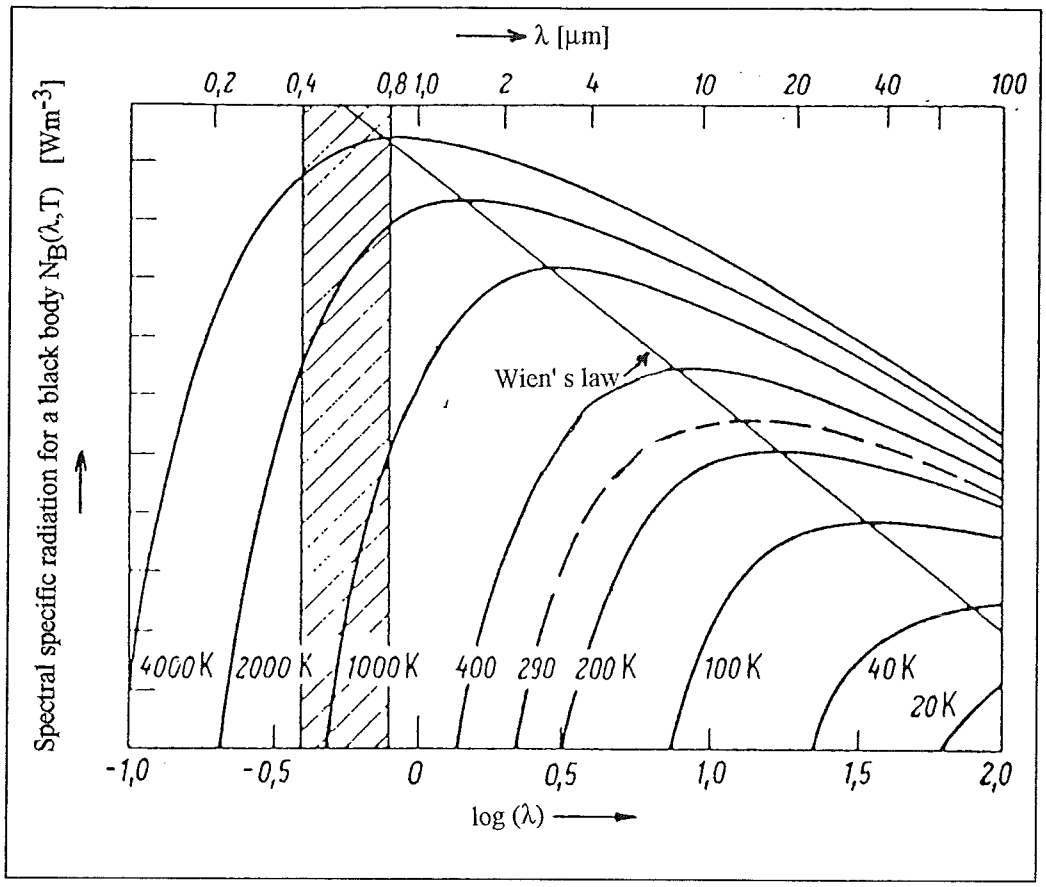

Fig. 5.4. Spectral specific radiation of a black body as function of λ and T [87].

5.2. Principles of Different Pyrometric Methods

It already has been stated that noncontact measuring of surface temperatures bases on a very simple principle and set-up's for such a system are numerously described [85-97].
By measuring, spectral radiance density L_λ at a chosen wavelength λ and by substituting appropriate values for ε_λ, C_1 and C_2, the temperature of the surface can be calculated, with the Planck radiation equation (4) or the Wien approximation (5). This is called one-colour-Pyrometry or one-wavelength-Pyrometry. Fig. 5.5 schematically gives the optical system of a Pyrometer. The lenses focus the emitted radiation of a surface on a detector (most of the time a semi-conductor, e.g. PbSe or PbS). Because the emission coefficient usually is unknown, several multiwavelength-Pyrometry methods are developed to eliminate this coefficient. A description of these methods gives the next part.

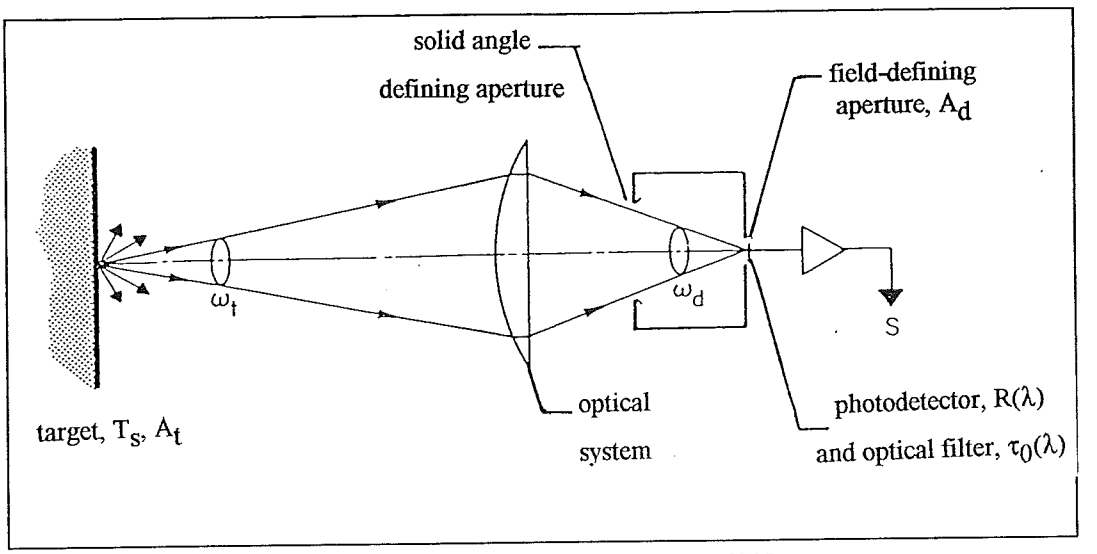

Fig. 5.5. Lenses system and detector of a Pyrometer system [88].

Planck's radiation law is integrated between wavelength λ_1 and λ_2 in Band-Pyrometry. The temperature can be calculated by substitution of the emissivity. An average value or function for the emission coefficient must be substituted.

When the total radiance is measured the Stefan-Boltzmann equation (6) is used to determine surface temperatures. This is called full-spectrum-Pyrometry or total-energy-Pyrometry. In full-spectrum-Pyrometry the thermal radiation emitted is measured in many channels over a broad spectral interval to include the peak of the emitted radiation. Assuming that the wavelength dependence of ε_λ can be explicitly represented by an analytical function and substituted into Planck's radiation law. When no analytical function for the emissivity is available, it is sometimes possible to determine the temperature with use of linear or non-linear least-squares curve fitting [95].

Historically there have been two distinct techniques for calculating or extrapolating the emissivity. The older technique is usually known as ratio-Pyrometry. This technique involves measurement of radiance emission at a number of different wavelengths in an attempt to eliminate the emissivity term by making ratios of the measured radiance's [96]. Ratio techniques assume that both (in the case of two-colour) or several numbers (in the cases of three- or four-colour) of the emissivities at the measured wavelengths are equal.

The other, newer, method of Pyrometry is known as multiwavelength-Pyrometry. In this method again, measurements of the spectral radiance emissions of the object are taken at several wavelengths. The processing of this data is than performed by a variety of techniques, the most accurate of which have proven to be least-squares-based multiwavelength techniques. Another method is fitting the radiance emission data to an assumed radiance functional form.

Generally, ratio techniques have do not provide adequately accurate temperature estimates for broad industrial usage. The often large inaccuracies of the ratio techniques are caused by unrealistic assumptions about the nature of the emissivity.

Multiwavelength, and particularly least-squares-based, techniques have been somewhat more successful, largely because they more reasonably assume a wavelength dependent emissivity function, rather than that all, or some of the emissivities, are equal. With certain materials these techniques report to be accurate to within 1 % [94]. With other materials, however, results have been unsatisfactory. It has been assumed by previous investigators that the unsatisfactory results have been due to two sources: first, incorrect form or lack of functions and second, the so-called "correlation effect", due to the inability of curve fitting routines, to distinguish in certain circumstances between changes in emissivity and in temperature.

Fig. 5.6. shows the problem of influence of radiation coming from surrounding objects.

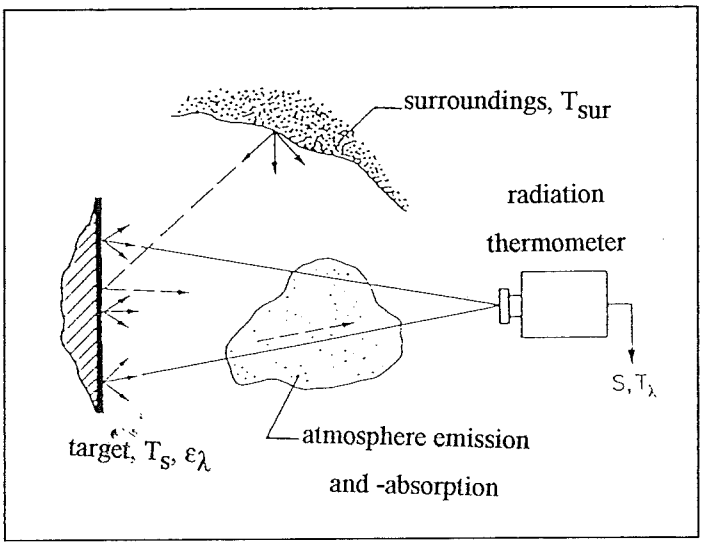

Fig. 5.6. Influence of radiation coming from surrounding objects [88].

5.3. Principles of Pyrometer Calibration

Three different components can be distinguished in the optical system of a Pyrometer measurement's system; optical lenses, radiation detector and converter. The spectral radiation density L_λ of a surface with temperature T must be translated to an electric output in volt, U(T). Correction factors to convert the radiation to an electrical output are [85]:

- The optical system of lenses, mirrors and filters, that images the radiation of the surface to a radiation detector. For the shape of the image, a correction factor K_1 is added to Planck's radiation law (10). Not all radiation passes through the lenses system and this is corrected by a relative spectral transitivity coefficient τ_λ;
- The radiation detector has a sensitivity $B(\lambda)=K_2S(\lambda)$. This sensitivity is divided in the responsivity K_2 (wavelength independent) and $S(\lambda)$ (wavelength dependent) of practical consideration [89];
- The electrical analysing circuit, which converts the signal to any output corrects multiplicationsfactor K_3.

The spectral radiation density distribution in integral form of Planck is:

$$L(T) = \int_{\lambda_1}^{\lambda_2} \varepsilon_\lambda \cdot L_B(\lambda, T) d\lambda \tag{11}$$

Now the electric output U(T) with the above mentioned correction factors and (11) is:

$$U(T) = \int_{\lambda_1}^{\lambda_2} \tau_\lambda \cdot S(\lambda) \cdot K_1 \cdot K_2 \cdot K_3 \cdot \varepsilon_\lambda \cdot L_B(\lambda, T) d\lambda \pm G \tag{12}$$

According to wavelength range the Pyrometry method is called one-colour-, band- or total-energy-Pyrometry. The parameter G, is a correcting factor, for the DC drift appearing by conversion, and for the drift of the background noise, from the radiation detector.

In the following the formulas to directly calculate temperatures from radiation densities are given

- one wavelength Pyrometry:

The measured temperature T_B is converted to the real temperature T of the non black body, using the Wien approximation (5) for Planck's distribution law. For this the Wien approximation for a black body is equated to the Wien approximation for a real body ($L=L_B$). After rewriting the temperature is found with the expression [86]:

$$T = \frac{1}{\frac{1}{T_B} + \frac{\lambda}{C_2} \ln \varepsilon} \left(L = L_B\right) \tag{13}$$

Eq. (12) shows that the measured "black" temperature T_B is smaller than the real temperature T. The sensitivity of one-colour-Pyrometer, i.e. the signal-change with temperature, depends on the wavelength.

Differentiation of equation (5) gives the sensitivity [86]:

$$\frac{dL_\lambda}{L_\lambda} = \frac{C_2}{\lambda T} \cdot \frac{dT}{T} \qquad (14)$$

If at a defined temperature change dT the wavelength increases, than the spectral radiation density change dL_λ decreases. A change in measured spectral radiation density caused by emissivity or apparatus inaccuracy leads to larger faults at larger wavelengths. It is also better to measure in one-colour-Pyrometry at shorter wavelengths. This is limited by the decreasing spectral radiation density at short wavelengths.

- band-Pyrometry:

The equations deduced for one-wavelength-Pyrometry are also valid for band-Pyrometry, but for wavelength λ an effective wavelength λ_{eff} must be substituted. Correction for the influence of the emissivity change is made by numerical integration of the spectral emissivity change.

- total-energy-Pyrometry or full-spectrum-Pyrometry:

If the Stefan-Boltzmann equation (6) for the total radiation density $N_B(T)$ and Kirchhoffs radiation law (9) are combined, the real temperature T can be calculated from the measured "black" body temperature T_B (for a non black body). By equating $N_B(T)$ with N(T) it is found that:

$$T = \frac{T_B}{\varepsilon_t^{1/4}}, \qquad (15)$$

where ε_t is the total emissivity. The radiation density change, dN, at temperature change dT is found by differentiating the Stefan-Boltzmann equation (6) :

$$\frac{dN}{N} = 4 \cdot \frac{dT}{T} \qquad (16)$$

Normally a radiation density change in total-energy-Pyrometry leads to greater temperature deviations. Comparing equation (14) to equation (16) shows that they are correct as long as $C_2/\lambda T > 4$ ($\lambda < C_2/4T$). At a temperature of 1000 K, the wavelength in one-colour-Pyrometry must be smaller as 3,6 µm to achieve this condition. In that case the sensitivity for radiation density change is better for the one-colour-Pyrometer.

- ratio-Pyrometry:

In ratio-Pyrometry the spectral radiation density is measured at two or more wavelengths and the temperature is calculated from these values. An assumption about the spectral change of the emissivity is made. The literature describes many different methods of multi-colour-Pyrometry. The two-colour-Pyrometer however has proven to be of good practical use. For a black body using the Wien approximation, the ratio R_B is:

$$R_B = \frac{L_{1B}}{L_{2B}} = \left(\frac{\lambda_2}{\lambda_1}\right)^5 \exp\left(\frac{C_2}{\lambda_2 T} - \frac{C_2}{\lambda_1 T}\right), \tag{17}$$

where L_{1B} and L_{2B} are the spectral radiation densities, at respectively wavelengths λ_1 and λ_2. For real bodies, the emissivity, must be taken into account:

$$R = \frac{\varepsilon_1}{\varepsilon_2} R_B \tag{18}$$

For grey bodies ($\varepsilon_1=\varepsilon_2$ and thus $R=R_B$) is the measured ratio temperature T_r equal to the real temperature T.

For a real body T_r is the real temperature equal to:

$$T = \left(\frac{1}{T_r} - \frac{\lambda_1 \cdot \lambda_2}{\lambda_1 - \lambda_2} \cdot \frac{1}{C_2} \cdot \ln\frac{\varepsilon_1}{\varepsilon_2}\right)^{-1} \tag{19}$$

To determine the real temperature, good knowledge about emissivity-ratio is essential. Due to this, an estimation of the fault is difficult. Temperature deviation differs in two directions depending on the emissivity change. Thus general criteria for the favourable wavelength-combination cannot be given and depend on the application.

5.4. Principles of Emission Coefficient

The foregoing showed that the key problem of noncontact temperature measurements, using Pyrometry, is missing knowledge of exact emissivity and functions with temperature. The most important variables that determine the emissivity:

- wavelength (Fig. 5.7);
- temperature (Fig. 5.8-9);
- material;
- surface roughness;
- microstructure;
- measurement angle (Fig. 5.10);
- degree of oxidation of the surface;
- in case of a substrate-coating-system, the thickness of the coating
- physical and chemical contamination.

Accurate temperature measurement in the case of grey surfaces ($\varepsilon<1$ and constant over all wavelengths) is done with full-spectrum-Pyrometry and non-linear least-squares curve fitting [95]. Unfortunately in most practical situations the surfaces act as non grey and extensive research is necessary. Appendix D gives a review of the emissivities of some materials [23]. For spectral Pyrometry the emissivity ε at wavelength λ=0,65 µm and the total emissivity ε_t for total energy Pyrometry is given. For all the materials the transmission grade was zero (τ=0). The materials are divided in three groups: high, medium, and low changing emissivity. The materials in group 3 are solid and fluid-state metals with bright surfaces. Metal melts and clean metals, which rapidly oxidise, show strongly changing emissivities.

Determination of the emissivity is done with following methods:

a) The surface temperature of a body is measured at the same time using noncontact Pyrometry, to determine the "black" temperature T_B and is measured with a thermocouple or another contact thermometer, to determine the real temperature T. In case of the contact temperature measurement care has to be taken to achieve good contact. When the material conducts heat well, the thermocouple can be put in a boring. In equations (20) and (21) the calculations of the emissivity are respectively given for the case of spectral Pyrometry (one-wavelength or band-Pyrometry) and total energy Pyrometry:

$$\varepsilon = \exp\left[\frac{C_2}{\lambda_{eff}} \cdot \left(\frac{1}{T} - \frac{1}{T_B}\right)\right] \tag{20}$$

$$\varepsilon_t = \left(\frac{T}{T_w}\right)^4 \tag{21}$$

b) In case that the material conducts heat well a hole is processed into the surface of the body. The temperature T_B is measured at the bottom of the boring and the real temperature T at the surface next to the boring at the same time. When the boring has a diameter depth ratio of 1:3 the boring radiates according to a black body (ε>0.97). This diameter is chosen according to the measurement spot area and the focal distance (Fig. 5.11).

c) In case of heat insulating materials a black coating is applied to the surface. A non black surface part is compared to a coated black part and again the temperature can be calculated according to (20) and (21).

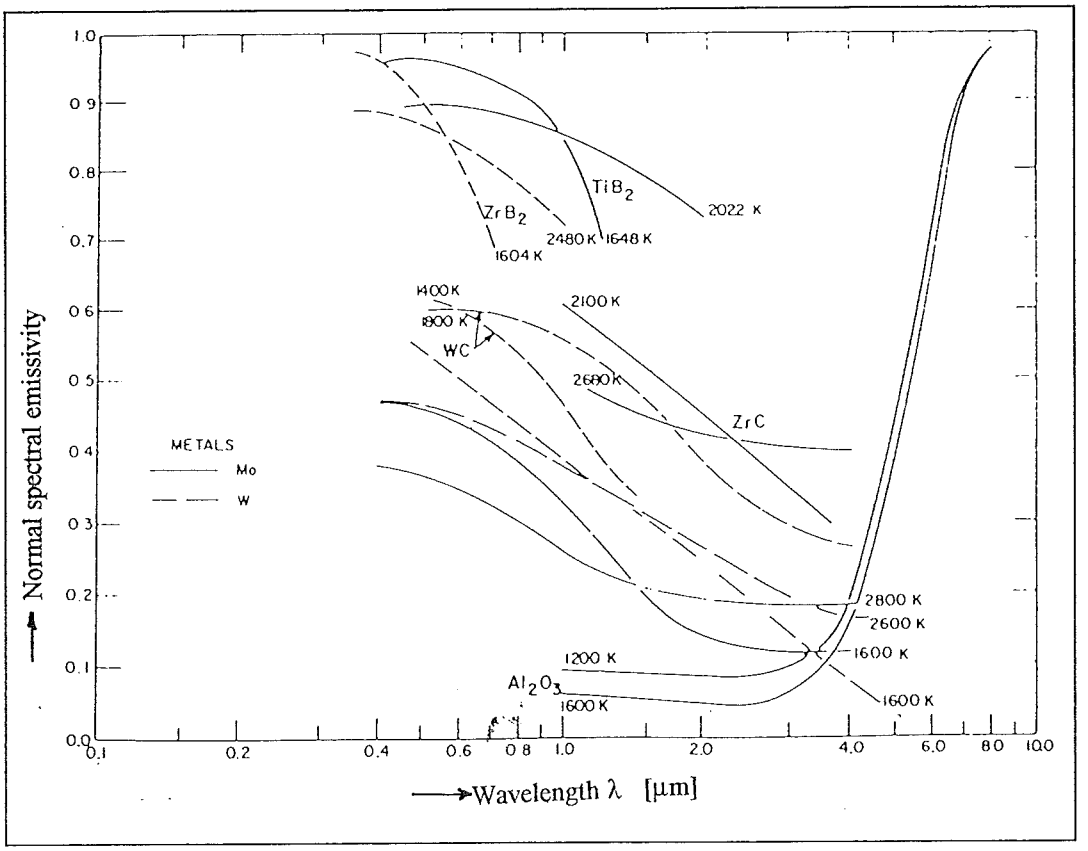

Fig. 5.7. Spectral emissivity coefficient as a function of wavelength [88].

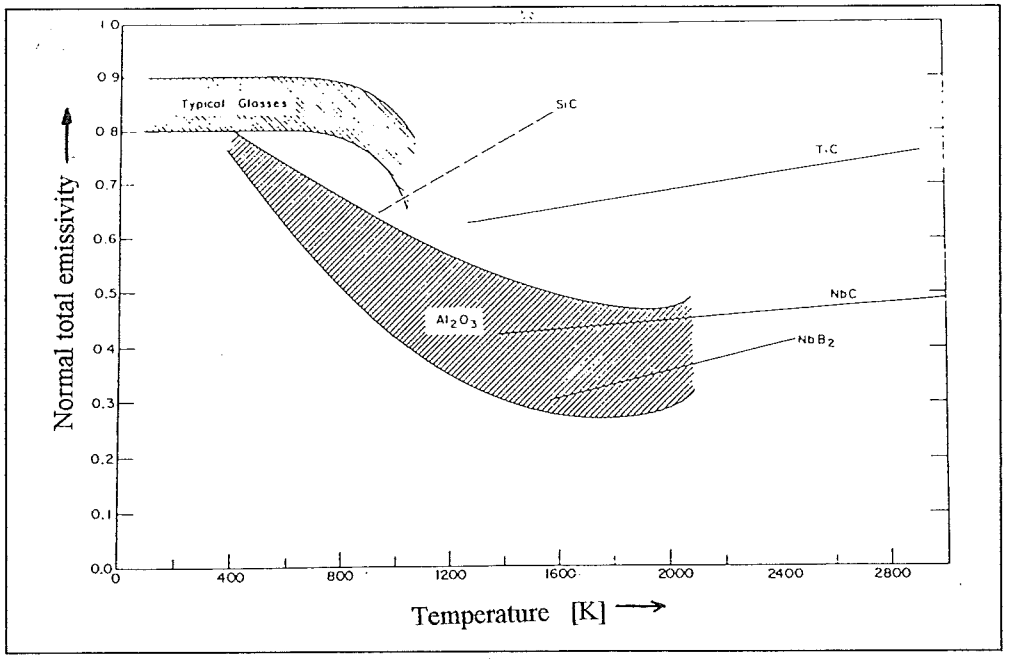

Fig. 5.9. Total emissivity as a function of temperature [88].

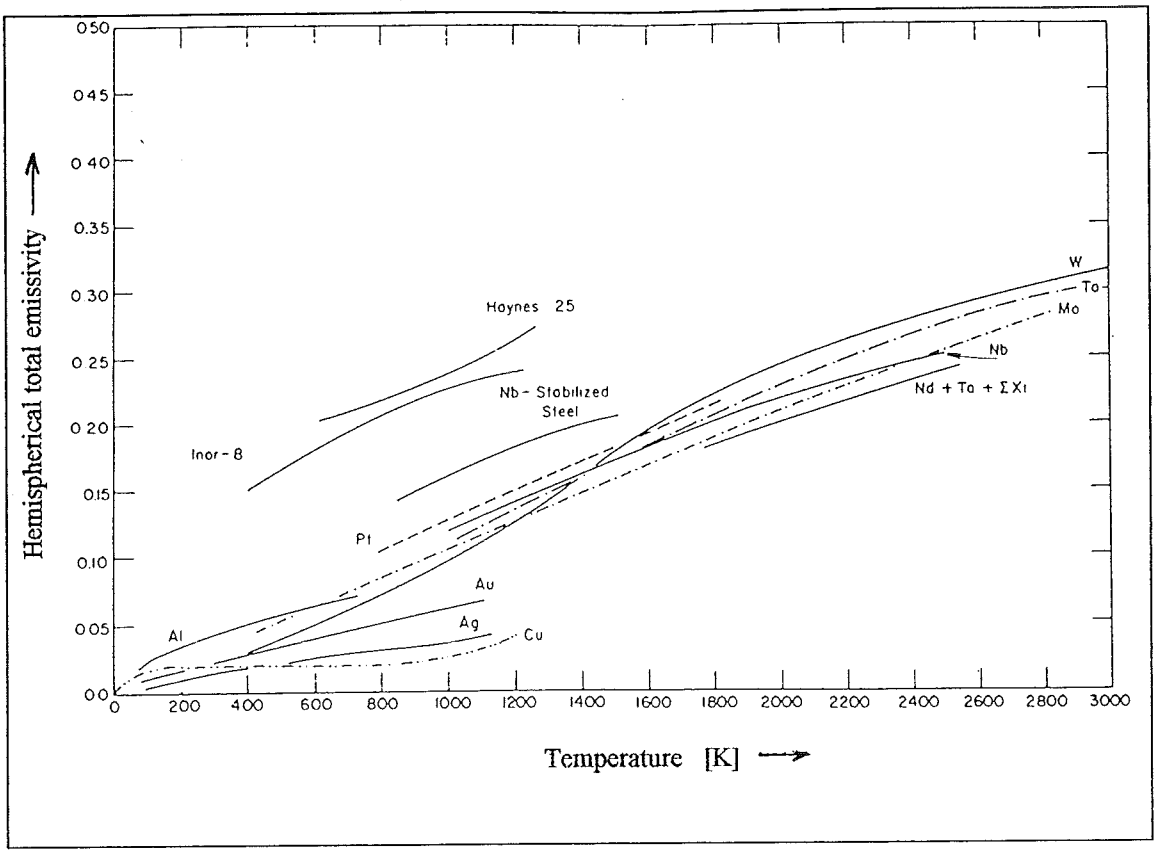

Fig. 5.8. Spectral emissivity coefficient as a function of temperature [88].

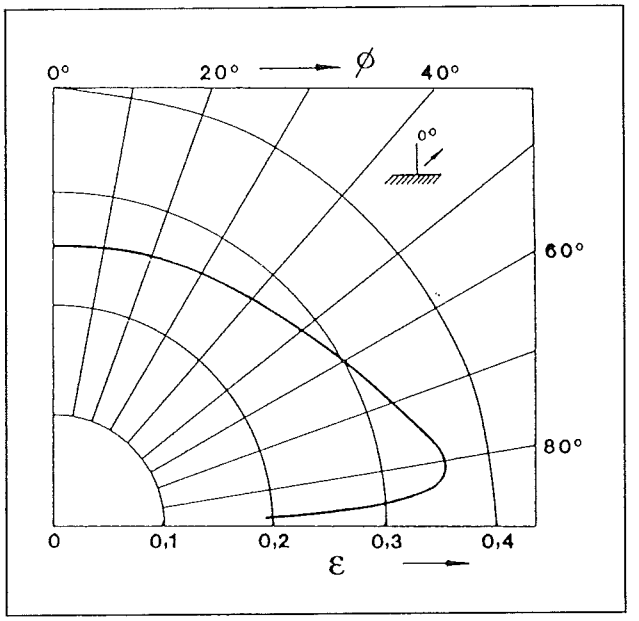

Fig. 5.10. The influence of measurements angle on the emissivity [87].

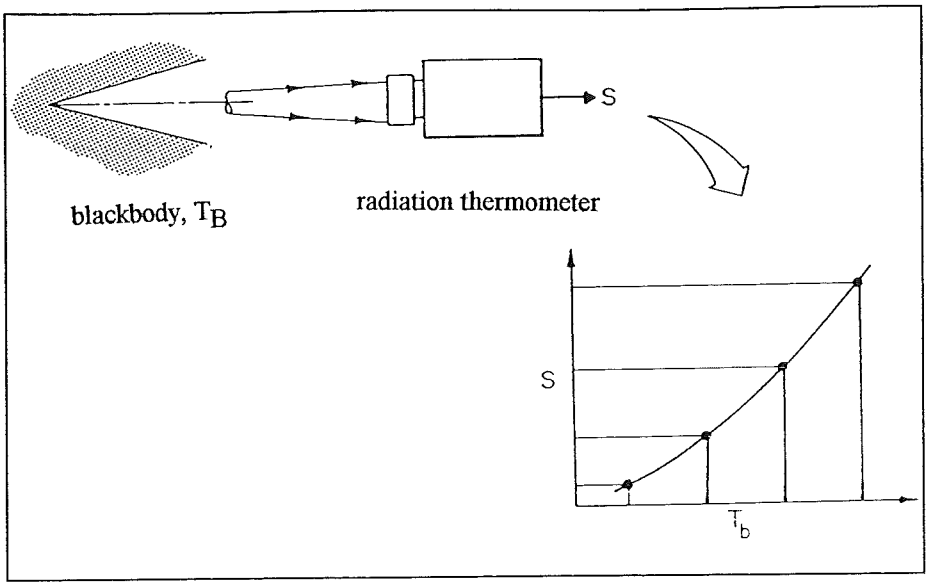

Fig. 5.11. Simulation of a black body to determine the emissivity [88].

6. Adaptation of the Pyrometric Process Control System for APS

This chapter describes the apparatus and the steps that were taken to complete the Pyrometric Process-Control System (PPCS) for Atmospheric Plasma Spraying (APS). It is divided in three parts where respectively the Plasmadyne system, the pyrometric hardware and the pyrometric software are described. First the systems are described followed by the adaptation that has bee undertaken.

6.1. The Plasmadyne system

6.1.1. Description of the Plasmadyne System

In this paragraph the Plasmadyne spray system, F4 plasma gun, the Posimo 3000 roboter and the powder feeder of Plasma-Technik AG Switzerland will be described (Fig. 6.1).

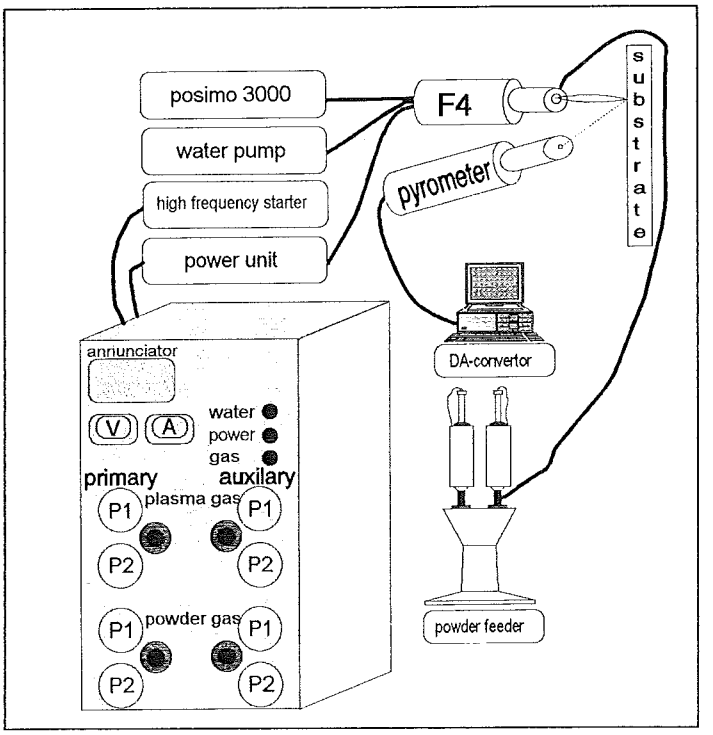

Fig. 6.1. The Plasma Process Control System.

A model NAU-E-1000DD4 control console controls power, cooling circuit, gas rates, powder rate and initiation of the plasma (Fig. 6). To prevent starting or operating under unsafe conditions, the console has safety interlocks on the gases, water and power.
The control console has a built in annunciator model 1070-1, which at a malfunction automatically shuts down the system, by its safety interlocks. The annunciator shows the cause of the malfunction [98].

The system consists of two PS-61M/S, 380-volt, 50 Hz power supplies, which produce 40 kW of power for each of the spray guns. In case of one plasma gun it can be used at a maximum power of 80 kW. Furthermore to initiate the plasma there is a model 1229 high frequency arc starter unit.

Main plasma gas is argon and with a three-way tap a second plasma gas (nitrogen, helium or hydrogen) gas can be chosen. The control console is used to open and adjust the gas rates. Critical orifice assemblies (a cylindrical body with a very small boring) control the gas flow rates. Various critical orifice inserts can be readily exchanged as required for specific gases and flow rates. Fig. 6.2 presents a gas flow rate chart for different orifice sizes and gases for the above mentioned orifice inserts. To determine the gas flow rate, the P_1 gas pressure is read in Pounds per Square Inch Gas (1 PSIG = 0,0689 Bar) and the gas flow rate is read in Standard Cubic Feet per Hour (SCFH) for the orifice being used. In the Thermal Spraying technology the gas rates are expressed in Standard Litres per Minute (SLPM). A second P_2 pressure gage insures that the orifice flow is critical. The P_2 pressure must always be less than one-half of the P_1 pressure.

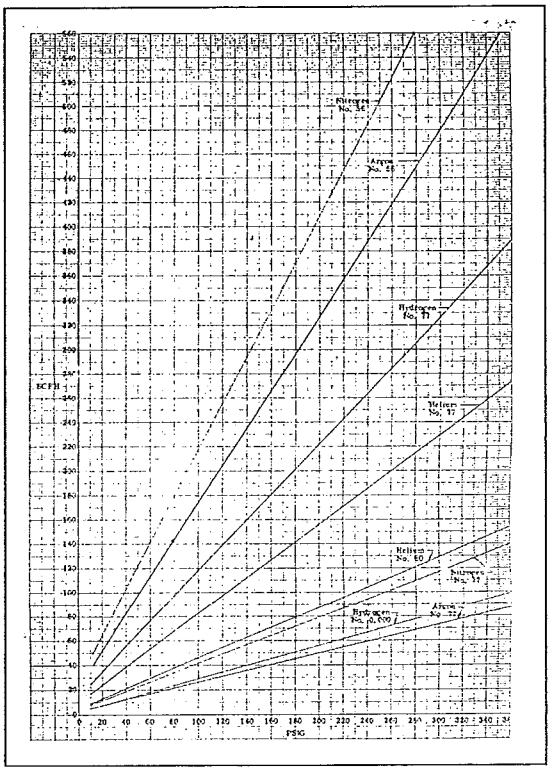

Fig. 6.2. PSIG against SCFH plot to determine the gas rate [98].

The powder feeder TWIN-10-V is of Plasma-Technique AG with the requirements [99][100]:

- highest precision of the powder flow;
- reproducible powder flow also during long operating periods;
- processing of bad flowing spray powders.

It has two powder containers, constructed of aluminium, with a capacity of 5 l. A cone guarantees a constant weight on the outlet of the cone shaped funnel independent of the power level in the container. A reproducible powder supply accuracy within 1 % of the set value is guaranteed.
Both containers have two high capacity resistance heaters and a thermostat to allow adjustment and control of the temperature. The maximum adjustable temperature is limited to 100 °C (Fig. 6.3).

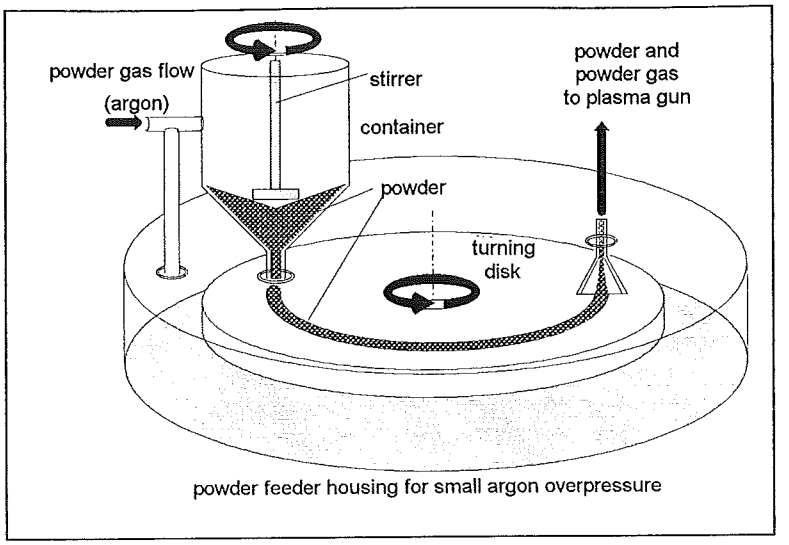

Fig. 6.3. Twin 10-V powder feeder.

The Posimo 3000 can move in two rectangular directions (Fig. 6.4). It consists of a computer and two electromotors, to move the table whit the plasma gun. It has a teach-mode to move the torch by hand with direction keys [101].

The F4 VB 8801 plasma burner (Fig. 6.5) is developed by Plasma-Technique AG Switzerland [101]. It is the most important part of a Plasma Spraying system and transfers the electric energy to heat energy. It has three circuits:

1. Gas circuit:
After the plasma gas has entered the gun, it flows through a gas dividing ring, which directs and stabilises the gas. Furthermore a rotation is introduced in the gas. Then the gas flows around the wolfram cathode in the nozzle, where it ionises and dissociates. The gas gets a high heat capacity and is accelerated by the expansion caused by the heat input. The nozzle concentrates the gas flow.

2. Power circuit:
The current flows from the positive connection over the front body to the anode. From the nozzle it flows (ionisation assumed) to the cathode and over the rear body to the negative connection.

3. Cooling water circuit:
The water flows from the positive connection (in the current-cable) in two canals through the centre body and front body and than to the end of the nozzle. Through canals in the nozzle body the water flows back and cools the cathode, before it flows out at the negative connection.

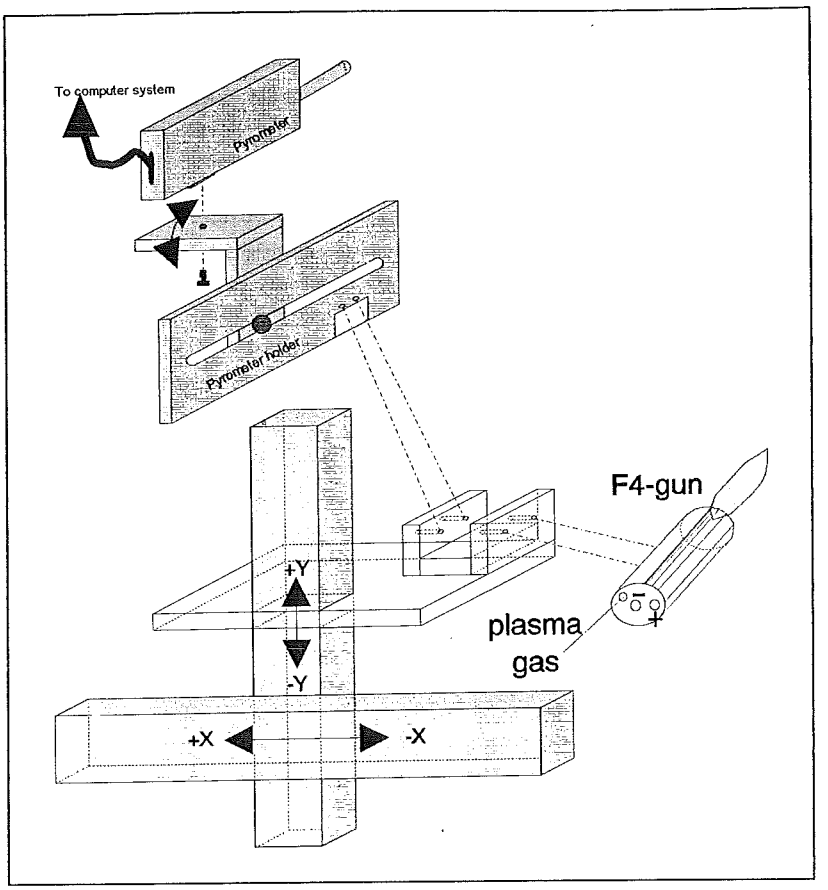

Fig 6.4. The Posimo 3000 xy-roboter system.

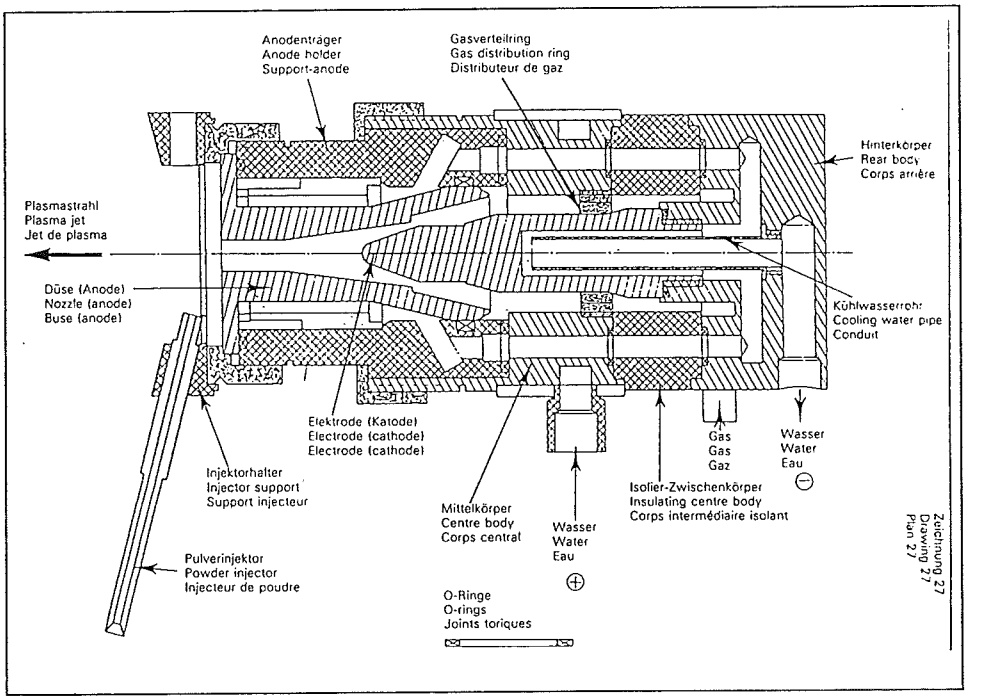

Fig. 6.5. Sectional drawing of the F4 gun [101].

Table 6.1. Technical specifications of the F4 VB 8801 machine plasma gun [101].

gas flow	1,5 - 20 m^3/h
continuous operation at:	maximum power: 55 kW
water pressure	p_{max} = 15 bar
minimal water flow	660 l/h
axial cable connection	

A Sulzer CP3-200N water pump gives cooling to the gun. Over 2900 l/min is passes through, with a power of 2,9 kW. A water flow meter controls the water flow (p_m=20 bar).

6.1.2. Calibration of the Plasmadyne System

The age of the control console is over 20 years and there was reason to doubt that the indicating instruments did not correctly show the values.

To calibrate the ammeter, used in a range between 400 and 1000 A, a calibrated ammeter was borrowed from the Institute for Electric Machines. The amperage was taken over a 2000 Ω resistor. A deviation of 25 amperes was found and corrected with the zero stand screw (2,5 % difference).

The gas flow is controlled and calibrated with help of critical orifices as was described in 4.1.1.. The pressure reduction over the critical orifice calibrate the manometers for the chosen gas. From given charts the gas flows are read-out. For an optimal process control it is expected that for the smaller auxiliary gas flows this method is not very exact and that the charts are not accurate. Data that was collected with the existing charts and maximum adjustable flows is summarised in Table 2.

Table 6.2. Maximal possible gasrates of the Plasmadyne.

Gas	Critical orifice number	Pressure from gas bottle	Pressure P1 (PSIG)	Pressure P1 (Bar)	SLPM
argon	56	10	120	8,3	105
nitrogen	56	5	56	3,9	56
helium	80	5	60	4,1	16
hydrogen	006	5	75	5,2	6

With a gas meter the argon and hydrogen gas rates at different PSIG pressures were determined from measured time at different gas volumes (Appendix B). The complete results of the calibration are given in a description of a practical work of the author [102].

6.2. The BP100 Pyrometer

6.2.1. Description of the BP100 Pyrometer

The Pyrometer-system, fabricated by CompoTherm in Syke Germany, consists of two measurement heads for different temperature ranges, a Digital-Analogue (DA) converter and a computer [103]. The Pyrometer-head has a water-cooled semi-conductor on which converging lenses focus the electromagnetic radiation from the surface. A DA-converter converts the current of the semi-conductor to a computer system (Fig. 6.6).

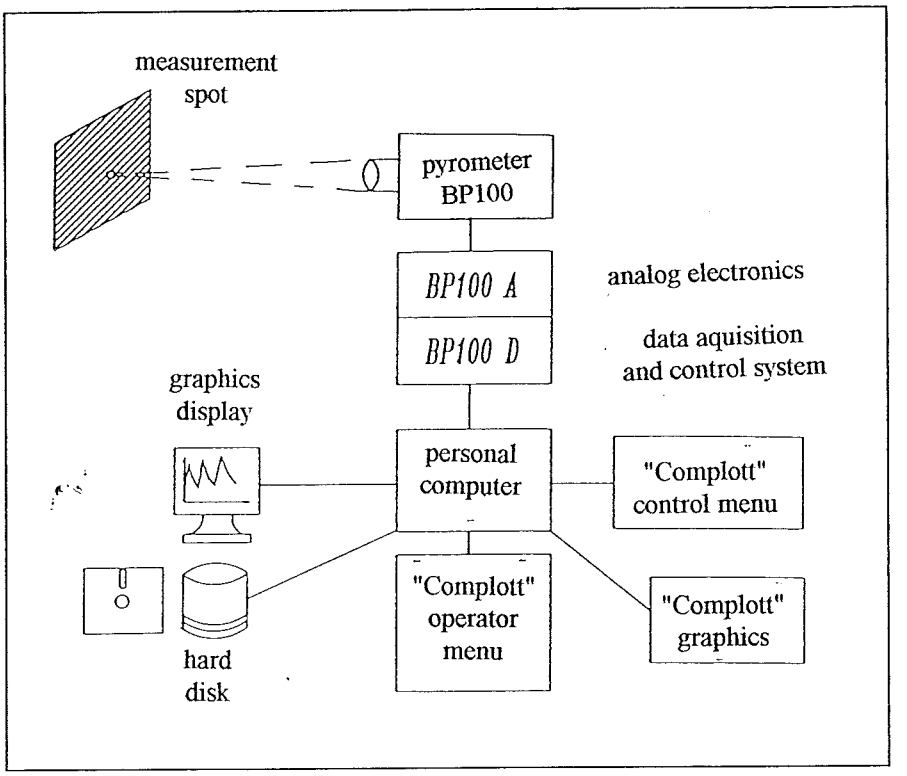

Fig. 6.6. The BP100 HS-Pyrometry system.

The pyrometric system can be used as a high-speed temperature measurements-system with a sample rate of 36 µs and for process control over longer times. For the authors research the latter is of interest.

Calibration was done by CompoTherm on a black body. The sensitivity of the semi-conductor to radiation was determined and saved in a file the software uses. The software package available is for high-speed and continuing measurements. Furthermore there is a graphical software package for analysing the high-speed measurements. The description and evaluation of the software gives 5.2. The technical specifications of the high-speed Pyrometer are listed in Table 6.3.

Table 6.3. Technical specifications of the high-speed Pyrometer BP 100.

Description	CC100/1	CC100/2
Temperature-range	300-3200 °C	40-600 °C
measurements range	2,0-5,0 µm	3,0-5,0 υm
IR-Optic	CaF_2	ZnSe
Aperture	22 mm	34 mm
Measurements distance	250 mm	150-250 mm
Measurements spot	1,5*1,5 mm	3,0*3,0 - 5,6*5,6 mm

6.2.2. Developments for the BP100 Pyrometer

To point the Pyrometer to the right spot it has an ocular with crosshairs. Because of high plasma temperatures, thus high intensities, the ocular has been exchanged for a laser pointer of 5 mW.

The F4 plasma-gun is assembled on an aluminium table and moved by the Posimo 3000. To move the Pyrometer head along with the gun it had to be mounted besides the gun. For this purpose a holder to position the head in 3 directions was designed and fabricated (Fig. 6.7).

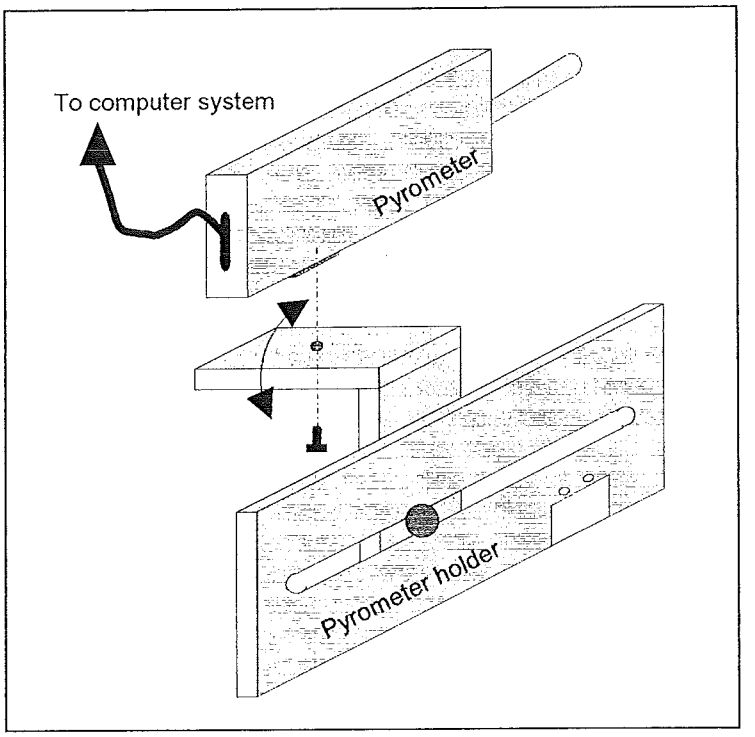

Fig. 6.7. Pyrometer holder.

6.3. The CC100- and Complott Software

6.3.1. Description of the CC100- and Complott Software

The software to be described in this paragraph is CC100 (Coating Control System) and the Complott graphical package [104]. The CC100 software is measures, evaluates and saves temperature profiles to harddisk. The Complott graphical software analyses the profiles and gives a graphical reproduction of high-speed measurements.

The system requires an IBM compatible computer with coprocessor. For comfortable use a 386-SX16 (or faster) computer is recommended. After connection of the serial cable (25 poles, attached 1 to 1) and the cooling water and starting of the computer a self-test inspects the Pyrometer. It takes about 10 minutes for the Pyrometer to get operational; the ammeter on the DA-convertor than must display 15 µ A. The Pyrometer control program is 'CC18.EXE'. The program is ended by pressing 'ALT+B' (Beenden).
At a continuing measurement 100 times per second, the temperature is measured with a sample rate of 36 µs. In the rest of the second the temperature is saved and evaluated. Saved to harddisk are minimal-, maximal-, mean- and differential temperature, 2 offset-values, date and time (every second takes 237 bytes).

The CC18 menu has 4 levels and can be switched by pressing the TAB key. To select F11 and F12 on the XT-keyboard 'SHFT+F1' and 'SHFT+F2' must be pressed.

The speed of a replay can be varied by pressing the direction keys. The left direction key decreases and the right direction key increases the speed (2 %). The up direction key decreases and the down direction key increases the speed (10 %).

The Complott graphical program exists of CM.EXE, TN.EXE, TP.EXE, PLOTT.EXE, SHOW.EXE, SPFIT.EXE and MODIT.EXE [7].

All programs are executable from the prompt or from a menu by executing 'CM.EXE LAST'. In LAST there is a pointer to M_DOS.FIL with the menu text. The menu can be changed to personal demands. Also are the last 16 loaded files saved in LAST.

SHOW.EXE and PLOTT.EXE have the same function. SHOW has been made to call the last saved file from the menu and plot it on the screen.

More information can be found in the CompoTherm documentary [103].

6.3.2. History of the CC100- and Complott Software

On the author's arrival at the Institute Materials Science three generations of the CC100 package existed:

In the first version CC12.EXE, the results of the high-speed measurements were saved in binary files with the names MESSXXX.BIN (XXXX = 0000, 0001, ...). These were automatically translated to MESSXXXX.TAB (table with time and measured voltages) and to TEMPXXXX.TAB (table with time and calculated temperatures, depending on chosen emissivity).

The continuing measurements' data were saved in the file CONTINUE.BIN. This temperature profile could be replayed but was overwritten at the start of an new measurement. If the user wanted to keep the file it had to be renamed for a new measurement was started.

The second version was CC13.EXE. The difference to the first version was that now more continue measurements, without renaming them, were possible. The files were named CONTXXXX.BIN (XXXX=0000, 0001, ...).

In the third generation CC15.EXE the problem that only the last file could be replayed was solved. Any CONTXXXX.BIN could be replayed.

The latest version CC18.EXE solved most of the problems that were discovered during use of the system. These were:

- Creation of ASCII-files instead of the specific Complott TAB-format, to be able to evaluate the temperature profiles in other graphical programs;
- Automatic saving of the used intensification, because by replay with a wrong intensity nothing useful is showed;
- Quitting the program should be changed into 'ALT+B' (Beenden) instead of ESC, because undeliberate pressing of the latter key;
- In the MOOSXXXX.TAB-file, created at a high-speed measurement, should in it 's head the Voltage be displayed instead of Temperature;
- The left part of the screen has to be cleaned before a new measurement is started;
- Replay should have different speed-steps;
- In the right corner the number of the level should be displayed.

7. Optimisation of the Al_2O_3 / TiO_2 Coating with Pyrometry

7.1. Background of the optimisation

This optimisation is the start of an AIF (Arbeitsgemeinschaft industrieller Forschungsvereinigungen) research project. This is a co-operative research between the Materials Science Institute, Aachen University of Technology and the Electronics Faculty, München University of armed forces. The goal is to gain information about the:

- properties of the plasma;
- properties of the particles in the plasma;
- temperatures of the substrate.

With this information, relations between primary parameters and plasma properties, particle properties, heat-input in the substrate on one side and coating quality on the other side will be determined. This will be done for Al_2O_3, Al_2O_3/TiO_2 (87/13) and ZrO_2 (+22,5 -45 µm) on St.-37/2 Substrates. For this München uses a LDA system and Aachen employs a HS-Pyrometric system.

The work for the authors engineering thesis is limited to the measuring of temperature profiles, testing of the mechanical properties and the microstructural analysis of APS sprayed samples. The research for this engineering thesis is limited to Al_2O_3/TiO_2 (87/13) powder and continuous process control temperature measurements.

7.2. Properties of the used Materials

- **The powder** [106]**:**

Al_2O_3	Mol wt.	101,96
	ρ	3,97
	T_m	2072
	T_b	2980
TiO_2	Mol wt.	79,88
	ρ	4,09
	T_m	1830-1850
	T_b	2500-3000

Grain size		+22,5 -45 µm
Chemical Composition:	SiO_2	0,40 %
	TiO_2	13,00 %
	Fe_2O_3	0,04 %
	Al_2O_3	rest

- **The substrate material St 37-2** [106]**:**

Tensile Strength	< 3 mm	360-510
	3 ≤ x ≤ 100 mm	340-470
Upper Yield Stress	≤ 16 mm	235
	16 ≤ x ≤ 40 mm	225
Elongation after rapture	3 ≤ x ≤ 40 mm	26
	40 ≤ x ≤ 63 mm	25

Chemical Composition:	C	≤ 0,17 %
	P	≤ 0,050 %
	S	≤ 0,050 %
	N	≤ 0,009 %

7.3. Spraying of the Al_2O_3 / TiO_2 Coating

Pyrometric temperature measurements form the basis of this work and may help with optimisation and process control. Two parameters that were expected to have an explicit influence on substrate temperatures and coating quality were chosen to be optimised: power level and powder feed rate. Standard parameters for Al_2O_3/TiO_2 coating system given by Plasma Technik AG Switzerland were used as starting parameters. These parameters are given for the Plasma Technik CAPS system, which also uses the F4 gun. Unfortunately because of the relatively high surrounding temperature the pyrometric system can not be used in the chamber.

The Plasmadyne system described in chapter 6 is not capable of such high voltages and such high H_2 gas flows. For this reason not the exact parameters were used. Table 7.1. gives these parameter values.

Table 7.1. Plasma Technik parameters for Al_2O_3/TiO_2 coatings.

parameter	dimension	value
powder size	µm	10-40
Argon	SLPM	41
Hydrogen	SLPM	14
Current	A	530
Voltage	V	72
Power	kW	38
Nozzle	mm Ø	6
Injector	mm Ø	1,5
Injector angle	°	90
Injector distance	mm	6
powder gas (Ar)	SLPM	3,4
Powder feed rate	g/min	28
Spray distance	mm	120
Surface speed	m/min	75
Traverse speed	mm/s	8
Air cooling		yes

Furthermore test samples were sprayed for microscopic research, wear resistance and adhesive strength in tension experiments. To insure the same adjustment for all samples they were sprayed in one procedure. For this reason a sample holder that could contain all the different samples was constructed (Fig. 7.1).

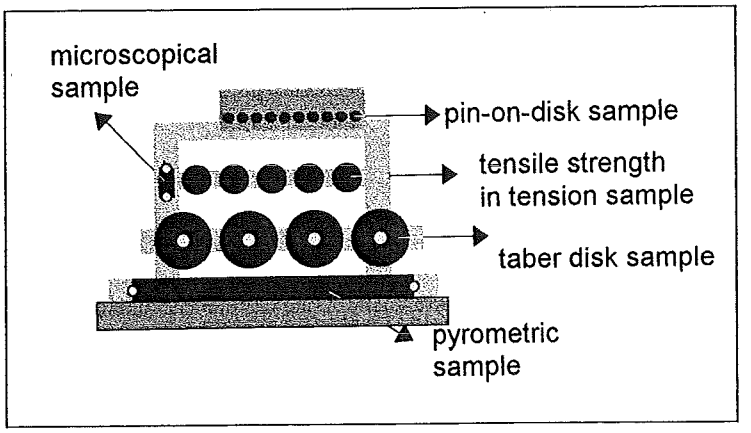

Fig. 7.1. Sample holder that was used to spray all samples in one procedure.

The samples desire a different coating thickness: for adhesive strength in tension 50 µm, for Taber Disk 200 µm and for Pin-on-Disk 300 µm. Disadvantage of different thickness is that the coatings cannot be compared to each other. For this reason an average thickness of 200 µm was chosen.
Traverse speed of the plasma gun was adapted to spraying of the desired thickness in one pass at three different powder feed rates. Try-out tests gave a speed of 1, 2 and 3,5 cm/s for respectively 5 %, 10 % and 15 % powder feed rate. All the measurements were done at a power adjustment of 40 kW.

The test series to be researched was a matrix of 9 combinations between power (35, 40 and 45 kW) and powder feed rate (5 %, 10 % and 15 %). Calibration of the powder mass flow gave respectively: 5,7; 11,4 and 17,1 g/min. Table 7.2 gives the spraying parameter variation and spraying consequence. Appendix F gives the exact spraying dates. This consequence was chosen because the following reasons:

- first the 'standard' Plasma Technik adjustment;
- than the time extensive 5 % powder feed samples (because of slow traverse speed);
- followed by the last series.

Table 7.2. Matrix of researched parameters.

Nr.	Adjustment
1	40 kW - 10 %
2	45 kW - 10 %
3	35 kW - 10 %
4	40 kW - 5 %
5	45 kW - 5 %
6	35 kW - 5 %
7	40 kW - 15 %
8	45 kW - 15 %
9	35 kW - 15 %

The numbers of the samples are based on the sequence of table 7.2. Double numbers exist, because the different samples easily can be divided. The numbers and sizes of the samples:

- Microscope; 1,2,... (50 x 20 x 5 mm);
- Taber; 10, 11,... and 20, 21,... (Ø 90 mm);
- Pin-on-disk; 10, 11,... and 20, 21,...(length 40 x Ø 14 mm);
- Tensile strength in tension; 10, 11,... and 20, 21,...(length 100 x Ø 40 mm);
- Pyrometry (50 x 500 x 5 mm).

Atmospheric Plasma Sprayed for each set were 4 Taber disks, 10 Pins-on-Disks and 5 tensile strength in tension samples and one pyrometric sample.

7.4. Pyrometric measurements

To compare the pyrometric measurement among one another a steady speed of 1,5 cm/s was found to fulfil this request. The ideal traverse speed was determined by too thick coatings splitting of at a too slow speed and a too limited measurements time at too high speed. Beside these factors, at a higher speed the vibrations of the positioner disturbed the temperature measurements more intensive.

The sensitive Pyrometer needs some time (5-20 s) to achieve steady reproduction temperature profiles. When the temperature is measurement next to the substrate, in air, the temperature scatters very much. This gives a problem at the direction turn at the end of one pass. To avoid this irritating deviation at the turn, the Pyrometer head must stay pointed on the substrate.
It was thus unfortunately not possible to measure temperatures profiles on the smaller samples. These parts are too small to reach a steady state. The plasma spray beam has a diameter of approximately 15 mm (at 120 mm spraying distance) and the turn has to be made at least 20 mm next to the substrate. This means that the Pyrometer would measure a lot next to the substrate and thus no reproducible temperatures are measured.

The pyrometric samples were chosen with a length of 500 mm. Turning about 50 mm before the end of the substrate gave good temperature results. A small temperature increase is detected at the turn, due to the fact that more particle arrive at this spot giving rise to the substrate temperature. It was found that with a traverse speed of 1,5 cm/s the vibrations of the table were limited and the thickness of the resulting coating was not to much at the 15 % powder feed rate. A distance between the passes of 15 mm gave better results than 5 and 10 mm. The samples were sprayed with a distance of 5 mm.
In this case three ways on the sample with a width of 50 mm could be measured. Three times 400 mm at a speed of 1,5 cm/s gives a total measurements time of 80 s.
For all measurements an emissivity of 0,2 was chosen. This is an estimation of values given in the literature. The exact temperature is also unknown, but differences and scattering of the temperature can be detected. By taken the same emissivity for all measurements, the same fault is made and this justifies comparison of the profiles.

At the try-out measurements it was discovered that the cooling pressurised air is more effective when it moves ahead of the gun. At the first measurements, the cooling air was only on one side. A temperature difference of 30-50 °C was found, depending on the adjustment of the primary parameters (the temperature was higher when the cooling came behind !).

Picture 1-3. HS-Pyrometric continuous measurements.

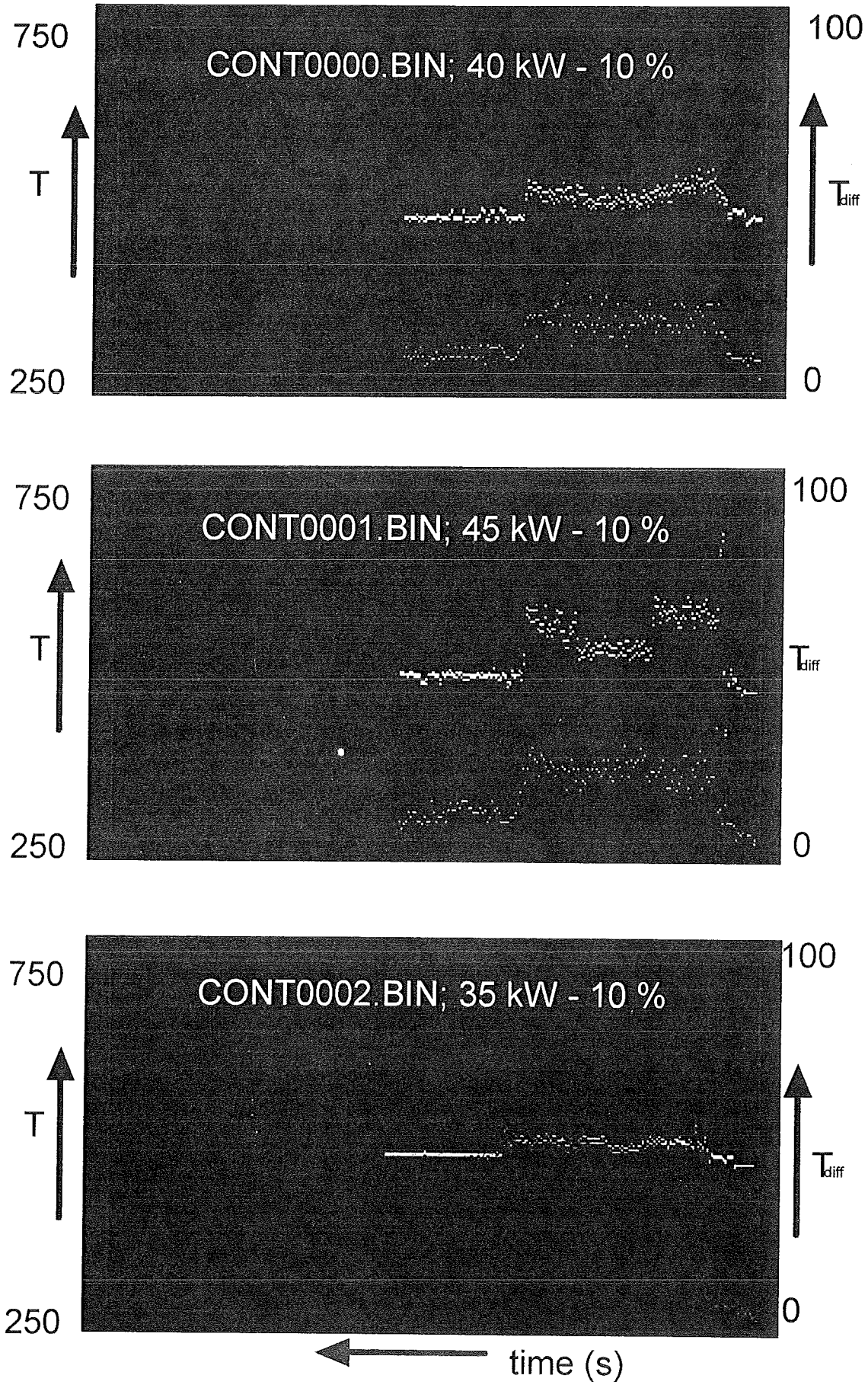

Picture 4-6. HS-Pyrometric continuous measurements.

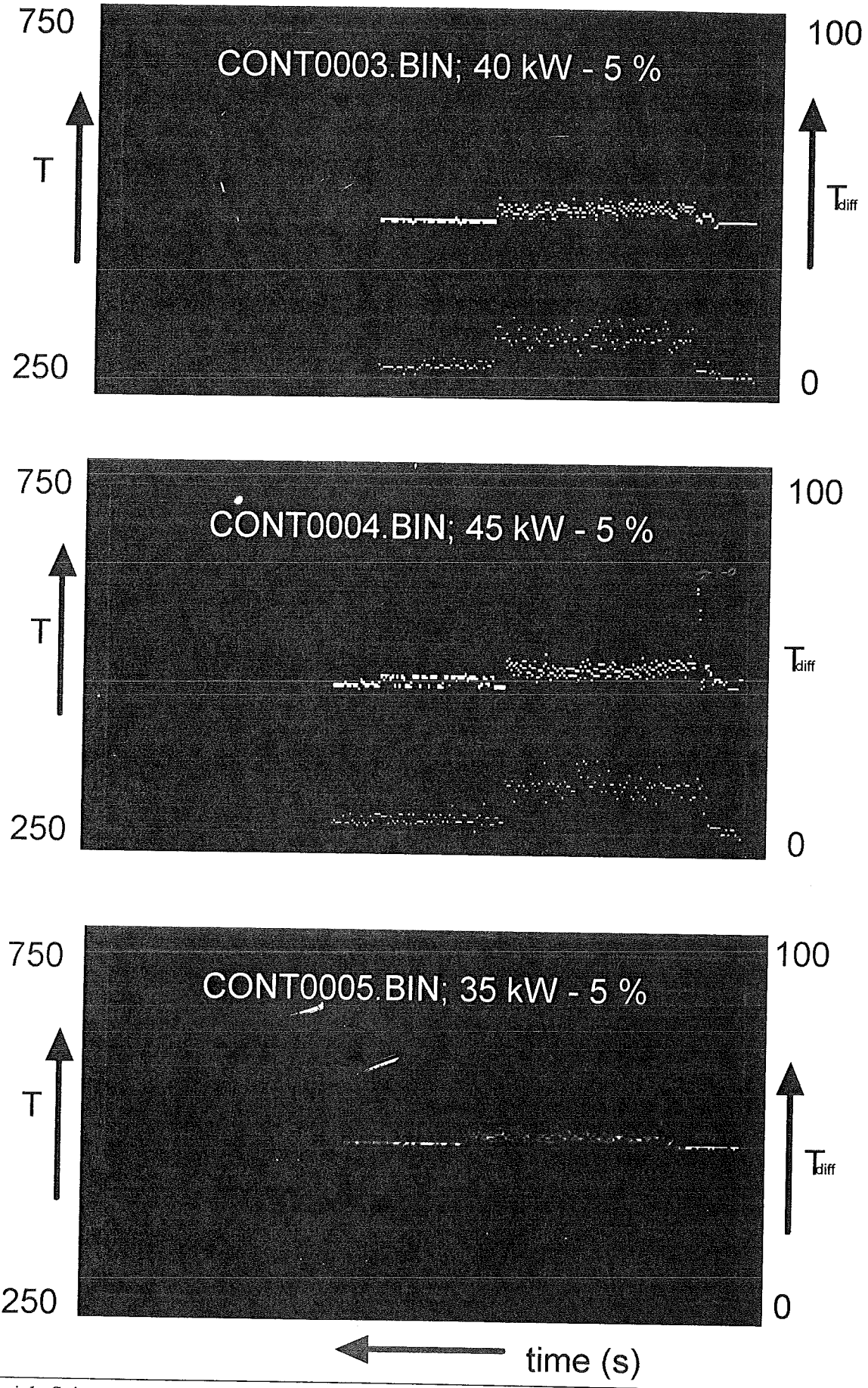

Picture 7-9. HS-Pyrometric continuous measurements.

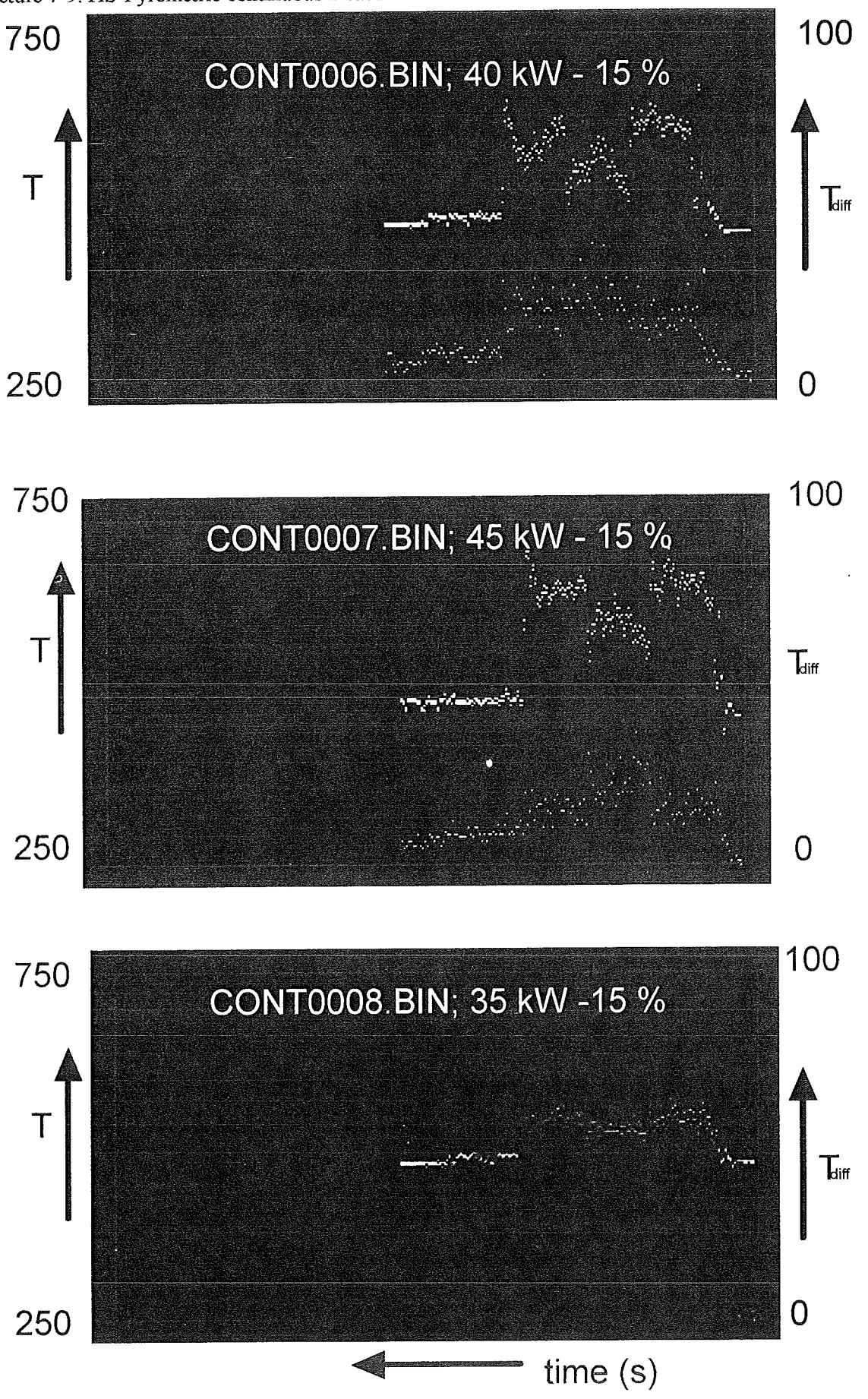

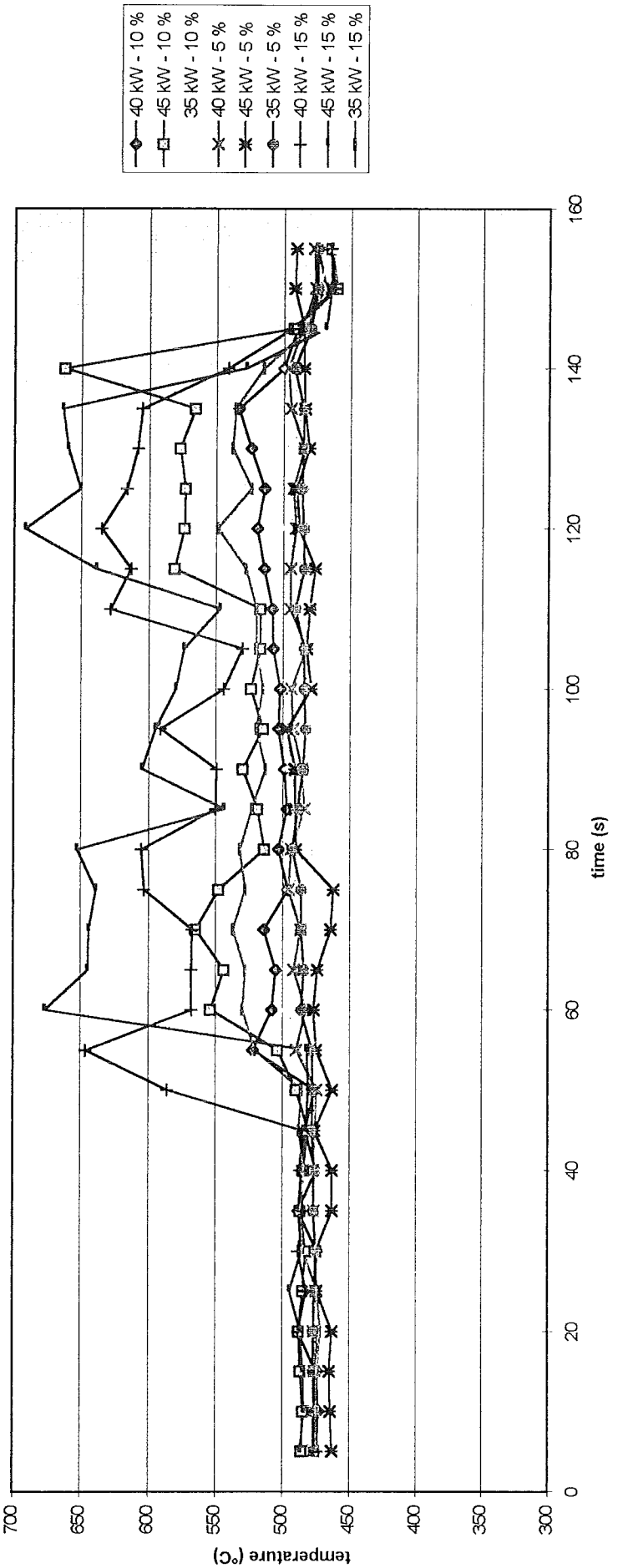

Fig. 7.2. HS-Pyrometric mean-temperature profiles.

The best reproducible temperatures were recorded, when the temperature was measured according to a fixed program. First 10 seconds was measured in the plasma (150 mm away on the right side of the substrate). To reach a stable powder flow, 40 seconds was waited and the temperature measured in the beam of plasma and powder gave only a very small rise in temperature.
Than the program of the positioner was started and a useful temperature profile with a length of 80 seconds was recorded. This was from right to left (400 mm), back and than one last time from right to left. It can be seen at the hard copy prints that the plasma has very limited influence on the temperature (Picture 7.1-7.9). The colours of the pictures 7.1-7.9 mean:

- white = maximum temperature;
- yellow = mean temperature;
- dark blue = minimal temperature;
- bright blue = difference temperature.

Every second these 4 temperature values are plotted to the screen from a total of 100 measurements.

The 5 % powder levels show almost no temperature increase of the substrate and the temperature load of to the substrate is limited. When less particles arrive, the pressurised air controls the cooling of the substrate better.

The 45 kW profiles show the most scattering in the difference temperature. This is caused by the high energy transfer. The gas expands more and is less stable. This was found back in the microstructural evaluation; the coating was less homogeneous and almost the same amount of porosity was found. Although at higher power level, higher gas and thus particle velocities give as a result, not necessarily results this in higher densities and better coatings.

The best result give the 10 % powder feed rate results. Although they show more scattering than 5 %, are they sprayed at a moderate traverse speed and this is of economical advantage.

The pictures 45 kW - 10 % and all 15 % show very clearly the turning points (3 times, see also the description of the continuously measurements in Appendix I).

For any unknown reason the cooling was moving from the right to left less effective as shown by all 15 % pictures.

Unfortunately at the moment the software does not offer the possibility of giving the temperatures as ASCII files to further more exact evaluation. The mean temperatures were transferred by hand to a spreadsheet program. This is the reason that this was done only every 5 seconds (Fig. 7.2).

7.5. Testing methods

The microscopic samples were cut into smaller parts and hot embedded in a plastic matrix (175 °C, 40 kN, 12 min). Than the samples were prepared on an Abramin type machine for light microscopic research according to the grinding and polishing program given in Table 7.3.
A light microscope, manufactured by Zeiss, type Axiophot, was used for the sample evaluation. The samples were researched and evaluated to a maximum magnification of 1000. The system is coupled to a 35 mm film camera.

Table 7.3. Sample preparation for light microscopic research.

abrasive SiC-graining	time (min)	force (N)	number of revolutions (min^{-1})
400	1,5	150	300
800	1,5	150	300
abrasive diamond plate	time (min)	force (N)	number of revolutions (min^{-1})
30 µm	2 x 2	200	300
20 µm	2 x 1	200	300
10 µm	2 x 1	200	300
polishing step cloth	time (min)	force (N)	number of revolutions (min^{-1})
3 µm	2 x 6	150	150
1 µm	2 x 8	100	150
end-polishing and etching	time (min)	force (N)	number of revolutions (min^{-1})
Op-chem OPS	1,5	50	150

An interactive image analysing system, IBAS 2000 of the firm Kontron, is used to estimate the porosity in the coating (Fig. 7.3). This system evaluates the prepared microscopic samples by estimating the total surface percentage of a marked phase. This marking is done manually by the user. Usually the porosity is the darkest phase of the microscopic image.

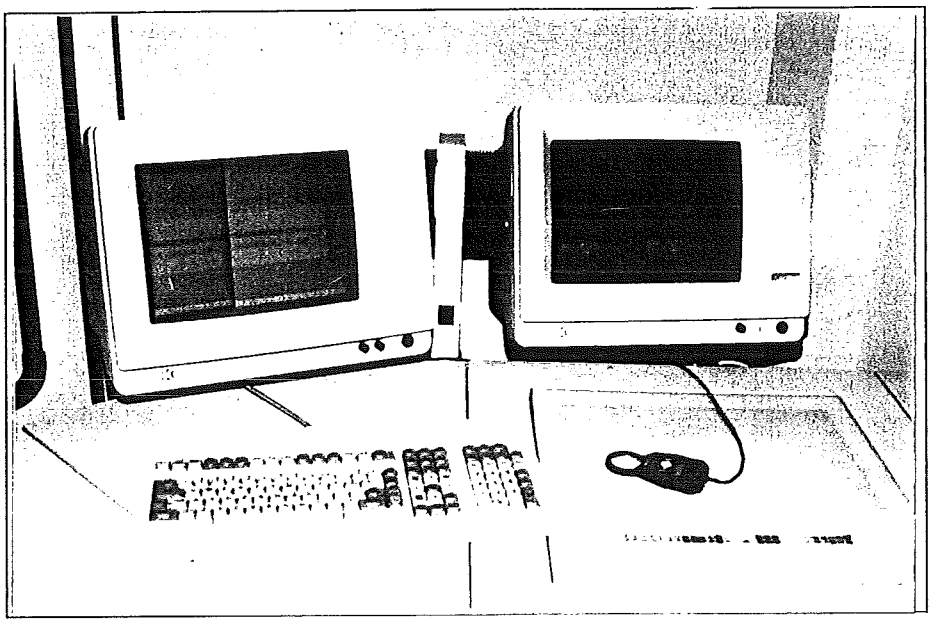

Fig. 7.2. The IBAS 2000 image analyses system.

To determine Vickers micro hardness a Micromet 1 tester of Buehler Ltd. was used. The magnification used is 400x for normal measurements and 1000x for single phases. The test force was 100 pounds (0,981 N) and the testing time 10 seconds. The testing body is a 4-side diamond-pyramid which locks-in an angle of 136 °. On the sample a quadrangle impression is made by plastic deformation caused by the diamond.. With a video graphical system the user marks the diagonals of the quadrangle and a computer calculates the Vickers hardness (Fig. 7.3).

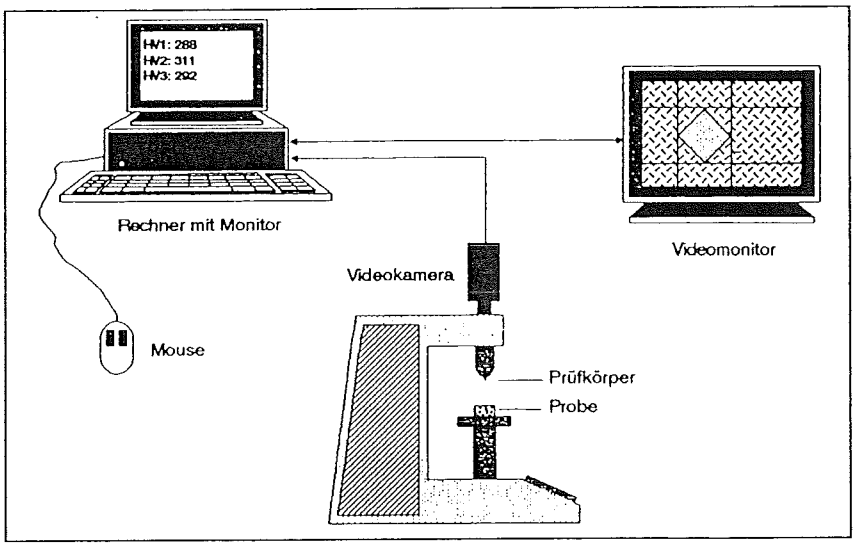

Fig. 7.4. The Micromet 1 microhardness test machine.

Determination of adhesive strength in tension is done according to DIN 50160 [107]. As substrate a cylinder with a diameter of 40 mm was coated (Fig. 7.5). For a regular test DIN needs at least 3 test samples sprayed under the same conditions. In this case 5 samples were sprayed.
With a special type HTK Ultrabond 100 (Hanseatisches Technologie Kontor GmbH) a counterpart was glued together with the coated substrate. The adhesive strength in tension sample is heated for 2 hours at 180 °C, to achieve reaction and good bonding of the glue.

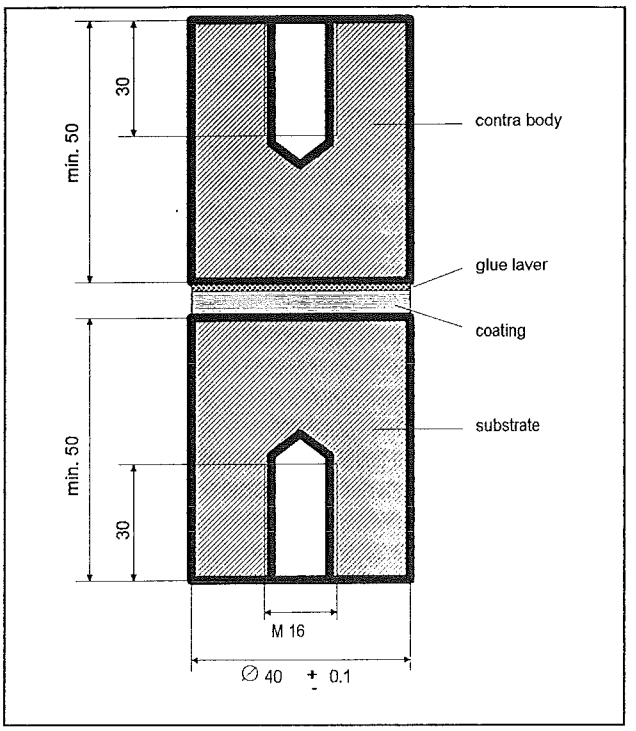

Fig. 7.5. Tensile Strength in Tension test sample

The sample is tested in an Amsler type UPN 10 SZD 560 machine. It has a maximum pull force of 100 kN.

Wear resistance was tested with two different methods;

- Taber disk are round samples and have diameter of 90 mm and a thickness of 4-6 mm. Two samples can simultaneously be tested to abrasive roll-gliding wear. The pressure on each side on two grinding rolls of sintered SiC is 1000 g (Fig. 7.6.).

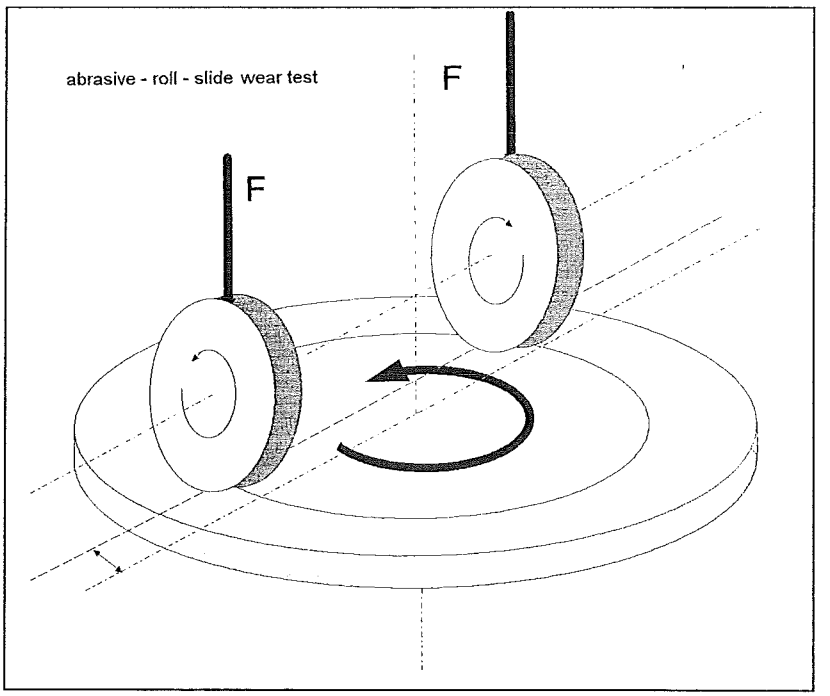

Fig. 7.6. Taber Disk abrasive wear test

- Pin-on-disk are cylindrical samples with a 14 mm diameter and a length of 40 mm. The wear is abrasively tested on SiC graining paper with a graining depending on the situation (120, 180, 240, 320, 400, 600 or 800). The pressure is 500 g and 4 samples can be tested simultaneously. Every 25 m the weight decrease of the sample is measured (Fig. 7.7).

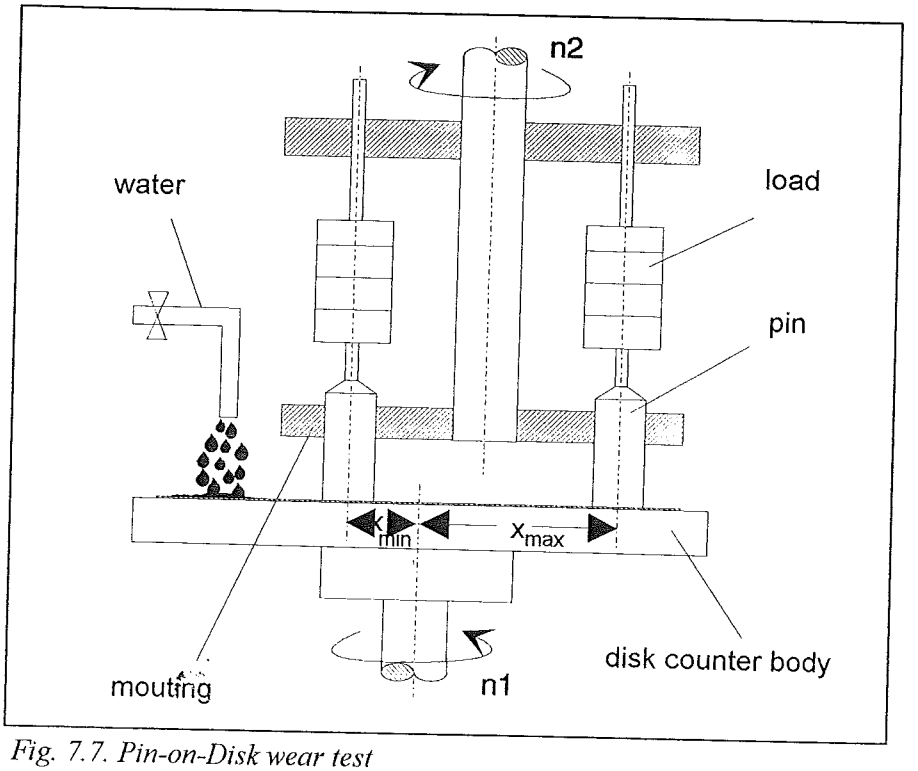

Fig. 7.7. Pin-on-Disk wear test

7.6. Results of Microstructural research

It was found that there were more particles broken out of the coating surface at the 35 kW sprayed samples, caused by preparation, although all the samples were prepared in the same way. This can be understood because a smaller power levels less energy is transferred to the plasma, resulting in smaller velocities and less heat input. Thus a smaller density and worse cohesion is the result. It was tried not to measure these out-breaks as porosity. The 45 kW coatings have lower porosity levels caused by better melting and thus better flowing around obstacles at the substrate.
It was expected that at a higher powder level (15 %), the heat is shared over more particles and the single particles would be heated less. This is also supported by the porosity measurements. Only at 45 kW the plasma has enough energy capacity, what is showed by the low porosity.

This also explains the coating thickness difference for same powder feed rates, but different power levels. Thickness vary 'very much'. At higher power levels, the particles were more effectively transported. This is the reason that the 35 kW coatings were sprayed too thin.

Table 7.4. Results of the porosity measurements (average over 5 measurements).

Nr.	Power-powder feed rate	porosity %	remarks
1	40 kW - 10 %	8,7	
2	45 kW - 10 %	7,3	
3	35 kW - 10 %	9,3	many break outs
4	40 kW - 5 %	10,3	
5	45 kW - 5 %	8,0	
6	35 kW - 5 %	9,0	many break outs
7	40 kW - 15 %	10,6	
8	45 kW - 15 %	6,3	
9	35 kW - 15%	11,5	many break outs

The aluminiumoxide (dark phase) has a much higher hardness and for this reason the phases were measured separately and together. For the hardness conclusions the mixed phase stays model, because this mixed phase determines the actual coating quality. Because the wide varying results it is difficult to give the trend here. Obviously 45 kW and 10 % powder feed rate gives the best hardness result. But the coating has as disadvantage that its brittle and contains cracks (Picture 7.13). By the way, it was the only crack of that size found in this substrate and all other substrates. A good cooling may prevent high temperature gradients during the spraying process and also prevent cracking of the coating.

Table 7.5. Results of the microhardness measurements (average over 3 measurements).

Nr.	Power-powder feed rate	grey phase $HV_{0.1}$	white phase $HV_{0.1}$	mixed phase $HV_{0.1}$
1	40 kW - 10 %	1025,9	761,4	840,4
2	45 kW - 10 %	1039,9	650,9	995,9
3	35 kW - 10 %	775,9	673,9	824,6
4	40 kW - 5 %	1079,8	727,1	927,7
5	45 kW - 5 %	1108,1	710,6	825,7
6	35 kW - 5 %	889,0	639,8	679,3
7	40 kW - 15 %	1021,1	752,3	793,7
8	45 kW - 15 %	1080,4	683,4	752,0
9	35 kW - 15%	978,1	549,2	718,3

Pictures of the 9 different coatings have been taken at magnifications of 200, 500 and 1000 x. It is extremely difficult to focus sharp over whole surface at a magnification and thus the picture of the 1000 times magnification is not perfectly focused (Picture 7.10-7.15).

Picture 7.10. shows the coating that was sprayed the most according to the adjustments given by Plasma Technik. The white at the top is the substrate material. It has little porosity and is a dense structure. The same coating is showed at a magnification of 500 x. It confirms the low porosity level and shows that they are 'very' small. Picture 7.12. shows the same coating at a magnification of 1000 x, which is not focused ideally, but the good quality is nevertheless recognised..

The brittle coating sprayed at 45 kW and 10 % powder feed rate is showed in Picture 7.13 At the left a long crack was developed.

Pictures 7.14 and 7.15 show the coating sprayed at 45 kW-15 % powder at magnifications of 200 x and 500 x respectively. Only the coatings of 15 % powder sprayed at this high power level showed good microstructure. The powder was well melted and the coating shows little break-out particles. But it contains more porosity than Picture 7.11.

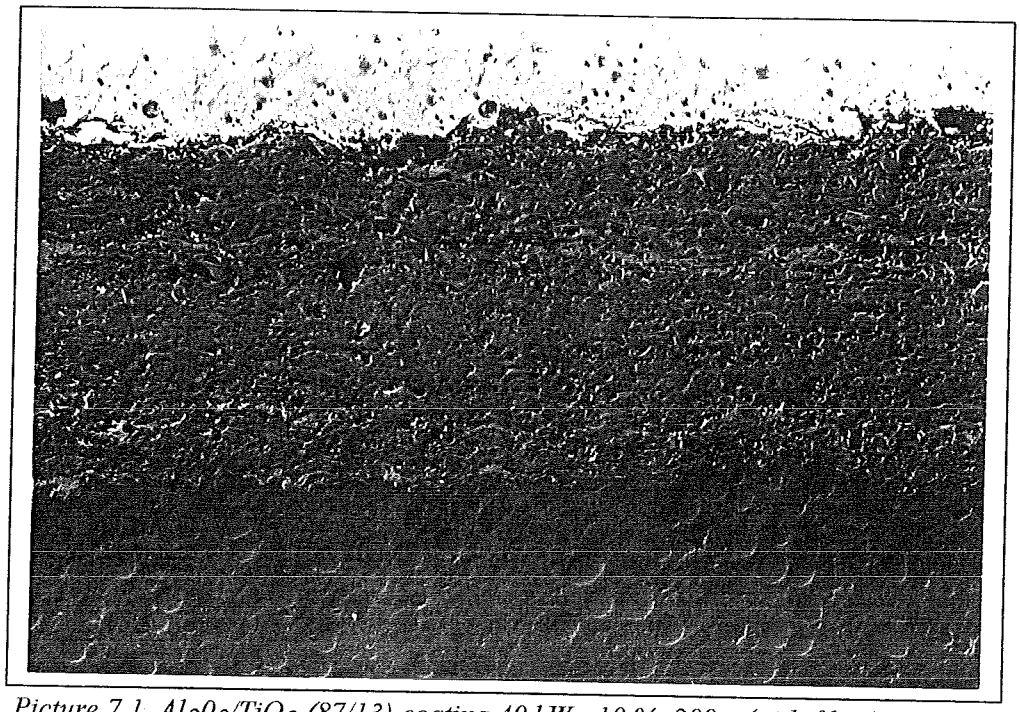

Picture 7.1. Al_2O_3/TiO_2 (87/13) coating 40 kW - 10 %, 200 x (with filter).

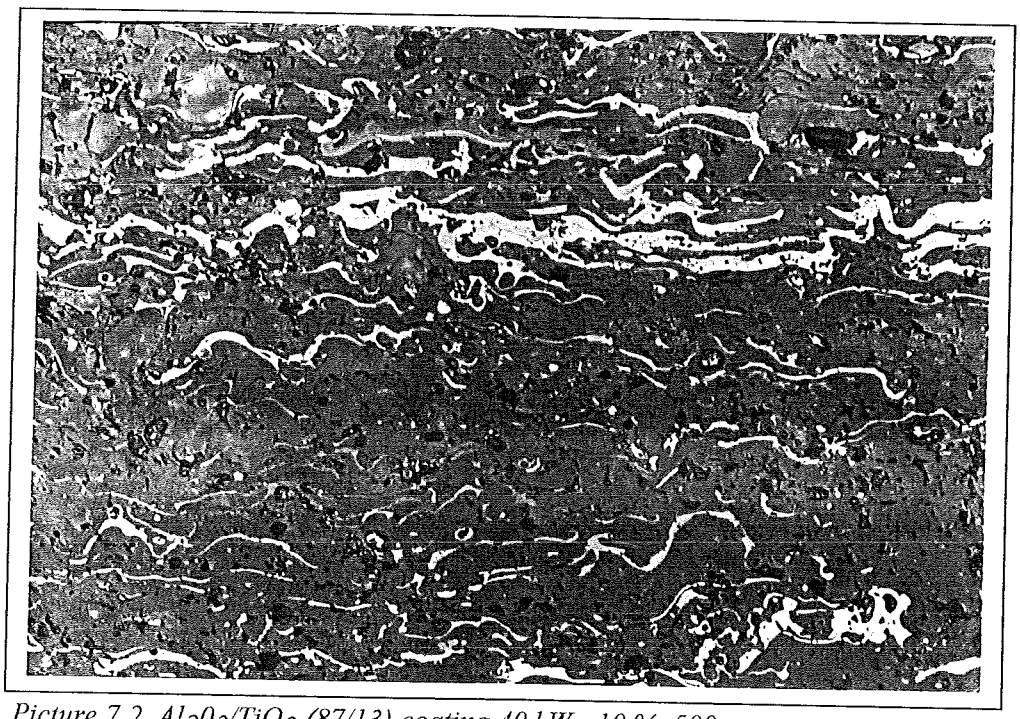

Picture 7.2. Al_2O_3/TiO_2 (87/13) coating 40 kW - 10 %, 500 x.

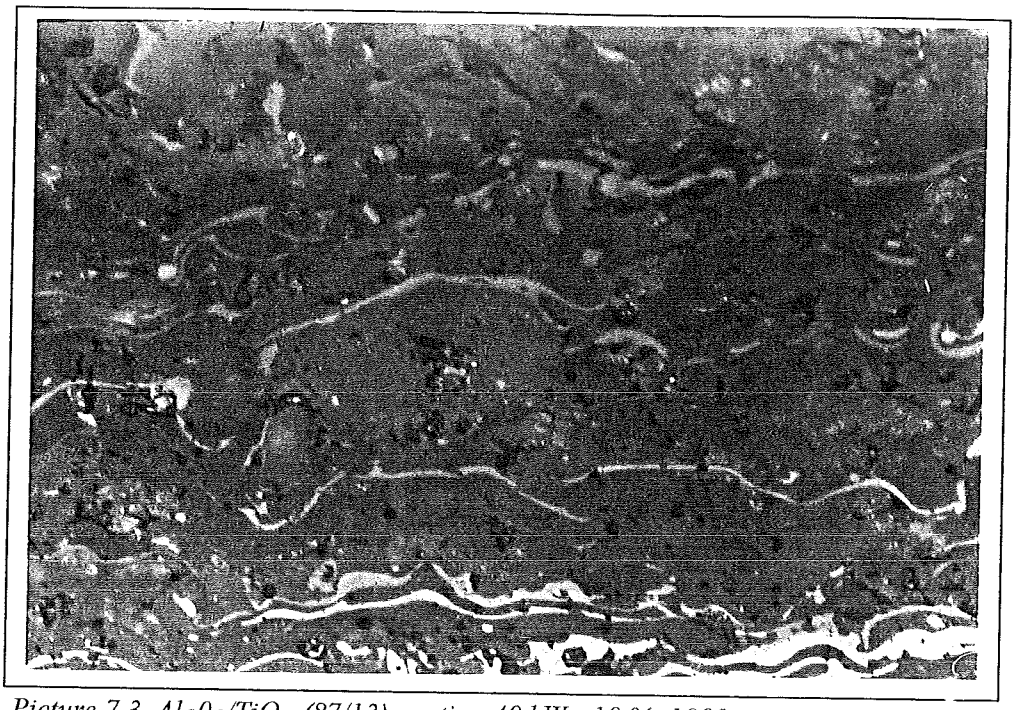

Picture 7.3. Al_2O_3/TiO_2 (87/13) coating 40 kW - 10 %, 1000 x.

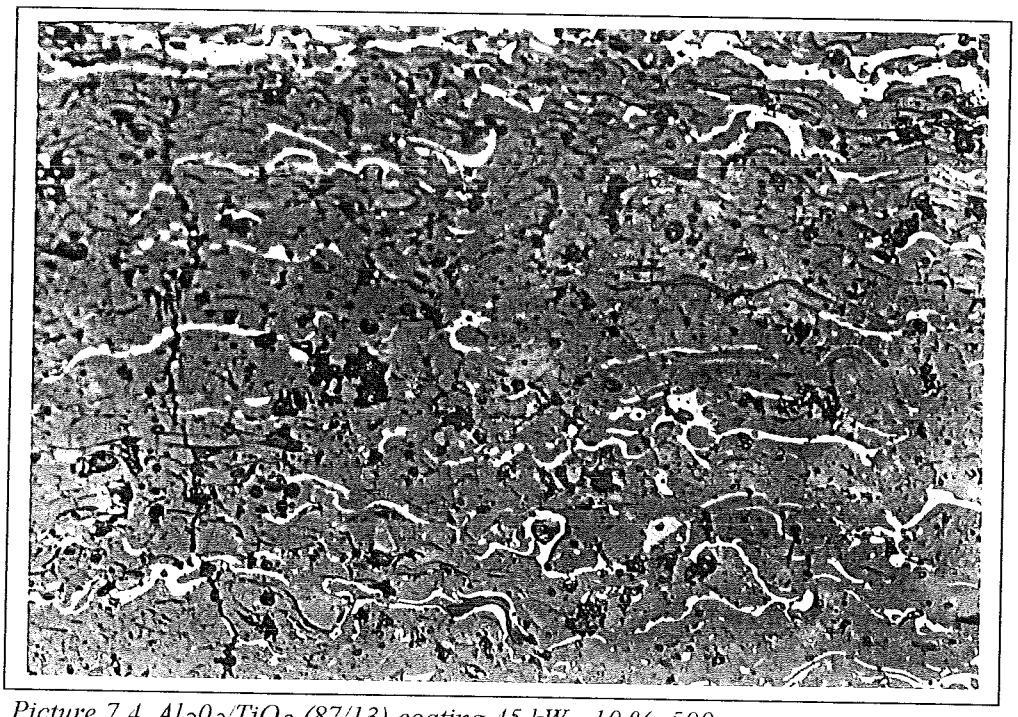

Picture 7.4. Al_2O_3/TiO_2 (87/13) coating 45 kW - 10 %, 500 x.

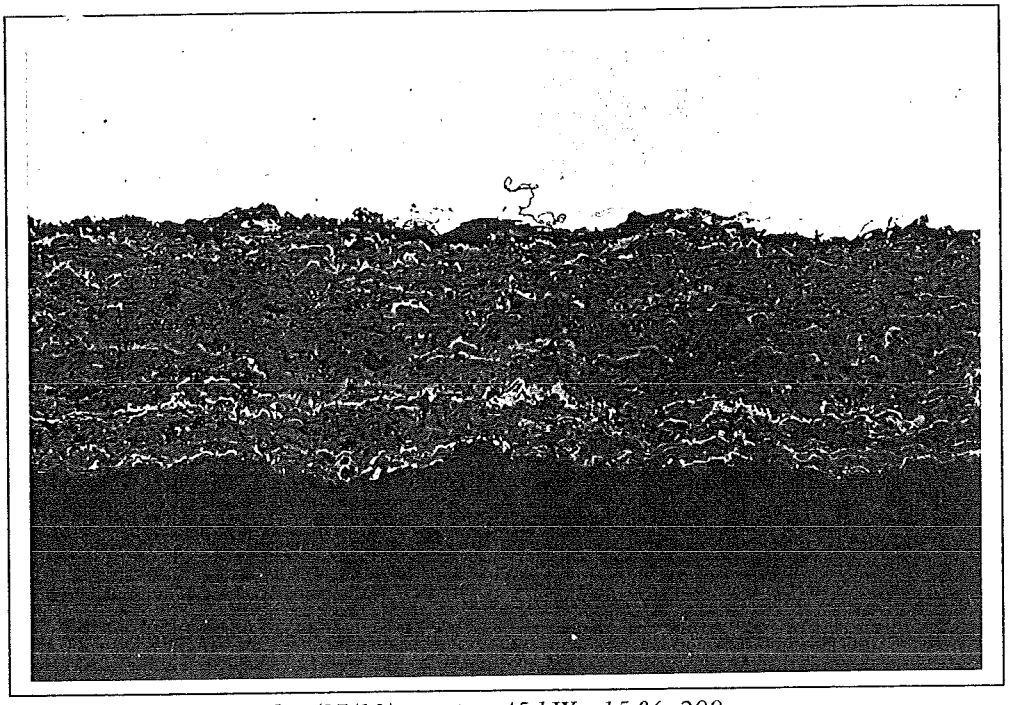

Picture 7.5. Al_2O_3/TiO_2 (87/13) coating 45 kW - 15 %, 200 x.

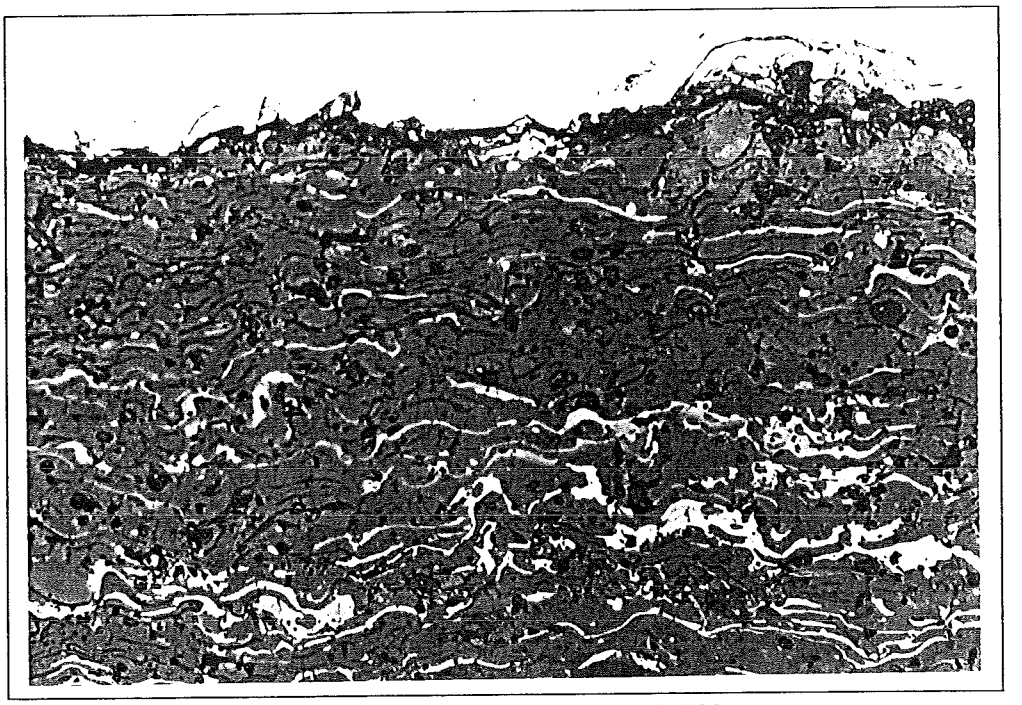

Picture 7.6. Al_2O_3/TiO_2 (87/13) coating 45 kW - 15 %, 500 x.

7.7. Results of Mechanical and Wear Tests

The adhesive strength in tension was calculated from only those of 5 test results of which the coating caused of the failure. A very good value has the series 6x, this can be explained by a relatively 'high' porosity level; and the glue searched his way through the relatively porous coating and contributed to the strength. Strange result is the higher strength of 7x compared to 8x. At this powder feed rate is a better melting at 45 kW expected and thus better coating. The difference however is not very different and is explained by the sensitivity of the process to mistakes during one of the preparation phases: plane turning, sand blasting, spraying process, applying the glue, heating phase and speed of the pull-machine that differs. Honest values seem to be the ones of 2x and 8x.

Table 7.6. Average values of Adhesive Strength in Tension Test:

Sample-Nr.	Power-powder feed rate	F_m (N / mm^2)
1x	40 kW - 10 %	54,9
2x	45 kW - 10 %	63,5
3x	35 kW - 10 %	64,6
4x	40 kW - 5 %	51,3
5x	45 kW - 5 %	48,4
6x	35 kW - 5 %	67,8
7x	40 kW - 15 %	58,6
8x	45 kW - 15 %	56,6
9x	35 kW - 15%	48,0

Before testing of the Taber disk samples they should be grinned to remove the surface roughness and to make a plain surface. This has been done for the numbers 10, 11, 20, 21, 30. Due to relatively thin coating on the 3x samples, the coating was worn out already after 2000 turns. Comparison was not possible and for this reason these results are left out.
The exact dates for the samples, tested without plain grinding are given in Appendix L. Figure 7.8. gives a summary of the Taber disk results. The 35 kW samples show the highest wear level. This is caused a by the less heat input and smaller plasma and particles velocities. Thus these coatings have a smaller density. It confirms the break-out particles observed by the for microstructure prepared samples. The lamellae have do not show optimal cohesion. The 35 kW - 5 % coating shows the best result for the 35 kW adjustments. Most heat available for the number of particles.

The relatively thin coating also gave problems at the Pin-on-Disk tests. At a graining paper of 400 the 35 kW samples were worn out already after 50 m. (exact dates are given in Appendix K). For this reason the samples were also tested on 800 graining paper. Fig. 7.9-11 give the results of the Pin-on-Disk experiments. The same trend here as at the Taber disks is observed: higher power levels show less wear. The 45 kW - 5 % adjustment shows the best result. High plasma velocity, high heat transfer to the particles. The particles were very good molten and follow the irregularities of the substrate surface at the impact.

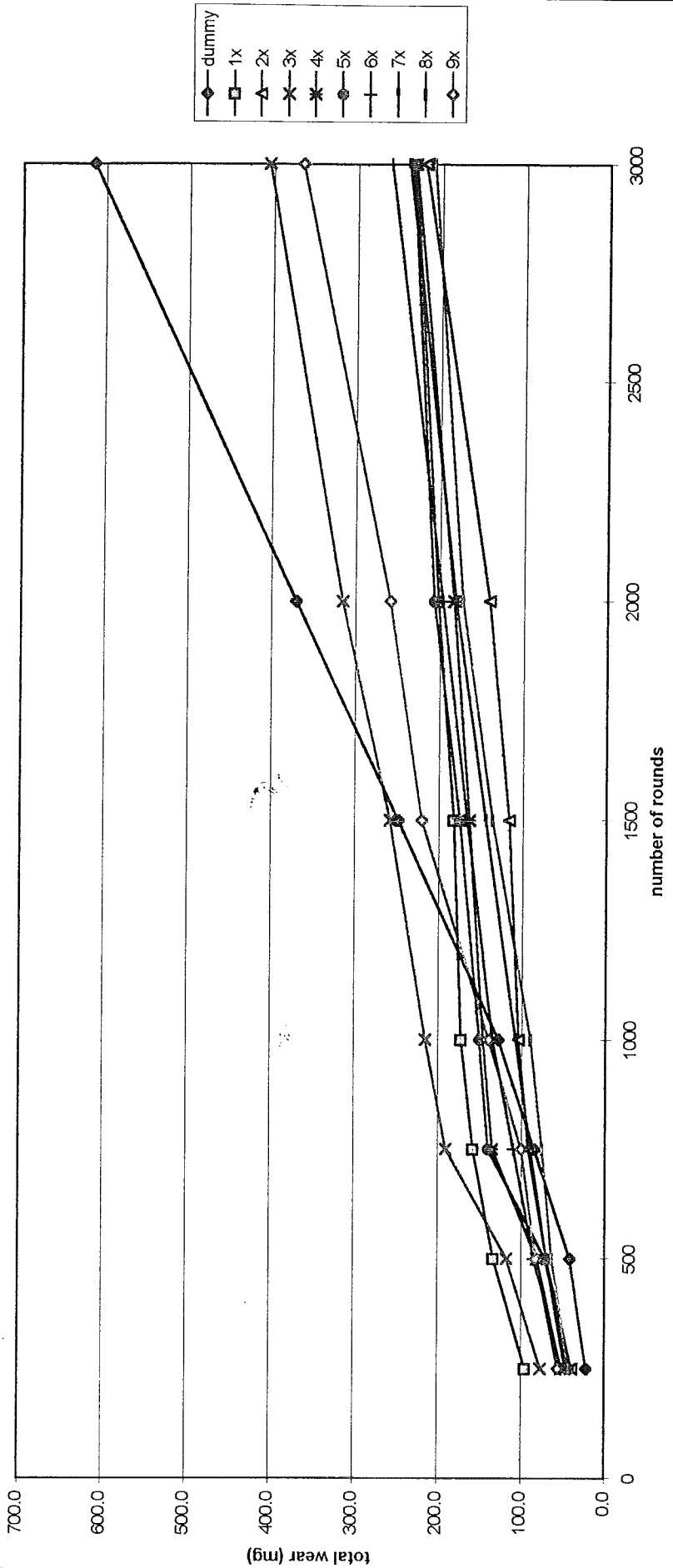

Fig. 7.8. Wear results of the Taber Disk test

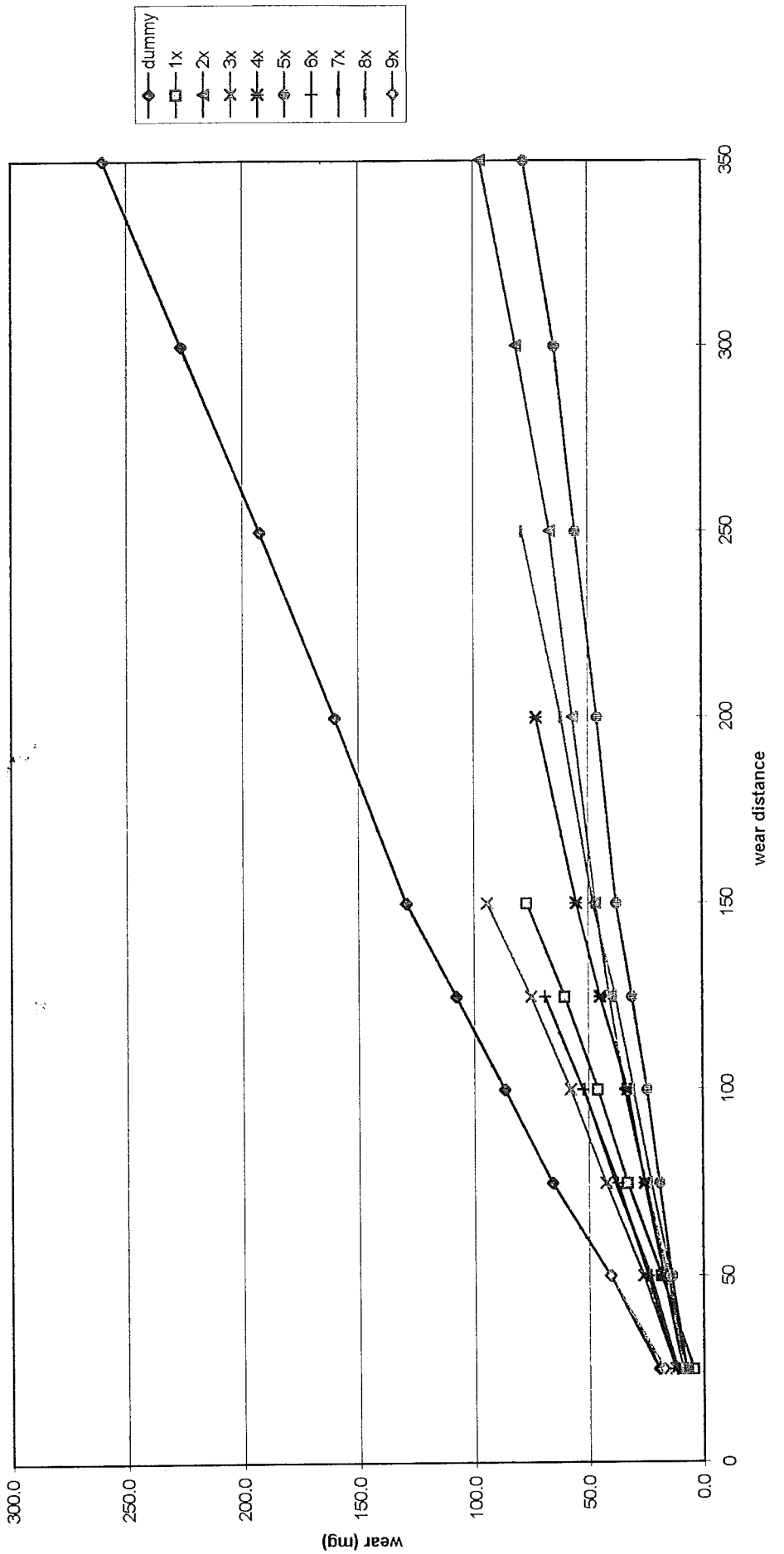

Fig. 7.9. Wear results of the Pin-on-Disk test

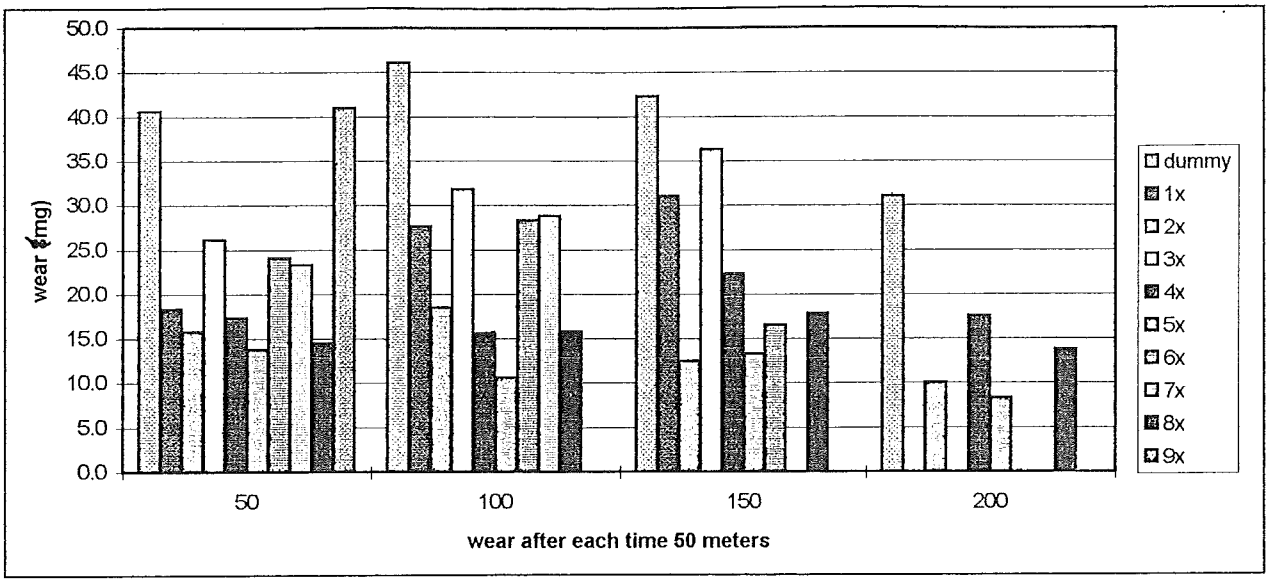

Fig. 7.10. Comparison of the wear of the Pin-on-Disk samples after 50 m each time.

7.8. Summary of the optimisation

Standard parameters published by the Plasma Technik AG were chosen as start parameters. To this a matrix of 9 combinations between power of 35, 40, 45 kW and powder feed rate 5, 10, 15 % has been researched.

The results summarised:

- The best pyrometric results with limited scattering were found at the 10 % powder feed rate adjustments;
- For adhesive strength in tension samples 2x gave the best reliable result: 63,5 N/mm^2;
- The microstructure of the first series was the most homogenous one and stable one (2x showed cracks);
- Low porosity levels showed the 45 kW samples;
- Microhardness was the best for 2x: 995,9 $HV_{0,1}$ (cracks were found);
- Best Taber sample was 45 kW - 10 %;
- Best Pin-on-Disk was 45 kW - 5 %.

The 5 % powder feed adjustment gave good results, this powder feed rate however has as disadvantage that the coating is sprayed at a low traverse speed to achieve a sufficient coating thickness. It took about 35 minutes to spray the whole set, which of course is ineffective and expensive. If it had been the case to much better coatings were produced it might be worthwhile.

The average 10 % powder feed rate showed good results and only for wear resistance, the 5 % coatings were better. For hardness, the 45 kW - 10 % was the best, but the substrate temperature should be better controlled to avoid cracking.

8. Conclusions and Discussion

This engineering thesis consists of an extended theoretical introduction to the wide Thermal Spraying field and also of the results of an experimental work that was carried out.

Nowadays an increasing number of machine parts for high-tech applications are coated to give protection against corrosive, oxidative, wear, erosion and chemical aggressive environments. Thermal Spraying is a very important coating method for depositing relatively thick protective layers. Among the different Thermal Spraying methods Plasma Spraying is the most versatile one. Several different Plasma Spraying techniques have been developed in the last decades. A modern Plasma Spraying system (CAPS) is capable of handling all these Plasma Spray variations.
The coatings are used for technical, chemical, optical, medical, electrical and decoration purposes and are employed in aerospace, automotive, chemical and offshore industries. Almost all combinations of metals, hard-metals, alloys, ceramics, cermets, plastics and fibre-reinforced plastics are possible. Before a coating is sprayed, the substrate material is thoroughly cleaned and roughened.

In the Plasma Spraying process more than 80 parameters influence the coating process and quality. A high quality coating leads to a good environmental resistance, long term stability and strong adhesion. Extensive and expensive research is necessary to find the best adjustment of the Plasma Spraying system. Research to improve coating systems in the last decades was mostly empirical. This 'trial and error' type of optimisation has many disadvantages:

- time intensive procedures, expensive resources and manpower;
- the optimised adjustment and coating quality may not be found;
- destructively testing of batch series necessary;
- the optimisation of indirect parameters is ineffective (power level, spraying distance, gas flow rate);
- no process control and quality control;
- not any suitable non destructive test method is available to inspect the coating after spraying and during its lifetime;
- for every new substrate-coating-system the process has to be repeated many times.

In order to meet new demands to coatings systems, to reduce research time and to save resources, new developments are necessary. Chapter 4 describes the actual developments, which may help the to fulfil the decreasing requirements. Their features and advantages as well as disadvantages are described.

Noncontact optical methods are suitable for measuring parameters that directly influence coating quality instead of indirect process parameters (e.g. spraying distance, powder rate, gas flow). It may lead to process monitoring and Quality Control; the process can be regulated when irregularities appear. For example the spraying system can immediately be regulated, when a decreasing power level, caused by wear of the nozzle, is detected by more scattering of the substrate temperature. When no deviations from ideal setting appear, the resulting coating-quality can be predicted in a much better way, without destructive testing.

Process Modelling and Simulation help to increase the scientific understanding of the process and this may lead to a reduction of the number of necessary experiments. Experiments remain necessary in order to gather information and to check calculations. Once a model has been developed it can be adjusted with limited effort to other materials geometry and materials. It may be possible to determine the complex internal stresses in coating systems and determine optimised coating thickness and

combination with different layers. Exact data of physical properties such as Reynolds numbers, heat capacity and modules of elasticity in a coating often fail and this leads to many estimations.

Statistical Design of Experiments is based on statistical mathematics. The goal is to find trends, which gives hand to experiments which might be useful and thus limit the necessary number of experiments. This tool must be handled with care and cannot be used without a good fundamental knowledge of the process, because estimations about the relations between the parameters to be optimised have to be made.

Non Destructive Testing methods are very important for coated parts which have to be used and for controlling parts that are in use. For detection of the small flaws ceramic coatings, new developments remain necessary.

The fifth chapter extensively describes the theory, set-up and problems of Pyrometry, based on the radiation law of Planck. For real bodies the Planck radiation formula for a black body (no reflection and transmission of radiation) is justified by adding an emission coefficient for regular bodies. The coefficient is a function of wavelength, temperature, surface roughness, measurements angle, etc.

For the start of the experimental work, the gas flows and the current-display of the APS Plasmadyne system were newly calibrated and furthermore a Pyromete-holder as well as a sample holder was designed and constructed. The pyrometric hard- and software was extensively tested and improved.

The HS-Pyrometer was used to optimise Al_2O_3/TiO_2 (87/13) coatings on St-37/2. Two parameters that were expected to influence the heat-input in the substrate were chosen to be optimised. Standard parameters published by the Plasma Technik AG were chosen as start parameters. A matrix of 9 combinations between power of 35, 40, 45 kW and powder feed rate 5, 10, 15 % had been researched. Temperature profiles were recorded, microstructure was examined and mechanical properties were tested.

Microscopic evaluation and mechanical destructive testing do not give explicit and indisputable the best adjustment of parameters and exactly this underlines the importance of the development of process control methods as Pyrometry.

It was found that the coatings sprayed at a power of 40 kW with 10 % powder feed rate gave good results. The microstructure was homogeneously, had a relatively low porosity level and good mechanical properties. The substrate temperature showed a stable profile with little scattering, which indicates to a steady constant process.

The 5 % powder feed adjustment also gave good results (not always the best!). The small powder feed rate however has as disadvantage that the coating is sprayed at a low traverse speed to achieve sufficient coating thickness. It took about 35 minutes to spray one whole set, which is ineffective and expensive. These sample showed the best wear resistance.

Although the pyrometric measurements do not totally convince to be 'the solution' for process control and optimisation, the results encourage further research. Other indirect parameters which are expected to have influence the heat input and coating quality are among other parameters spray distance and powder gas rate and. will be optimised in the near future.

Appendix A: List of symbols

Symbol	Value	Dimension	Quantity
α	0...1		absorption grade
ε	0...1		emissivity (or spectral emission coefficient)
ε_λ	0...1		spectral emissivity
ε_t	0...1		total emissivity
λ		m	wavelength
λ_0		m	wavelength in vacuum
λ_{eff}		m	effective wavelength in band-Pyrometry
λ_{max}		m	wavelength, where spectral radiation-density is maximal at T-isotope
σ	5,6697 E-8	$Wm^{-2}K^{-4}$	constant of Stefan-Boltzmann
ρ	0...1		reflections grade
ε	0...1		transmissions coefficient
Φ		W	radiation flow
$C1=2\pi \cdot c_0^2 h$	3,7418 E-16	Wm^2	constant of Planck's radiation law
$C2=c_0 \cdot h/k$	1,4388 E-2	m•K	constant of Planck's radiation law
c_0	2,99792458 E8	ms^{-1}	light speed in vacuum
$d\lambda$		m	wavelength interval
dL_λ		m	spectral radiation density interval
dT		K	temperature interval
G		V	correcting factor for DC drift
h	6,62618E-34	Js	Planck 's constant
I		Wsr^{-1}	radiation intensity
K_1			correcting factor for optical system
K_2			sensitivity
K_3			multiplicationsfactor
k	1,38066E-23	JK^{-1}	constant of Boltzmann
k_w	2,8978E-3	m•K	constant of Wien
L		$Wm^{-2}sr^{-1}$	radiation density
L_B		$Wm^{-2}sr^{-1}$	radiation density for black body
L_λ		$Wm^{-3}sr^{-1}$	spectral radiation density
$L_{\lambda B}$		$Wm^{-3}sr^{-1}$	spectral radiation density for black body
L_{1B}		$Wm^{-3}sr^{-1}$	spectral radiation density at wavelength 1
M		Wm^{-2}	spectral radiation
M_B		Wm^{-2}	spectral radiation for black body
N		Wm^{-3}	total radiance density
N_B		Wm^{-3}	total radiance density for black body
n			index of refraction
Q		J	Radiation energy
R			temperature ratio
R_B			temperature ratio for black body
$S(\lambda)$			wavelength dependent part for radiation density detector
T		K	absolute real temperature
T_B		K	temperature of black body
T_r		K	ratio temperature
T_{sur}		K	temperature of the surrounding
U(T)		V	electric output

Appendix B: List of used Abbreviations

AG	Arbeitsgemeinschaft
AIF	Arbeitsgemeinschaft industrieller Forschungsvereinigungen
APS	Atmospheric Plasma Spraying
ASM	American Society for Materials
CAP	Controlled Aspiration Plasma Spraying
CAPS	Controlled Atmosphere Plasma Spraying
CCD	Charge Coupled Device
DA-convertor	Digital-Analogue converter
DIN	Deutsche Industrie Norm
DVS	das Deutschen Verbandes für Schweißtechnik e.V.
FE	Finite Element
HGP	Hochgeschwindigkeits-Pyrometrie
HS-Pyrometry	High-speed Pyrometry
HVOF	High Velocity Oxygen Fuel Spraying
IPS	Inert Plasma Spraying
IR	Infrared
IRP	Infrarot-Pyrometrie
ITSC	International Thermal Spraying Conference
LDA	Laser Doppler Anemometry
LDV	Laser Doppler Velocimetry
LPPS	Low Pressure Plasma Spraying
MCP	Micro Channel Plate
MCrAlY	Anti Hot-corrosion Coating, M=Fe,Ni,Co
NTSC	National Thermal Spraying Conference
PPCS	Pyrometric Process Control System
PSIG	Pound per Square Inch Gas
RSM	Responce Surface Methods
RWTH	Rheinisch-Westfälische Technische Hochschule
SCFH	Standard Cubic Feet per Hour
SDE	Statistical Design of Experiments
SEP	Statistical Experiment Planning
SPS	Shrouded Plasma Spraying
QC	Quality Control
SLPM	Standard Litre per Minute
TBC	Thermal Barrier Coating
UPS	Underwater Plasma Spraying
UV	Ultraviolet
WW	Werkstoffwissenschaften

Appendix C: Review of Functions of Coatings

Table C1. Functions of the most important materials [4]:

Coating		Application							Maximum temperature
		Corrosion protection	Oxidation protection	Wear protection	Gliding coating	Bonding coating	Repairing coating	Other	[°C]
M	Aluminium	•							400
e	Zinc	•							250
t	Nickel					•			500
a	Mb			•	•	•			320
l	Lead	•						radiation protection	200
s	Al-Mg	•							200
	alloyed steel	•		•			•		~ 500
a n	Co substrate with Al_2O_3 or Cr_2O_3		•	•					~ 1000
d	CoMoSi (Tribaloy)			•	•				~ 1000
A	NiAl, NiCr					•	•		950
l	Nickel-graphite				•				500
l o	MeCrAlY Me=Fe, Co, Ni	•	•						~ 1000
y	Brass, Bronze				•				< 200
s	Hardalloys with matrix Fe, Co, Ni and Borides, Carbides, Silicides with elements V, Cr, Mo, W			•					800
Bori de	TiB_2, ZrB_2			•					*
Car- bide	TiC, Cr_3C_2, NbC, TaC, WC			•					400 TiC 500 WC
	WC-TiC TaC-NbC			•					
	Cr_3C_2-NiCr WC-Co			v					800 500
Oxi- de	Al_2O_3, TiO_2 Cr_2O_3, ZrO_2			•				TBC (**)	*
	Al_2O_3-TiO_2 Al_2O_3-MgO Cr_2O_3-TiO_2			•				TBC (**)	*
	ZrO_2-MgO ZrO_2-CaO ZrO_2-SiO_2			•				TBC (**)	*

*) Temperature is limited by the substrate

**) Thermal Barrier Coating

Appendix D: Survey of some Emission Coefficients

Table D1. Emissivities according to Glückert [87]:

Material		temperature (K)	$\varepsilon_{\perp}$
aluminium:	highly polished	480	0,038
	oxidised	370	0,2-0,35
gold	highly polished	370	0,018
copper	highly polished	310	0,02
	black oxidised	310	0,78
brass	polished	370	0,09
	mat	370	0,2
	oxidised	370	> 0,6
nickel	polished	370	0,1
	oxidised	370	> 0,6
steel	polished sheet metal	310	0,1
	rough oxidised sheet metal	310	0,8
	stainless steel	300	0,15
tungsten	wire	310	0,03
		3500	< 0,4
concrete	rough	310	0,94
plaster		310	0,9
glass		340	0,93
wood		310	0,90
marble		310	0,94
paper		310	0,96
sand		300	0,94
water	large layer	300	0,96
	ice	270	0,98
	snow	270	0,82

Table D2. Emissivities according to Engel [23].

Radiator-group	Radiator	Total emissivity coefficient	Spectral emissivity at ε=0,65 µm
High emissivity ε < 0,7	Carbon	----	0,84...0,98
	Graphite	0,71...0,76 (100...500 °C)	0,75...0,82 (smooth)
	Iron oxide (thick layer)	0,71...0,9	0,8...0,98 (1600 °C)
	Copperoxid (thick layer)	----	0,7...0,8
Semi-Large emissivity 0,3...0,7	Iron oxide (thin layer)	0,8	0,8
	Copperoxid (thin layer)	0,57	0,6...0,7
	Nickel oxide (thin layer)	0,37...0,48	0,68...0,75
	Oxidised brass	0,59...0,61 (200...600 °C)	----
low ε < 0,3	Pure iron	0,05...0,08	0,33 (925...977 °C) 0,43...0,5 (1530...1930 °C)
	Steel	0,05...0,10	0,41...0,52 (1510...1650 °C)
	high-grade steel	----	0,15...0,36
	Copper	0,15 (1000 °C)	0,11...,014 (solid) 0,15 (liquid)
	Nickel	0,06...0,19 (400...1000 °C)	0,36 (solid) 0,37 (liquid)
	Aluminium	0,06 (500 °C)	0,12...0,17 (700...1000 °C)
	Brass	0,02...0,05	----
Very changeable emissivity 0...1	Nickel as delivered	0,625	----
	Nickel cleaned	0,592	----
	Nickel polished	0,334	----
	Nickel heavily oxidised	0,9	----
	Iron	0,2...0,98	----
	Aluminium clean	0,04...0,06	0,12...0,17
	Aluminium oxidised	0,1...0,2	0,22...0,4
	Brass mat	0,07	0,22
	Brass browned	0,4	0,4
	Brass polished	0,03...0,04	0,04...0,05

Table D3. Spectral emissivity of oxides [106].

material		observed value	probable value for oxide formed on smooth metal
oxide	aluminium	0,22-0,40	0,30
	beryllium	0,07-0,37	0,35
	cerium	0,58-0,37	----
	chromium	0,58-0,80	0,70
	cobalt	0,60-0,80	0,75
	columbium	----	0,70
	copper	0,55-0,71	0,70
	iron	0,60-0,80	0,70
	magnesium	0,63-0,98	0,20
	nickel	0,10-0,43	0,90
	thorium	0,85-0,96	0,50
	tin	0,20-0,57	----
	titanium	0,32-0,60	0,05
	uranium	----	0,30
	vanadium	----	0,70
	yttrium	----	0,60
	zirconium	----	0,40
oxidised	alumel	----	0,87
	cast iron	----	0,70
	chromel P (90 Ni-10Cr)	----	0,87
	80Ni-20Cr	----	0,90
	60Ni-24Fe-16Cr	----	0,83
	55Fe-35.5Cr-7.5Al	----	0,78
	70Fe-23Cr-5Al-2Co	----	0,75
	constantan (55Cu-45Ni)	----	0,84
	carbon steel	----	0,80
	stainless steel	----	0,85
	porcelain	0,25-0,50	----

Appendix E: Calibration of the PPCS

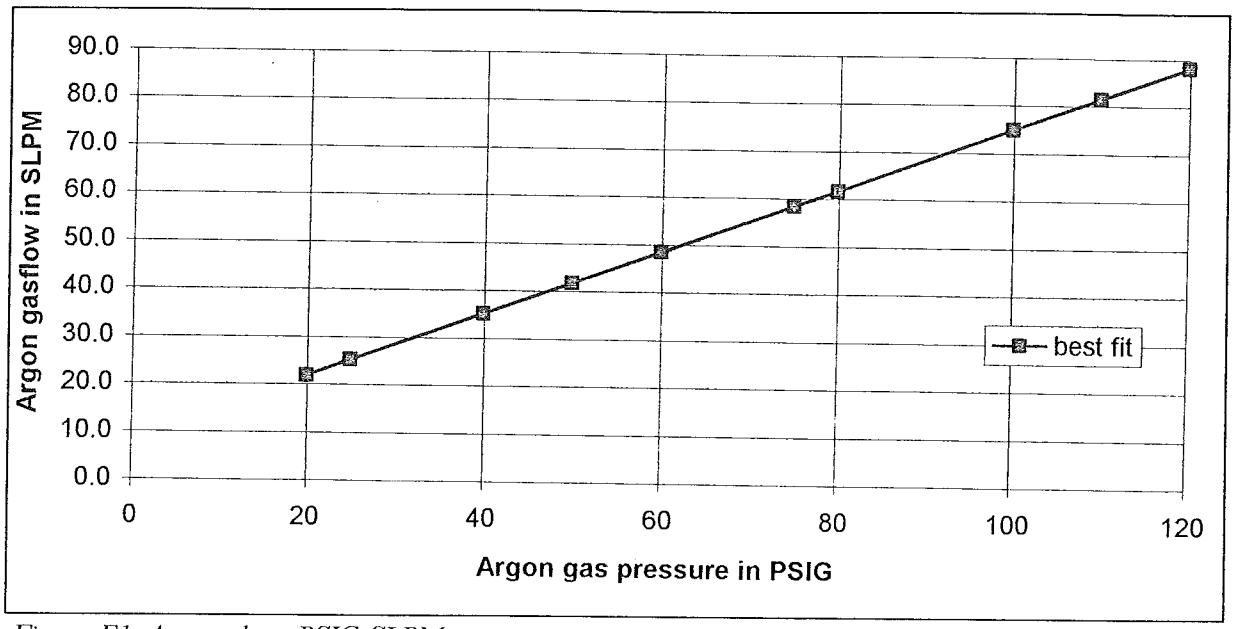

Figure E1. Argon chart PSIG-SLPM.

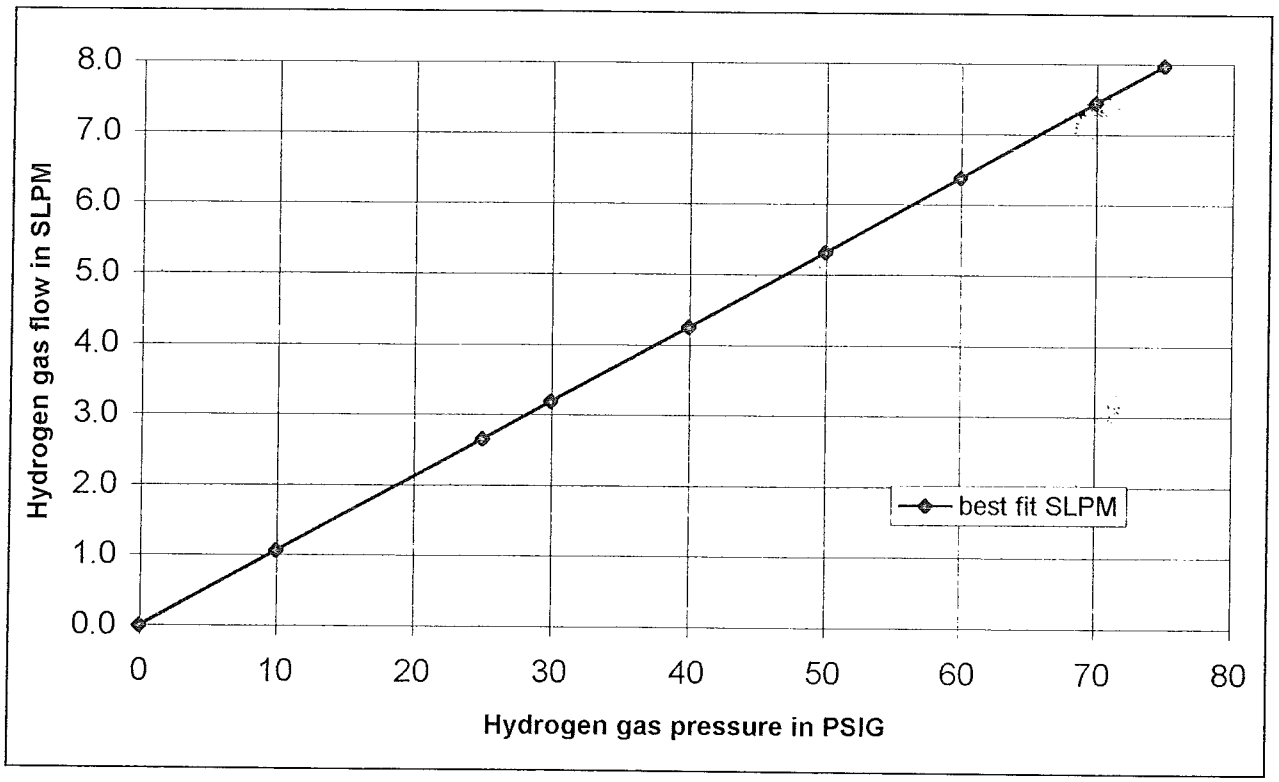

Figure E2. H_2 chart PSIG-SLPM:

Table E3. Powder mass flow calibration for 5 %, 10 % and 15 % at 5 SLPM gas flow.

percentage	time (min)	weight (g)	flow (g/min)	average (g/min)
5 %	4	24,068	6,017	**5,8**
5 %	3.30'	19,895	5,684	---
10 %	3.45'	44,263	11,804	**11,6**
10 %	3.30'	39,803	11,372	---
15 %	4.30'	77,223	17,161	**17,1**
15 %	3.30'	59,377	16,960	---

Appendix F: Plasma Spraying Protocols

Spritzprotokoll Plasmadyne		Brenner:	F4
		Pulvergeber:	PT Twin-10C
		Pulver-Material:	Al_2O_3/TiO2 (87/13)
Bearbeiter:	F. Ladru	Korngrößenvert.:	-45 +22,5
Datum:	26-05-1994	Typ:	744,1 HC Starck
		Behandlung:	none

Proben			
Nummer:	1x	2x	3x
Versuchszweck:	optimization, engineering thesis		
Material:	St.-37		
Geometrie:	complete set		
Plasmadyne			
Strom (A):	800	900	710
Spannung (V):	50 (49,6-50,1)	50 (49,9-50,4)	50 (48,8-49,0)
Leistung (kW):	40	45	35
Ar (PSIG-SLPM):	50-41,8	50-41,8	50-41,8
H_2 (PSIG-SLPM):	20-2,2	20-2,2	20-2,2
N_2 (PSIG-SLPM):	none	none	none
He (PSIG-SLPM):	none	none	none
Pulvergeber			
Trägergasrate (SLPM):	5	5	5
Pulverförderrate (%-g/min):	10-11,4	10-11,4	10-11,4
Rührer (Umdrehungen/min):	40	40	40
Heizung (°C):	40	40	40
Verfahr-Parameter			
Vorschub; FMAX X-RAMPE X:	580-200	580-200	580-200
Vorschubgeschwindigkeit (cm/s):	2	2	2
Bahnbreite (mm):	5	5	5
Sonstiges			
Spritzabstand (mm):	120	120	120
Übergänge:	1	1	1
Kühlung (bar):	2,5 (L+R)	2,5 (L+R)	2,5 (L+R)
Schicht			
Qualität der Schicht:	optisch very good, equal surface	optisch very good, equal surface	optisch very good, equal surface
Substrat-Dicke (mm):			
Nach Beschichten (mm):			
Dicke der Schicht (µm)	~210	~275	~120
Gewicht vorher (g):			
Gewicht nachher (g):			
Gewicht der Schicht (mg):			
Pyrometer BP 100			
Geschwindigkeit (cm/s)	1,5	1,5	1,5
Verzeichnis:	240594	240594	240594
Datei-Name:	CONT0002.BIN	CONT0004.BIN	CONT0003.BIN
Screen-kopie-Name:	GRAB1040.TIF	GRAB1045.TIF	GRAB1035.BIN
ε:	0,2	0,2	0,2
Totale Zeit (s):	157	155	160

Spritzprotokoll Plasmadyne			
		Brenner:	F4
		Pulvergeber:	PT Twin-10C
		Pulver-Material:	Al_2O_3/TiO2 (87/13)
Bearbeiter:	F. Ladru	Korngrößenvert.:	-45 +22,5
Datum:	02-06-1994	Typ:	744,1 HC Starck
		Behandlung:	none

Proben			
Nummer:	4x	5x	6x
Versuchszweck:	optimization, engineering thesis		
Material:	St.-37		
Geometrie:	complete set		
Plasmadyne			
Strom (A):	800	900-910	710-720
Spannung (V):	50 (49,5-50,4)	50 (49,6-50,2)	50 (47,6-48,9)
Leistung (kW):	40	45	35
Ar (PSIG-SLPM):	50-41,8	50-41,8	50-41,8
H_2 (PSIG-SLPM):	20-2,2	20-2,2	20-2,2
N_2 (PSIG-SLPM):	none	none	none
He (PSIG-SLPM):	none	none	none
Pulvergeber			
Trägergasrate (SLPM):	5	5	5
Pulverförderrate (%-g/min):	5-5,7	5-5,7	5-5,7
Rührer (Umdrehungen/min):	40	40	40
Heizung (°C):	40	40	40
Verfahr-Parameter			
Vorschub; FMAX X-RAMPE X:	250-200	250-200	250-200
Vorschubgeschwindigkeit(cm/s):	1	1	1
Bahnbreite (mm):	5	5	5
Sonstiges			
Spritzabstand (mm):	120	120	120
Übergänge:	1	1	1
Kühlung (bar):	2,5 (L+R)	2,5 (L+R)	2,5 (L+R)
Schicht			
Qualität der Schicht:	less plane surface as 10 % powder	less plane surface as 10 % powder	less plane surface as 10 % powder
Substrat-Dicke (mm):			
Nach Beschichten (mm):			
Dicke der Schicht (µm)	~190	~220	~100
Gewicht vorher (g):			
Gewicht nachher (g):			
Gewicht der Schicht (mg):			
Pyrometer BP 100			
Geschwindigkeit (cm/s)	1,5	1,5	1,5
Verzeichnis:	250594	250594	250594
Datei-Name:	CONT0002.BIN	CONT0001.BIN	CONT003.BIN
Screen-kopie-Name:	GRAB0540.TIF	GRAB0545.TIF	GRAB0535
ε:	0,2	0,2	0,2
Totale Zeit (s):	182	165	180

Spritzprotokoll Plasmadyne		Brenner:	F4
		Pulvergeber:	PT Twin-10C
		Pulver-Material:	$Al_2O_3/TiO2$ (87/13)
Bearbeiter:	F. Ladru	Korngrößenvert.:	-45 +22,5
Datum:	05-06-1994	Typ:	744,1 HC Starck
		Behandlung:	none

Proben			
Nummer:	7x	8x	9x
Versuchszweck:	optimization, engineering thesis		
Material:	St.-37		
Geometrie:	complete set		
Plasmadyne			
Strom (A):	800	900	710
Spannung (V):	49,5-50,5	49,8-50,2	48,2-48,7
Leistung (kW):	40	45	35
Ar (PSIG-SLPM):	50-41,8	50-41,8	50-41,8
H_2 (PSIG-SLPM):	20-2,2	20-2,2	20-2,2
N_2 (PSIG-SLPM):	none	none	none
He (PSIG-SLPM):	none	none	none
Pulvergeber			
Trägergasrate (SLPM):	5	5	5
Pulverförderrate (%-g/min):	15-17,1	15-17,1	15-17,1
Rührer (Umdrehungen/min):	40	40	40
Heizung (°C):	40	40	40
Verfahr-Parameter			
Vorschub; FMAX X-RAMPE X:	1000-100	1000-100	1000-100
Vorschubgeschwindigkeit (cm/s):	3,5	3,5	3,5
Bahnbreite (mm):	5	5	5
Sonstiges			
Spritzabstand (mm):	120	120	120
Übergänge:	1	1	1
Kühlung (bar):	2,5 (L+R)	2,5 (L+R)	2,5 (L+R)
Schicht			
Qualität der Schicht:			
Substrat-Dicke (mm):			
Nach Beschichten (mm):			
Dicke der Schicht (µm)	~145	~185	~60
Gewicht vorher (g):			
Gewicht nachher (g):			
Gewicht der Schicht (mg):			
Pyrometer BP 100			
Geschwindigkeit (cm/s)	1,5	1,5	1,5
Verzeichnis:	240594	240594	240594
Datei-Name:	CONT0005.BIN	CONT0007.BIN	CONT0006.BIN
Screen-kopie-Name:	GRAB1540.TIF	GRAB1545.TIF	GRAB1535.BIN
ε:	0,2	0,2	0,2
Totale Zeit (s):	170	152	155

Appendix G: Weight and Thickness Results of the Samples

Codes: P = Pin on disk, T = Taber, M = Microscope

Wear-samples:

number:	weight before (g):	weight after (g):	increase: (mg)
P10	47,758	47,870	112
P11	47,461	47,563	102
P12	47,119	47,220	101
P13	47,684	47,795	111
P14	47,622	47,701	79
P15	47,792	47,915	123
P16	47,815	47,936	121
P17	47,228	47,351	123
P18	47,452	47,574	122
P19	47,422	47,545	123
P20	47,552	47,684	132
P21	47,891	48,023	132
P22	47,902	48,032	121
P23	47,692	47,829	137
P24	47,208	47,346	138
P25	47,764	47,899	153
P26	45,883	46,025	142
P27	47,877	48,015	138
P28	47,656	47,797	141
P29	48,230	48,373	143
P30	47,552	47,599	47
P31	47,690	47,746	56
P32	47,853	47,901	48
P33	48,160	48,210	50
P34	47,425	47,475	50
P35	47,244	47,302	58
P36	47,520	47,577	57
P37	47,990	48,053	63
P38	48,060	48,108	48
P39	44,530	44,579	49

number:	weight before (g):	weight after (g):	increase (g):
T10	185,716	189,946	4,230
T11	186,211	190,305	4,094
T12	186,088	190,284	3,912
T13	186,067	190,256	4,189
T20	186,336	191,454	5,118
T21	186,562	191,677	5,115
T22	184,673	189,702	5,029
T23	186,689	191,764	5,075
T30	181,073	183,435	2,362
T31	186,376	188,761	2,385
T32	187,113	189,446	2,333
T33	185,622	188,015	2,393
number:	thickness before:	thickness after:	increase (µm):
T10	4,05	4,25	200
T11	4,06	4,27	210
T12	4,06	4,27	210
T13	4,05	4,27	220
T20	4,05	4,33	280
T21	4,06	4,33	270
T22	4,05	4,33	280
T23	4,06	4,33	270
T30	3,97	4,10	130
T31	4,05	4,17	120
T32	4,06	4,22	160
T33	4,05	4,16	110

Microscope-samples:

number:	weight before:	weight after:	increase (mg):
M1	43,201	44,075	874
M2	43,100	44,146	1046
M3	43,318	43,811	493
number:	thickness before:	thickness after:	coating thickness:
M1	5,02	5,24	220 µ
M2	5,06	5,33	270 µ
M3	5,05	5,16	110 µ

Wear-samples:

number:	weight before (g):	weight after (g):	increase: (mg)
P40	48,030	48,117	114
P41	47,372	47,455	83
P42	47,803	47,889	86
P43	47,622	47,706	84
P44	47,654	47,732	78
P45	47,887	47,973	86
P46	47,238	47,323	85
P47	48,008	48,096	88
P48	48,163	48,240	77
P49	47,737	47,808	71
P50	47,137	47,252	115
P51	47,760	47,872	112
P52	47,776	47,890	114
P53	47,844	47,957	113
P54	48,386	48,499	113
P55	47,276	47,385	109
P56	46,760	46,869	109
P57	47,378	47,496	118
P58	47,688	47,803	115
P59	48,013	48,130	117
P60	48,103	48,161	58
P61	47,845	47,901	56
P62	47,924	47,983	59
P63	48,492	48,550	58
P64	46,441	46,499	58
P65	47,860	47,917	57
P66	47,897	47,951	54
P67	46,276	46,335	59
P68	48,129	48,189	60
P69	47,375	47,430	55

number:	weight before (g):	weight after (g):	increase (g):
T40	186,585	190,110	3,525
T41	185,467	188,989	3,522
T42	186,157	189,655	3,498
T43	186,693	190,232	3,539
T50	186,658	190,737	4,044
T51	186,509	190,658	4,149
T52	185,438	189,624	4,186
T53	186,022	190,156	4,134
T60	186,824	188,674	1,850
T61	187,014	188,845	1,831
T62	185,491	187,372	1,881
T63	186,988	188,916	1,928

number:	thickness before:	thickness after:	increase (µm):
T40	4,05-4,07	4,25	200-220
T41	4,03-4,07	4,18-4,22	150
T42	4,06-4,10	4,23-4,27	170
T43	4,05	4,25	200
T50	4,06	4,28	220
T51	4,05	4,28	230
T52	4,02-4,05	4,25-4,26	210-230
T53	4,05	4,26	210
T60	4,06	4,16	100
T61	4,06	4,16	100
T62	4,03-4,06	4,11-4,20	80-140
T63	4,07	4,17	100

Microscope-samples:

number:	weight before:	weight after:	increase (mg):
M4	45,516	46,281	765
M5	42,758	43,618	860
M6	42,888	43,239	351
number:	thickness before:	thickness after:	coating thickness:
M4	5,05-5,09	5,25-5,27	180-200
M5	4,97-5,02	5,19-5,23	210-220
M6	4,97-5,01	5,04-5,12	70-110

Wear-samples:

number:	weight before (g):	weight after (g):	increase: (mg)	number:	weight before (g):	weight after (g):	increase (g):
P70	48,588	48,642	54	T70	186,858	189,010	2,152
P71	47,248	47,301	53	T71	186,483	188,647	2,165
P72	47,680	47,735	55	T72	186,598	188,790	2,192
P73	47,629	47,686	57	T73	185,871	188,060	2,189
P74	47,516	47,570	59	T80	186,865	190,164	3,299
P75	48,391	48,444	53	T81	186,062	189,345	3,283
P76	47,877	47,933	56	T82	185,543	188,857	3,314
P77	47,928	47,981	53	T83	186,540	189,809	3,269
P78	48,313	48,368	55	T90	186,996	188,155	1,159
P79	47,735	47,791	56	T91	186,376	187,520	1,144
P80	47,077	47,164	87	T92	186,451	187,630	1,179
P81	47,991	48,072	81	T93	186,035	187,223	1,188
P82	47,328	47,414	86	number:	thickness	thickness	increase
P83	48,096	48,182	86		before:	after:	(µm):
P84	47,798	47,880	82	T70	4,06	4,21	150
P85	47,812	47,894	82	T71	4,06	4,20	140
P86	47,953	48,036	83	T72	4,06	4,20	140
P87	46,935	47,018	83	T73	4,04	4,19	150
P88	47,030	47,114	84	T80	4,06	4,24	180
P89	47,848	47,939	91	T81	4,04	4,21	170
P90	47,466	47,494	28	T82	4,03-4,04	4,23	200
P91	48,001	48,032	31	T83	4,06	4,22	160
P92	47,861	47,891	30	T90	4,06	4,12	60
P93	47,855	47,883	28	T91	4,05	4,11	60
P94	47,553	47,585	32	T92	4,05	4,11	60
P95	47,359	47,389	30	T93	4,04	4,10	60
P96	47,954	47,985	31				
P97	46,310	46,338	28				
P98	48,006	48,038	32				
P99	48,010	48,042	32				

Microscope-samples:

number:	weight before:	weight after:	increase (mg):
M7	42,860	43,315	455
M8	42,983	43,674	691
M9	43,222	43,466	244
number:	thickness before:	thickness after:	coating thickness:
M7	4,96-5,00	5,10-5,15	140-150
M8	4,98-5,02	5,15-5,21	190
M9	5,01-5,06	5,08-5,15	70-90

Appendix H: Listing of Pyrometric Procedure

Distance of substrate-holder is 700 mm from the right side of the APS cabine.

1	MOP	1
2	MOP	2
3	Y-ACHSE	3625
4	TIMER	10
5	X-ACHSE	2400
6	JUMP	9
7	COUNTER	2
8	JUMP	18
9	FMAX X	1000
10	RAMPE X	100
11	X-ACHSE	3050
12	Y-ACHSE	-50
13	FMAX X	1000
14	RAMPE X	100
15	X-ACHSE	-3050
16	Y-ACHSE	-50
17	JUMP	7
18	Y-ACHSE	-500
19	JUMP	22
20	RAMPE X	4
21	JUMP	31
22	FMAX X	1000
23	RAMPE X	100
24	X-ACHSE	3350
25	Y-ACHSE	-50
26	FMAX X	1000
27	RAMPE X	100
28	X-ACHSE	-3350
29	Y-ACHSE	-50
30	JUMP	20
31	Y-ACHSE	-300
32	JUMP	35
33	RAMPE X	9
34	JUMP	1
35	FMAX X	1000
36	RAMPE X	100
37	X-ACHSE	4650
38	Y-ACHSE	-50
39	FMAX X	1000
40	RAMPE X	100
41	X-ACHSE	-4650
42	Y-ACHSE	-50
43	JUMP	33

Appendix I: Description of Continuous Measurements

Table I1.High-speed Pyrometric Temperature measurements description:

10 % - 40 kW		
time (s):	measurements situation:	temperature (°C):
0-10	plasma	500-530
10-50	plasma+powder	
50	start	
82	turn left	
109	turn right	
137	power off	
157	end of recording	

Table I2.High-speed Pyrometric Temperature measurements description:

10 % - 45 kW		
time (s):	measurements situation:	temperature (°C):
0-10	plasma	520-570
10-50	plasma+powder	
50	start	
81	turn left	
110	turn right	
137	power off	
155	end of recording	

Table I3.High-speed Pyrometric Temperature measurements description:

10 % - 35 kW		
time (s):	measurements situation:	temperature (°C):
0-10	plasma	485-495
10-50	plasma+powder	
50	start	
80	turn left	
109	turn right	
135	power off	
160	end of recording	

Table I4.High-speed Pyrometric Temperature measurements description:

5 % - 40 kW		
time (s):	measurements situation:	temperature (°C):
0-10	plasma	480-490
10-75	plasma+powder	
75	start	
100	turn left	
	turn right	
162	power off	
182	end of recording	

Table I5.High-speed Pyrometric Temperature measurements description:

5 % - 45 kW		
time (s):	measurements situation:	temperature (°C):
0-10	plasma	490-500
10-50	plasma+powder	
50	start	
80	turn left	
108	turn right	
135	powder off	
157	end of recording	

Table I6.High-speed Pyrometric Temperature measurements description:

5 % - 35 kW		
time (s):	measurements situation:	temperature (°C):
0-10	plasma	475-485
10-50	plasma+powder	
50	start	
83	turn left	
111	turn right	
137	powder off	
180	end of recording	

Table I7.High-speed Pyrometric Temperature measurements description:

15 % - 40 kW		
time (s):	measurements situation:	temperature (°C):
0-10	plasma	550-620
10-50	plasma+powder	
50	start	
79	turn left	
107	turn right	
134	powder off	
170	end of recording	

Table I8.High-speed Pyrometric Temperature measurements description:

15 % - 45 kW		
time (s):	measurements situation:	temperature (°C):
0-10	plasma	600-650
10-50	plasma+powder	
53	start	
82	turn left	
110	turn right	
138	powder off	
152	end of recording	

Table I9.High-speed Pyrometric Temperature measurements description:

15 % - 35 kW		
time (s):	measurements situation:	temperature (°C):
0-10	plasma	515-525
10-50	plasma+powder	
50	start	
81	turn left	
108	turn right	
135	powder off	
155	end of recording	

Table I10. Continuous Pyrometric Results of the Mean Temperatures.

time (s)	CONT 0000	CONT 0001	CONT 0002	CONT 0003	CONT 0004	CONT 0005	CONT 0006	CONT 0007	CONT 0008
0	476	488	474	475	462	477	475	487	476
5	474	486	474	477	463	476	474	487	474
10	473	485	476	477	464	476	475	484	475
15	474	487	476	476	465	477	475	485	474
20	475	488	475	477	463	477	488	487	472
25	475	485	475	475	474	476	482	495	474
30	474	483	475	475	475	475	488	486	485
35	488	487	474	477	463	477	484	488	486
40	475	485	474	477	463	476	487	486	484
45	483	481	474	476	476	478	485	483	488
50	476	490	476	475	463	477	586	481	486
55	522	504	488	490	475	478	646	482	521
60	508	554	497	483	477	486	568	677	530
65	505	544	486	492	474	484	568	645	528
70	514	565	490	487	464	486	567	644	537
75	496	548	495	496	462	486	603	639	528
80	503	514	483	494	490	493	605	653	532
85	497	519	485	484	491	489	550	544	523
90	499	530	496	486	491	485	549	605	513
95	503	515	494	493	497	483	591	595	520
100	502	524	482	494	479	484	544	580	515
105	507	517	483	483	482	484	530	574	520
110	508	517	480	495	480	491	628	547	520
115	514	581	492	495	476	484	613	639	528
120	519	574	497	491	488	485	635	692	549
125	514	573	494	493	490	486	616	651	524
130	524	577	494	485	481	485	608	660	538
135	533	566	487	495	484	485	605	664	536
140	500	663	498	497	485	492	541	528	515
145	490	493	474	487	485	480	494	469	482
150	469	461	474	477	492	475	462	465	477
155	475	465	465	478	491	475	465	465	476
160	----	----	465	477	496	477	464	----	----
165	----	----	----	----	496	476	465	----	----
170	----	----	----	----	477	477	----	----	----

Appendix J: Results of Dummy tests

Table J1. Dummy microhardness $HV_{0,1}$ on St.-37

Nr.	$HV_{0,1}$
1	195,8
2	204,5
3	189,0
4	187,7
5	187,7
average	192,9

Table J2. Pin-on-disk test (weight in g, 400 graining):

Nr.	Start	25 m	50 m	75 m	100 m	125 m	150 m	200 m	250 m	300 m	350 m	400 m
A	47,027	47,009	46,996	46,969	46,953	46,935	46,920	46,890	46,846	46,809	46,771	46,737
B	50,208	50,193	50,181	50,159	50,142	50,125	50,109	50,090	50,054	50,013	49,983	49,944
C	49,452	49,438	49,426	49,403	49,388	49,367	49,348	49,325	49,291	49,262	49,224	49,198
D	50,002	49,987	49,938	49,917	49,900	49,881	49,865	49,846	49,806	49,773	49,743	49,708

Table J3. Wear of dummy pin-on-disk test in mg (400 graining):

Nr.	25 m	50 m	75 m	100 m	125 m	150 m	200 m	250 m	300 m	350 m	400 m
A	18	13	27	16	18	15	30	44	37	38	34
B	15	12	22	17	17	16	19	36	41	30	39
C	14	12	23	15	21	19	23	34	29	38	26
D	15	49	21	17	19	16	19	40	33	30	35
average	15,5	21,5	23,3	16,3	18,8	16,5	22,8	38,5	35,0	34	33,5
total	15,5	37,0	60,3	76,6	95,4	111,9	134,7	173,2	208,2	242,2	275,7

Table J4. Pin-on-disk test (weight in g, 800 graining):

Nr.	Start	25 m	50 m	75 m	100 m	125 m	150 m	200 m	250 m	300 m	350 m
E	50,099	50,081	50,058	50,030	50,010	49,985	49,964	49,923	49,889	49,848	49,805
F	50,266	50,246	50,226	50,201	50,183	50,162	50,140	50,113	50,086	50,061	50,029
G	50,314	49,294	49,273	50,250	50,227	50,210	50,192	50,166	50,134	50,100	50,066
H	50,086	50,067	50,046	50,021	49,999	49,979	49,954	49,924	49,887	49,854	49,828

Table J5. Wear of dummy pin-on-disk test in mg (800 graining):

Nr.	25 m	50 m	75 m	100 m	125 m	150 m	200 m	250 m	300 m	350 m
E	18	23	28	20	25	21	41	34	41	43
F	20	20	25	18	21	22	27	27	25	32
G	20	21	23	23	17	18	26	32	34	34
H	19	21	25	22	20	25	30	37	35	26
average	19,3	21,3	25,3	20,8	20,8	21,5	31,0	32,5	33,8	33,8
total	19,3	40,6	65,9	86,7	107,5	129,0	160,0	192,5	226,3	260,1

Table J6. Taber disk dummy test:

sample-Nr.:	A		B		average
weight (g):	182,915		186,492		
rounds:	weight (g)	wear (mg)	weight (g)	wear (mg)	(mg)
250	182,915	20	186,468	24	22
500	182,877	18	186,447	21	20
1000	182,832	44	186,319	128	86
1.500	182,708	124	186,203	116	120
2.500	182,464	244	185,879	324	284
5.000	181,943	521	184,624	1255	888
10.000	180,384	1559	180,982	3642	2601
20.000	173,581	6,803	173,804	7178	6991

Appendix K: Results of Microstructural Measurements

Table K1. Results of porosity measurements.

Nr.	DA-1	DA-2	DA-3	DA-4	DA-5	DA-6	DA-7	DA-8	DA-9
1	5,0	6,3	9,3	7,0	5,9	11,4	12,1	4,7	8,7
2	7,4	8,8	5,6	6,4	7,5	8,2	13,4	6,7	10,3
3	7,3	6,4	11,4	6,4	12,0	11,2	7,9	8,8	15,6
4	11,4	6,6	9,8	10,7	6,4	6,3	8,5	5,7	13,4
5	11,3	8,4	10,5	10,7	8,4	7,7	11,2	5,4	9,4
average	8,7	7,3	9,3	10,3	8,0	9,0	10,6	6,3	11,5

Table K2. Grey phase microhardness; $HV_{0,1}$.

Nr.	DA-1	DA-2	DA-3	DA-4	DA-5	DA-6	DA-7	DA-8	DA-9
1	1014,6	966,9	599,6	1160,7	998,3	982,4	1048,4	1121,4	1084,0
2	1048,4	1121,4	761,3	1181,1	1223,7	842,3	894,5	1121,4	982,4
3	1014,6	1031,3	966,9	894,5	1102,4	842,3	1048,4	998,3	867,8
average	1025,9	1039,9	775,9	1079,8	1108,1	889,0	1021,1	1080,4	978,1

Table K3. White phase microhardness: $HV_{0,1}$.

Nr.	DA-1	DA-2	DA-3	DA-4	DA-5	DA-6	DA-7	DA-8	DA-9
1	750,7	638,9	700,8	710,4	730,1	673,2	655,7	754,9	584,9
2	772,1	563,8	710,4	720,1	691,4	638,9	881,0	664,4	543,9
3	761,3	750,1	610,4	750,7	710,4	607,2	720,1	630,8	518,9
average	761,4	650,9	673,9	727,1	710,6	639,8	752,3	683,4	549,2

Table K4. Mixed phase microhardness: $HV_{0,1}$.

Nr.	DA-1	DA-2	DA-3	DA-4	DA-5	DA-6	DA-7	DA-8	DA-9
1	829,9	936,9	982,4	817,8	936,9	622,8	806,0	700,8	622,8
2	607,2	1084,0	761,3	998,3	829,9	664,4	720,1	772,1	664,4
3	1084,0	966,9	730,1	966,9	710,4	750,7	854,9	783,2	867,8
average	840,4	995,9	824,6	927,7	825,7	679,3	793,7	752,0	718,3

Appendix L: Pin-on-Disk Results

Table L1. 400 grinding paper, weigths in g

Nr.	Start	25 m	50 m	75 m	100 m	125 m	150 m	200 m
10	47,504	47,496*	47,480	47,454**	----	----	----	----
11	47,268	47,259*	47,243	47,224**	----	----	----	----
12	46,906	46,897*	46,879	46,861**	----	----	----	----
13	47,463	47,449*	47,428	47,408**	----	----	----	----
20	47,543	47,529	47,518	47,505	47,500*	47,482	47,469**	----
21	47,709	47,693	47,685*	47,672	47,658	47,639**	47,626	----
22	47,266	47,252	47,243	47,233	47,226	47,214	47,197*	----
23	47,421	47,408	47,397*	47,384	47,374	47,356	47,339**	----
30	47,461	47,441*	47,431**	----	----	----	----	----
31	48,031	48,015*	47,998**	----	----	----	----	----
32	47,537	47,519*	47,502**	----	----	----	----	----
33	47,244	47,226*	47,206**	----	----	----	----	----
40	48,114	48,096	48,084*	48,073	48,065	48,053**	----	----
41	47,452	47,434	47,426	47,413*	47,403	47,385**	----	----
42	47,887	47,865	47,853	47,838*	47,831	47,816**	----	----
43	47,707	47,683	47,668*	47,653	47,644	47,633**	----	----
50	47,245	47,231	47,228	47,222	47,213	47,204	47,194	47,177*
51	47,865	47,848	47,848	47,843	47,834	47,821*	47,811	47,791**
52	47,883	47,870	47,867	47,860	47,849	47,840*	47,826	47,808
53	47,950	47,935	47,933	47,923	47,916*	47,907	47,890	47,878**
60	48,158	48,124*	48,109**	48,093	----	----	----	----
61	47,900	47,894	47,868*	47,849**	----	----	----	----
62	47,981	47,967*	47,954	47,938**	----	----	----	----
63	48,546	48,531	48,511*	48,493**	----	----	----	----
70	48,639	48,622*	48,602**	48,582	----	----	----	----
71	47,300	47,284	47,262*	47,244**	----	----	----	----
72	47,730	47,722	47,705*	47,682**	----	----	----	----
73	47,681	47,665	47,644**	47,622	----	----	----	----
80	47,161	47,147	47,137	47,122*	47,106	47,091**	----	----
81	48,067	48,056	48,044	48,030*	48,017	48,002**	----	----
82	47,410	47,396	47,386	47,375	47,362*	47,346**	----	----
83	48,178	48,166	48,156	48,148	48,131*	48,122**	----	----
90	47,491	47,474**	47,446	----	----	----	----	----
91	48,027	48,003**	47,982	----	----	----	----	----
92	47,888	47,865**	47,847	----	----	----	----	----
93	47,883	47,860**	47,838	----	----	----	----	----

*) Part of coating gone at the edge (10 %)

**) Coating gone for more than 50 %

Table L3. 800 grinding paper, weigths in g.

Nr.	Start	25 m	50 m	75 m	100 m	125 m	150 m	200 m	250 m	300 m	350 m	400 m
14	47,279	47,275	47,263	47,249*	47,232	47,220	47,204**	----	----	----	----	----
15	46,777	46,770	46,755*	46,737	46,724	46,706	46,692**	----	----	----	----	----
16	45,950	45,949	45,935*	45,920	45,910	45,898	45,880**	----	----	----	----	----
17	47,375	47,369*	47,355*	47,343	47,332	47,316	47,298**	----	----	----	----	----
24	47,026	47,020	47,013	47,003	46,992	46,986	46,981	46,974*	46,963	46,948	46,935	----
25	45,520	45,513	45,504	45,495	45,487	45,481	45,475	45,464*	45,458	45,443	45,431**	----
26	47,559	47,550	47,541	47,533	47,525	47,518	47,513	47,504	47,494*	47,481	47,460**	----
27	47,909	47,901	47,893	47,882	47,873	47,866	47,858	47,845*	47,833	47,817	47,801**	----
34	47,349	47,335*	47,319	47,301	47,285	47,268	47,248**	----	----	----	----	----
35	47,156	47,146	47,135	47,120*	47,108	47,091**	47,071	----	----	----	----	----
36	47,734	47,723	47,709*	47,694	47,677**	47,661	47,642	----	----	----	----	----
37	46,989	46,975*	46,961	46,943	46,927**	46,908	46,891	----	----	----	----	----
44	47,976	47,966	47,960	47,952	47,943	47,931*	47,920	47,903**	----	----	----	----
45	47,323	47,313	47,302	47,294	47,289	47,277*	47,267	47,245**	----	----	----	----
46	48,095	48,087	48,078	48,071	48,065	48,055	48,043	48,029*	----	----	----	----
47	48,240	48,231	48,225	48,215	48,206*	48,193	48,184	48,167**	----	----	----	----
54	48,500	48,492	48,487	48,482	48,477	48,471	48,465	48,459	48,447*	48,435	48,422	48,403**
55	47,385	47,378	47,370	47,366	47,359	47,353	47,346	47,334*	47,327	47,318	47,304	47,292**
56	47,496	47,489	47,483	47,476	47,472	47,466	47,458	47,449	47,439	47,432	47,417	47,404**
57	48,130	48,122	48,115	48,109	48,104	48,097	48,090	48,084	48,076	48,067	48,056	48,043**
64	46,498	46,485	46,471*	46,459	46,445	46,432**	----	----	----	----	----	----
65	47,951	47,938	47,924*	47,912	47,897**	47,878	----	----	----	----	----	----
66	48,189	48,179	48,169	48,156*	48,141	48,124**	----	----	----	----	----	----
67	47,432	47,421	47,410*	47,395	47,378**	47,361	----	----	----	----	----	----
74	48,442	48,429*	48,419	48,402	48,387**	----	----	----	----	----	----	----
75	47,931	47,922	47,907*	47,895	47,885**	----	----	----	----	----	----	----
76	47,979	47,966	47,954*	47,935**	47,921	----	----	----	----	----	----	----
77	47,787	47,775*	47,766	47,754	47,738**	----	----	----	----	----	----	----
84	47,876	47,867	47,861	47,850	47,840*	47,833	47,822	47,806	47,782**	----	----	----
85	47,891	47,880	47,873	47,867	47,859	47,851	47,843*	47,831	47,813**	----	----	----
85	48,033	48,026	48,021	48,014	48,008	48,001	47,991	47,978*	47,963**	----	----	----
87	47,015	47,004	46,999	46,990	46,984	46,975*	46,964	46,950**	46,939	----	----	----
94	47,586	47,568*	47,547**	----	----	----	----	----	----	----	----	----
95	47,389	47,371*	47,349**	----	----	----	----	----	----	----	----	----
96	46,337	46,320*	46,291**	----	----	----	----	----	----	----	----	----
97	48,035	48,014*	47,992**	----	----	----	----	----	----	----	----	----

*) Part of coating gone at the edge (10 %)

**) Coating gone for more than 50 %

Table L4. Wear of Pin-on-Disk test, 800 graining (wear in mg)

Nr.	25 m	50 m	75 m	100 m	125 m	150 m	200 m	250 m	300 m	350 m	400 m
14	4	12	14	17	12	16	----	----	----	----	----
15	7	15	18	13	18	14	----	----	----	----	----
16	1	14	15	10	12	18	----	----	----	----	----
17	6	14	12	11	16	18	----	----	----	----	----
average	4,5	13,8	14,8	12,8	14,5	16,5	----	----	----	----	----
24	6	7	10	11	6	5	7	11	15	13	----
25	7	9	9	8	6	6	11	6	15	12	----
26	9	9	8	8	7	5	9	10	13	21	----
27	8	8	11	9	7	8	13	12	16	16	----
average	7,5	8,3	9,5	9,0	6,5	6,0	10,0	9,8	14,8	15,5	----
34	14	16	18	16	17	20	----	----	----	----	----
35	10	11	15	12	17	20	----	----	----	----	----
36	11	14	15	17	16	19	----	----	----	----	----
37	14	14	18	16	19	17	----	----	----	----	----
average	12,3	13,8	16,5	15,3	17,3	19,0	----	----	----	----	----
44	10	6	8	9	12	11	17	----	----	----	----
45	10	11	8	5	12	10	22	----	----	----	----
46	8	9	7	6	10	12	14	----	----	----	----
47	9	6	10	9	13	9	17	----	----	----	----
average	9,3	8,0	8,3	7,3	11,8	10,5	17,5	----	----	----	----
54	8	5	5	5	6	6	6	12	12	13	19
55	7	8	7	7	6	7	12	7	9	14	12
56	7	6	4	4	6	8	9	10	7	15	13
57	8	6	5	5	7	7	6	8	9	11	13
average	7,5	6,3	5,3	5,3	6,3	7,0	8,3	9,3	9,3	13,3	14,3
64	13	14	12	14	13	----	----	----	----	----	----
65	13	14	12	15	19	----	----	----	----	----	----
66	10	10	13	15	17	----	----	----	----	----	----
67	11	11	15	17	17	----	----	----	----	----	----
average	11,8	12,3	13,0	15,3	16,5	----	----	----	----	----	----
74	13	10	17	15	----	----	----	----	----	----	----
75	9	15	12	10	----	----	----	----	----	----	----
76	13	12	19	14	----	----	----	----	----	----	----
77	12	9	12	16	----	----	----	----	----	----	----
average	11,8	11,5	15,0	13,8	----	----	----	----	----	----	----
84	9	6	11	10	7	11	16	24	----	----	----
85	11	7	6	8	8	8	12	18	----	----	----
86	7	5	7	6	7	10	13	15	----	----	----
87	11	5	9	6	9	11	14	11	----	----	----
average	9,5	5,0	8,3	7,5	7,8	10,0	13,8	17,0	----	----	----
94	18	21	----	----	----	----	----	----	----	----	----
95	18	22	----	----	----	----	----	----	----	----	----
96	17	29	----	----	----	----	----	----	----	----	----
97	21	22	----	----	----	----	----	----	----	----	----
average	17,5	23,5	----	----	----	----	----	----	----	----	----

Appendix M: Taber Disk Results

Table L1. Taber Disk test.

sample-Nr.:	12		13		average
weight (g):	190,259		190,236		
rounds:	weight (g)	wear (mg)	weight (g)	wear (mg)	(mg)
250	190,158	98	190,143	93	95,5
500	190,128	30	190,097	46	38,0
750	190,114	14	190,062	35	24,5
1.000	190,100	14	190,046	16	15,0
1.500	190,090	10	190,037	9	9,5
2000	190,071	19	190,017	20	19,5
3000	190,046	25	190,981	36	30,5

Table L2. Taber Disk test.

sample-Nr.:	22		23		average
weight (g):	189,679		191,745		
rounds:	weight (g)	wear (mg)	weight (g)	wear (mg)	(mg)
250	189,639	40	191,707	38	39,0
500	189,613	26	191,670	37	31,5
750	189,601	12	191,640	30	21,0
1.000	189,592	9	191,624	16	12,5
1.500	189,583	24	191,609	15	12,0
2000	189,559	119	191,584	25	24,5
3000	189,440		191,545	39	79,0

Table L3 Taber Disk test.

sample-Nr.:	32		33		average
weight (g):	189,428		187,997		
rounds:	weight (g)	wear (mg)	weight (g)	wear (mg)	(mg)
250	189,355	73	187,915	82	77,5
500	189,319	36	187,870	45	40,5
750	189,262	57	187,782	88	72,5
1.000	189,240	22	187,755	27	24,5
1.500	189,204	36	187,704	51	43,5
2000	189,154	50	187,641	63	56,5
3000	189,059	95	187,556	85	90,0

Table L4. Taber Disk test.

sample-Nr.:	42		43		average
weight (g):	189,647		190,221		
rounds:	weight (g)	wear (mg)	weight (g)	wear (mg)	(mg)
250	189,599	48	190,165	56	52,0
500	189,572	27	190,134	31	29,0
750	189,528	44	190,070	64	54,0
1.000	189,516	12	190,059	11	11,5
1.500	189,501	15	190,041	18	16,5
2000	189,489	12	190,013	28	20,0
3000	189,444	45	189,962	51	48,0

Table L5. Taber Disk test.

sample-Nr.:	52		53		average
weight (g):	189,613		190,143		
rounds:	weight (g)	wear (mg)	weight (g)	wear (mg)	(mg)
250	189,572	41	190,098	45	43,0
500	189,556	16	190,057	41	28,5
750	189,484	72	189,992	65	68,5
1.000	189,474	10	189,981	11	10,5
1.500	189,452	22	189,955	26	24,0
2000	189,420	32	189,923	32	32,0
3000	189,392	28	189,895	28	28,0

Table L6. Taber Disk test.

sample-Nr.:	62		63		average
weight (g):	187,360		188,906		
rounds:	weight (g)	wear (mg)	weight (g)	wear (mg)	(mg)
250	187,313	47	188,851	55	51,0
500	187,284	29	188,813	38	33,5
750	187,268	16	188,779	34	25,0
1.000	187,248	20	188,748	31	25,5
1.500	187,222	26	188,712	36	31,0
2000	187,196	26	188,678	34	30,0
3000	187,151	45	188,595	83	64,0

Table L7. Taber Disk test.

sample-Nr.:	72		73		average
weight (g):	188,771		188,048		
rounds:	weight (g)	wear (mg)	weight (g)	wear (mg)	(mg)
250	188,725	46	187,999	49	47,5
500	188,706	19	187,973	26	22,5
750	188,689	17	187,950	23	20,0
1.000	188,673	16	187,931	19	17,5
1.500	188,639	34	187,891	40	37,0
2000	188,606	33	187,851	40	36,5
3000	188,558	48	187,782	69	58,5

Table L8. Taber Disk test.

sample-Nr.:	82		83		average
weight (g):	188,838		189,794		
rounds:	weight (g)	wear (mg)	weight (g)	wear (mg)	(mg)
250	188,798	40	189,748	46	43,0
500	188,772	26	189,732	16	21,0
750	188,759	13	189,721	11	12,0
1.000	188,745	14	189,707	14	14,0
1.500	188,676	69	189,684	23	46,0
2000	188,636	40	189,651	33	36,5
3000	188,599	37	189,614	37	37,0

Table L9. Taber Disk test.

sample-Nr.:	92		93		average
weight (g):	187,619		187,211		
rounds:	weight (g)	wear (mg)	weight (g)	wear (mg)	(mg)
250	187,569	50	187,148	63	56,5
500	187,549	20	187,115	33	26,5
750	187,538	11	187,091	24	17,5
1.000	187,507	31	187,043	48	39,5
1.500	187,423	84	186,967*	76	80,0
2000	187,391	32	186,921	46	39,0
3000	187,307*	84	186,793**	128	106,0

*) Coating came through

**) Coating almost gone

Appendix N: Results of Adhesive Strength in Tension Test

diameter: 40 mm
surface: 1256,7 mm^2

sample nr.	force (kN)	F_m (N / mm^2)	break down factor
10	66,0	52,5	2 % coating, 98 % glue
11	74,0	58,9	70 % coating, 30 % glue
12	66,8	53,2	100 % coating, 0 % glue
13	45,6	-----	0 % coating, 100 % glue
14	79,4	-----	0 % coating, 100 % glue
20	88,6	70,5	99 % coating, 1 % glue
21	88,0	70,0	100 % coating, 0 % glue
22	45,8	-----	0 % coating, 100 % glue
23	89,6	71,3	98 % coating, 2 % glue
24	50,8	40,4	10 % coating, 90 % glue
30	-----	-----	glue did not helt
31	80,0	-----	0 % coating, 100 % glue
32	88,4	-----	0 % coating, 100 % glue
33	96,6	-----	0 % coating, 100 % glue
34	81,2	64,6	1 % coating, 99 % glue
40	46,0	36,6	30 % coating, 70 % glue
41	72,2	----	0 % coating, 100 % glue
42	55,8	44,4	20 % coating, 80 % glue
43	82,4	----	0 % coating, 100 % glue
44	98,4	78,3	1 % coating, 100 % glue
50	68,4	54,4	100 % coating, 0 % glue
51	60,2	47,9	75 % coating, 25 % glue
52	78,0	62,1	50 % coating, 50 % glue
53	78,8	----	0 % coating, 100 % glue
54	36,8	29,3	2 % coating, 98 % glue
60	84,8	----	0 % coating, 100 % glue
61	79,2	63,0	2 % coating, 98 % glue
62	91,2	----	0 % coating, 100 % glue
63	93,8	----	0 % coating, 100 % glue
64	91,2	72,6	20 % coating, 80 % glue
70	86,8	69,1	2 % coating, 98 % glue
71	81,6	----	0 % coating, 100 % glue
72	79,4	63,2	2 % coating, 98 % glue
73	54,6	43,4	10 % coating, 90 % glue
74	82,0	----	0 % coating, 100 % glue
80	50,2	----	0 % coating, 100 % glue
81	81,0	64,5	70 % coating, 30 % glue
82	73,8	58,7	10 % coating, 90 % glue
83	87,2	69,4	50 % coating, 50 % glue
84	42,4	33,7	10 % coating, 90 % glue
90	52,4	41,7	5 % coating, 95 % glue
91	55,4	44,1	70 % coating, 30 % glue
92	60,0	47,7	15% coating, 85 % glue
93	75,2	59,8	5 % coating, 95 % glue
94	58,4	46,5	30 % coating, 70 % glue

References

[1] Deutsche Norm, *Thermisches Spritzen- Begriffe, Einteilung*, DIN 32530, 1989

[2] E. Lang, *Coatings for high temperature applications*, Joint Research Centre, Petten Establishment, The Netherlands, Applied Science Publishers, London and New York, 1983

[3] D.S. Rickerby, A. Matthews, *Advanced Surface Coatings: a Handbook of Surface Engineering*, Blackie & Son Ltd, 1991

[4] Several Writers, *Course 51 - Thermal Spray Technology*, ASM International, Materials Engineering Institute, Materials Park, OHIO, 1992

[5] H. Simon, M. Thoma, *Angewandte Oberflächentechnik für metallische Werkstoffe*, Carl Hanser Verlag München, 1985

[6] Univ.-Prof. Dr. techn. E. Lugscheider, *Beschichtungstechnik*, Vorlesungsumdruck für die Vertiefrichtung Werkstofftechnik, 1993

[7] H.-D. Steffens, K. Nassenstein, *Thermal Spraying: A Review of 1993*, pmi vol. 25, no. 6, 1993, 280-284

[8] S. Sampath, H. Herman, *Plasma Spray, Forming Metals, Intermetallics, and Composites*, The Journal of The Minerals, Metals & Materials Society (JOM), vol. 45, no. 7, 1993, 42-49

[9] E. Lugscheider, U. Westermann, *Werkstoff- und Prozeßentwicklung in der Beschichtungstechnik*, Ingenieur-Werkstoffe 5, no. 3, 1993, 42-45

[10] H. Eschnauer, E. Lugscheider, U. Müller, T. Weber, *Quo vadis, Thermisches Spritzen?*, Keramische Zeitschrift, no. 9, 1991

[11] E. Lugscheider, P. Jokiel, *Thermal spraying - An overview on processes, materials and applications*, Euromat, 1991

[12] K.D. Borbeck, *Marktübersicht über das thermische Spritzen*, Schweissen und Schneiden 42, DVS, no. 8, 1990

[13] T.N. Rhys-Jones, *Applications of Thermally Sprayed Coating Systems in Aero Engines*, ITSC, vol. 1, 1989

[14] U. Ströder, M. Mayr, *Vakuumplasmaspritzen als vielfältiges Beschichtungsverfahren (II)*, Werkstoff und Innovation 3, no. 5, 1992, 41-44

[15] E. Lugscheider, I. Rass, *Plasma Processing of Materials Underwater*, NTSC, Anaheim, CA, 1993, 329-334

[16] R.J. Glovan, J.C. Tierney, *Controlled Aspiration - A new Thermal Spray Process*, NTSC, Anaheim, CA, 1993, 111-119

[17] H. Benninghof, *Die wichtigen Parameter beim thermischen Spritzen*, Technische Rundschau 40, 1990, 58-61

[18] E. Lugscheider, P. Jokiel, *Characterization of Particle Reinforced Nickel Hard Alloys Produced by Thermal Spraying*, NTSC, Anaheim, CA, 1993, 411-416

[19] E. Lugscheider, R. Mathesius, G. Spur, A.Kranz, *Mechanical Properties of Thermal Sprayed Coatings on CFRP*, NTSC, Anaheim, CA, 1993, 569-573

[20] P. Sahoo, *High-Performance Wear Coatings - the Quest Continues*, pmi vol. 25, no. 2, 1993, 73-78

[21] K.H. Born, *Verarbeitung nanokristalliner Hartstoffe durch die Verfahren des thermischen Spritzens*, dissertation,. Materials Science Institute, RWTH Aachen, 1992

[22] P. Lichtmanneger, W. Mayr, A. Reusch, K. Landes, *Bedeutung der Messung von Partikeleigenschaften in der Praktis*, DVS 130, 253-256

[23] F. Engel, *Temperaturmessungen mit StrahlungsPyrometern*, VEB Verlag Technik Berlin, 1974

[24] H.-J. Sölter, U. Müller, E. Lugscheider, *High-Speed Temperature Measurement for On-Line Process Control and Quality Assurance during Plasma Spraying*, pmi vol.24, no 3, 1992

[25] C. Moreau, P. Cielo, M. Lamontagne, *Flattening and Solidification of Thermal Sprayed Particles*, Industrial Materials Institute, Canada, ITSC, 1992, 761-766

[26] P. Fauchais, A. Vardelle, M. Vardelle, *Modelling of Plasma Spraying of Ceramic Coatings at Atmospheric Pressure*, Lab. Céramiques Nouvelles, France, High Performance Ceramic Films and Coatings, P. Vincenzini (Editor), Elsevier Science Publishers B.V., 1991, 3-25

[27] S. Kuroda, T. Fukushima, S. Kitahara, Y. Tomita, T. Horiuchi, *Monitoring of Thermally Sprayed Particles using Thermal Radiation*, ITSC, 1989, 145-153

[28] M. Vardelle, A. Vardelle, P. Fauchais, *Spray Parameters and Particle Behaviour During Plasma Spraying*, Journal of Thermal Spray Technology, vol. 2, no. 1, 1992, 79-91

[29] S. Fantassi, M. Vardelle, A. Vardelle, P. Fauchais, *Influence of the Velocity of Plasma Sprayed Particles on the Splat Formation*, University of Limoges, France, NTSC, 1993, 1-6

[30] P. Goucheon, C. Moreau, *In-Flight Particle Surface Temperature Measurement: Influence of the Plasma Light Scattered by the Particles*, NTSC, Anahein, CA, 1993, 13-18

[31] J.F. Coudert, M.P. Planche, O.Betoule, M. Vardelle, P. Fauchais, *Measurement of Flow Velocity and Correlation to Particle Velocity Under Plasma Spraying Conditions*, University of Limoges, France, NTSC, Anaheim, CA, 1993, 19-24

[32] S. Fantassi, M. Vardelle, P. Fauchais, C. Moreau, *Investigation of the Splat Formation Versus Different Particulate Temperatures and Velocities Prior to Impact*, ITSC, 1992, 755-760

[33] F. Durst, A. Melling, J.H. Whitelaw, *Principles and Practice of Laser-Doppler-Anemometry*, Academic press, London, New York, San Fransisco, 1976

[34] J. Wiedemann, *Laser-Doppler-Anemometrie*, Springer Verlag, Berlin und Heidelberg, 1984

[35] G. Gouesbet, *A review on Measurements of Particle Velocities and Diameters by Laser Techniques, with Emphasis on Thermal Plasmas*, Plasma Chemistry and Plasma Processing, vol. 5, no. 2, 1985

[36] H.-H. Flögel, *Modifizierte Laser-Doppler-Anemometrie zur Simultanen bestimmung von Geschwindigkeit und Größe einzelner Partikeln*, VDI Verlag, 1987

[37] T. Hoffman, *Real-Time Imaging for Process Control*, Advanced Materials and Processes, no. 9, 1991, 37-43

[38] J. Agapakis, T. Hoffman, *Real-Time Imaging for Thermal Spray Process Development and Control*, Journal of Thermal Spray Technology, ASM International, vol. 1, 1992, 19-25

[39] T.T. Hoffman, *Real-Time Video Imaging for High-Luminosity Processes*, pmi vol. 25, no. 2, 1993, 86-90

[40] E. Pfender, *Fundamental Studies Associated with the Plasma Spray Process*, NTSC, USA, 1987, 1-10

[41] P. Fauchais, J.F. Coudert, A. and M. Vardelle, A. Grimaud, P. Roumilhac, *State of the Art for the Understanding of the Physical Phenomena Involved in Plasma Spraying at Atmospheric Pressure*, NTSC, USA, 1987, 11-19

[42] K.-H. Busse, H. Sobbe, *Spray Particle Behaviour during Atmospheric Arc Spraying*, ITSC, vol. 2, 1989, 105-117

[43] D. Wang, C.C. Berndt, *Particle/Substrate Interactions during Thermal Spraying, Key engineering Materials*, vol. 53-55, 1991, 499-504

[44] A. Essoltani, P. Proulx, M.I. Boulos, A. Gleizes, *The Importance in the Heat Transfer to a Single Particle in a Thermal Plasma*, HTD, vol. 161, Heat Transfer in Thermal Plasma Processing, ASME, 1991, 145-150

[45] B. Borgerding, H.-J. Sölter, *Computer Simulation of Temperature Distribution within Thermally Sprayed Coatings during the Plasma Spraying Process*, 2nd Plasma-Technik-Symposium, vol. 1, 1991, 65-73

[46] U. Balting, O. Knotek, R.Elsing, T. Cosack, *Comparison of Temperature Curve Calculations and Measurements in Coating-Substrate Composites during Plasma Spraying*, NTSC, Long Beach, CA, 1990, 87-91

[47] H.-J. Sölter, B. Borgerding, *Das Simulationsprogramm 'Splash' zur Optimierung von plasmagespritzten Schichtsystemen*, VDI Berichtenr. 936, 1991, 181-195

[48] B. Borgerding, H.-J. Sölter, E. Lugscheider, K. Simhan, *Modelling of Temperature Gradients and Stress-Strain Distributions during the Plasma Spraying Process*, pmi vol. 24, no. 4, 1992, 240-245

[49] O. Knotek, R. Elsing, U. Balting, T*he Influence of Thermophysical Data and Spraying Parameters on the Temperature curve in Thermally Sprayed Coatings during Production*, Surface and Coatings Technology, no. 36, 1988, 99-110

[50] R. Elsing, O. Knotek, U. Balting, *The Influence of Spraying Parameters, Substrate Materials and Coating Materials on the Temperature Curve in Coatings during Thermal Spraying*, ITSC, vol. 2, 1989, 133-143

[51] O. Knotek, U. Schnaut, U. Balting, K. Ebert, C. Verpoort, J. Owinski, *Simulation of the Jet-Kote® Process*, NTSC, Pittsburg, PA, 1991, 269-272

[52] O. Knotek, U. Schnaut, *Process Modelling of HVOF Thermal Spraying Systems*, ITSC, Orlando, Florida, 1992, 811-816

[53] O. Knotek, U. Schnaut, *Anwendung der Simulation auf neue Hochgeschwindigkeits Flammspritzsysteme*, VDI, Kosten senken durch EDV-Anwendungen in der Werkstofftechnik, Düsseldorf, 1993, 105-119

[54] O. Knotek, U. Schnaut, *Numerical Simulation of the Influences of HVOF Spraying Parameters on Coating Properties*, NTSC, Anaheim, CA, 1993, 7-12

[55] M. Knepper, *Prozeßsimulation in der Thermischen Spritztechnik*, Manuskript + Bilder, Promotionsvortrag, Materials Science Institute, RWTH Aachen, 1993

[56] G.E.P. Box, W.G. Hunter, J.S. Hunter, *Statistics for Experimenters*, J. Wiley & Sons, New York, 1978

[57] S. Bisgaard, *Optimizing Thermal Spray Processes going beyond Taguchi Methods*, Thermal Spray Research and Applications, NTSC, 1990

[58] W.G. Kleppmann, *Statistische Versuchsplanung - Klassisch, Taguchi oder Shainin?*, QZ 37, Carl Hanser Verlag, München, 1992

[59] G. Box, S. Bisgaard, C. Fung, *An Explanation and Critique of Taguchi's Contributions to Quality Engineering*, Quality and Reliability Engineering Int., vol. 4, 1988, 123-131

[60] C. Nedeß, G. Holst, *Hilfen für die statistische Versuchsplanung?*, QZ 37, part 1-3, 1992

[61] J. Krottmaier, *Versuchplanung: Der Weg zur Qualität des Jahres 2000*, 2. überarbeite Auflage, Verlag Industrielle Organisation, Köln, Verlag TÜV Rheinland, 1991

[62] P.J. Ross, *Loss Function, Ortogonal Experiment Parameter and Tolerance Design*, McGraw-Hill Book Company, 1988

[63] E. Lugscheider, D. Hofmann, D. Schubert, A.R. Nicoll, *Anwendung der Zwei-Niveau-Faktoren-Analyse zur Optimierung thermisch gespritzter Schichten am Beispiel des Plasmaspritzens*, Schweißen und Schneiden 43, no. 10, 1991, 591-593

[64] E. Lugscheider, M. Knepper, *Mathematische Statistik zur Optimierung des Plasmaspritzens - anhand von Beispielen vorgestellt*, DVS-Berichte 136, 1991, 88-92

[65] T.J. Steeper, W.L. Riggs, A.J. Rotolico,m J.E. Nerz, D.J. Varacalle, Jr.,G.C. Wilson, *Optimizing Plasma Sprayed Aluminia-Titania Coatings Using Statistical Methods*, NTSC, 1993, 37-48

[66] T.J. Steeper, W.L. Riggs, A.J. Rotolico, J.E. Nerz, D.J. Varacalle Jr.,G.C. Wilson, *A Taguchi Design of Experiment Study of Plasma Sprayed Alumina Coatings*, NTSC, 1993, 31-36

[67] C.A. Sciammarella, D.S. Kupperman, *Holographic Techniques for Nondestructive Evaluation of Structural Ceramics*, Materials Evaluation, no. 44, 1986, 1551-1559

[68] W.J. Harris, D.C. Woods, *Thermal Stress Studies Using Holographic Interferrometry*, Materials Evaluation, march, 1993, 50-56

[69] E.H. Meyer, K.-J. Pohl, *Further Development of the Holographic Sound Field Imaging Method for Testing Thermal Sprayed Coatings*, ITSC, Thermal Spraying, vol. 1., 1989, 29-38

[70] M.P. Connolly, *A Review of Factors Influencing Defect Detection in Infrared Thermography: Applications to Coated Materials*, Journal of Nondestructive Evaluation, vol. 10, no. 3, 1991, 89-96

[71] D. Harris, M. Kelly, *The potential for NDE of Thermal Sprayed Coatings Using Infrared Video Thermography*, Thermal Spray - Advances in Coating Technology, Orlando, 1987, 185-189

[72] J. Morris, P.M. Patel, D.P. Almond, H. Reiter, *The Influence of Coating Properties on the Sensitivity of Thermal Wave Testing Techniques*, Thermal Spray - Advances in Coating Technology, Orlando, 1987, 321-324

[73] J. Morris, P.M. Patel, D.P. Almond, H. Reiter, *Developments in Thermal Wave non-destructive Testing Systems for Thermal Spray Coatings*, ITSC, Thermal Spraying, vol. 1, 1989, 49-54

[74] Deutscher Verband für Scheißtechnik e.V., *Zerstörfreies Prüfen von thermisch gespritzten Schichten - Schichtdickemessung*, Merkblatt DVS 2303, Teil 1, DVS-Verlag GmbH, Düsseldorf, 1991

[75] R. Borchert, W. Jubitz, *Infrarottechnik*, VEB Verlag Technik, Berlin, 1958

[76] Deutsche Norm, *Spectral Measurement of radiation*, DIN 5030, 1982

[77] R. Siegel, J.R. Howell, J. Lohrengel, *Wärmeübertragung durch Strahlung, Teil 1 - Grundlagen und Materialeigenschaften*, Springer Verlag, Berlin, 1988

[78] K. Stahl, G. Miosaga, *Infrarottechnik - Grundlagen; Strahlungssender und Detektoren; Infrarotbildaufnahmen und -wiedergabe; Fernmeßverfahren*, Dr. Albert Hüthig Verlag, Heidelberg, 1986

[79] G. Bauer, *Strahlungsmessung im optischen Spektralbereich - Messung electromagnetischer Strahlung vom Ultraviolett bis zum Ultrarot*, Friedr. Vieweg & Sohn, Braunschweig, 1962

[80] Deutsche Norm, *Thermal Radiation of Volume Radiators*, DIN 5496, 1991

[81] Bergmann, Schaefer, *Lehrbuch der Expirimentalphysik*, band 1, 9. edition, de Gruyter, 612-619

[82] U. Renz, *Grundlagen der Wärmeübertragung*, Lehrstuhl für Wärmeübertragung und Klimatechnik, RWTH, Aachen, 1992

[83] H.-G. Schöpf, *Von Kirchhoff bis Planck - Theorie der Wärmestrahlung in historisch-kritischer Darstellung*, Akademie Verlag, Berlin, 1978

[84] H. Kangro, *Vorgeschichte des Planckschen Strahlungsgesetzes - Messungen und Theorien der Spektralen Energieverteilung bis zur Begründung der Quantenhypothese*, Franz Steiner Verlag GmbH, Wiesbaden, 1970

[85] E. Kühn, *Ein FarbPyrometer zur Messung rasch veränderlicher Oberflächen-temperaturen*, dissertation, TH Hannover, 1967

[86] F. Güntert, *Bestimmung des einflusses der Oxidation auf den emissionsgrad von Metallen am beispiel von Stählen und Titan*, dissertation, TU Stuttgart, 1990

[87] U. Glückert, *Erfassung und Messung von Wärmestrahlung - Eine Praktische Einführung in die Pyrometry und Thermographie*, Franzis-Verlag GmbH & Co, München, 1992

[88] D.P. DeWitt, G.D. Nutter, *Theory and practice of radiation thermometry*, John Wiley & Sons, Inc., U.S.A., 1988

[89] M.C. Lee, *Noncontact Temperature Measurement*, NASA Office of Space Science and Applications, Washington, D.C., 1988, 149

[90] H. Schreiber, *Infrarot-Elektrotechnik - Eine Einführung in die Infrarottechnik mit Hobbyschaltungen und Experimenten*, Franzis-Druck GmbH, München, 1992

[91] L. Fiessler, *Möglichkeiten und Grenzen der Mehrwellenlängenpyrometrie als emissionsgradunabhängiges Temperaturmeßverfahren*, Institut für Kernenergetik und Energiesysteme, Stuttgart, dissertation, 1990

[92] M. Delfino, D.T. Hodul, *Wavelength-Specific Pyrometry as a Temperature Measurement Tool*, IEEE, vol. 39, no. 1, 1992, 89-95

[93] G.R. Gathers, *Monte Carlo Studies of Multiwavelength Pyrometry Using Linearized Equations*, International Journal of Thermophysics, Plenum Press, vol. 13, no. 2, 1992

[94] P.B. Coates, *Multi-Wavelength Pyrometry*, Metrologia 17, 1981, 103-109

[95] D. Ng, W.D. Williams, *Full-spectrum multiwavelength Pyrometry for nongrey surfaces*, Thermosense XIV, SPIE, vol. 1682, 1992, 260-262

[96] M.A. Khan, C. Alemand, T.W. Eagar, *Noncontact Temperature Measurement II - Least Squares Based Techniques*, Rev. Sci. Instrum. vol. 62, no. 2, 1991, 403-409

[97] G. Ruffino, *A New Multiwavelength Pyrometer: Design and Feasibility Study*, International Journal of Thermophysics, Plenum Press, vol. 13, no. 1, 1992

[98] Plasmadyne, *Dual Plasma Spray System Instruction Manual*, 9/76

[99] Plasma-Technik AG Switzerland, *TWIN 10-2 Referenzhandbuch*, 1991

[100] Plasma-Technik AG Switzerland, *TWIN 10-V, Instruction Manual*, 1991

[101] Posimo 3000, *Benutzerhandbuch für die Programmierebene 3*

[101] Plasma-Technik AG Switzerland, *F4 Plasma gun*, Instruction Manual

[102] F.J. Ladru, *Adaptation of a Pyrometric Process-Control System for Atmospheric Plasma Spraying*, Materials Science Institute, RWTH Aachen, 1994

[103] CompoTherm, Bedienungsanleitung, *Prozeßkontrollsystem CC100 für das thermische Spritzen*, 1992

[104] CompoTherm, *Dokumentation zum Grafikpaket Complott*, 1992

[105] R.C. West, *Handbook of Chemistry and Physics*, 1ST Student Edition, CRC Press, Florida, 1988

[106] C.W. Wegst, *Nachschlagwerk Stahlschlüssel 1989*, Verlag Stahlschlüssel Wegst GmbH, 1989

[107] Deutsche Norm, *Thermisches Spritzen- Begriffe, Einteilung*, DIN 50160, 1990